JOURNAL OF MATHEMATICAL SCIENCES AND MODELLING

ISSN: 2636-8692

VOLUME VI
ISSUE III

VOLUME VI ISSUE III
ISSN 2636-8692

December 2023
http://dergipark.gov.tr/jmsm

JOURNAL OF MATHEMATICAL SCIENCES AND MODELLING

Editor in Chief

Mahmut Akyiğit
Department of Mathematics,
Faculty of Science, Sakarya University,
Sakarya-TÜRKİYE
makyigit@sakarya.edu.tr

Assistant Editor

Emrah Evren Kara
Department of Mathematics,
Faculty of Science and Arts, Düzce University,
Düzce-TÜRKİYE
eevrenkara@duzce.edu.tr

Editorial Board of Journal of Mathematical Sciences and Modelling

İrem Bağlan
Kocaeli University,
TÜRKİYE

Olena Sierikova
National University of Civil Protection of Ukraine,
UKRAINE

Hadi Roopaei
Islamic Azad University Marvdasht Branch,
IRAN

Dağıstan Şimşek
Konya Technical University,
TÜRKİYE

Galip Oturanç
Karamanoglu Mehmet Bey University,
TÜRKİYE

Statistics Editor

Melek Eriş Büyükkaya
Karadeniz Technical University,
TÜRKİYE

Language Editor

Tolga Aktürk
Yıldız Technical University,
TÜRKİYE

Technical Editor

Ayla Erdur Kara
Tekirdag Namık Kemal University,
TÜRKİYE

Contents

Journal of Mathematical Sciences and Modelling, 6(3) (2023) 87-96
Research Article

Journal of Mathematical Sciences and Modelling

Journal Homepage: www.dergipark.gov.tr/jmsm
ISSN 2636-8692
DOI: http://dx.doi.org/10.33187/jmsm.1241918

μ-Symmetries and μ-Conservation Laws for the Nonlinear Dispersive Modified Benjamin-Bona-Mahony Equation

Bahadır Kopçasız[1] **and Emrullah Yaşar**[2*]

[1,2]*Department of Mathematics, Faculty of Arts and Sciences, Bursa Uludag University, 16059 Bursa, Turkey*
[*]*Corresponding Author*

Article Info

Keywords: *μ-conservation laws, μ-symmetries, μ-symmetry reductions and invariant solutions*
2010 AMS: *22E46, 53C35, 54H15, 58J70, 57S20, 74J15, 83C15*
Received: *24 January 2023*
Accepted: *5 April 2023*
Available online: *25 July 2023*

Abstract

This work discusses the μ-symmetry and conservation law of μ procedure for the nonlinear dispersive modified Benjamin-Bona-Mahony equation (NDMBBME). This equation models an approximation for surface long waves in nonlinear dispersive media. It can also describe the hydromagnetic waves in a cold plasma, acoustic waves in inharmonic crystals, and acoustic gravity waves in compressible fluids. First and foremost, we offer some essential pieces of information about the μ-symmetry and the conservation law of μ concepts. In light of such information, μ-symmetries are found. Using characteristic equations, the NDMBBME is reduced to ordinary differential equations (ODEs). We obtained the exact invariant solutions by solving the nonlinear ODEs. Furthermore, employing the variational problem procedure, we get the Lagrangian and the μ-conservation laws. The exact solutions and conservation laws are new for the NDMBBME that are not reported by the other studies. We also demonstrate the properties with figures for these solutions.

1. Introduction

Nonlinear partial differential equations (NLPDEs) play a paramount role in the investigation of considerable problems in physics and geometry. The struggle to discover exact solutions to nonlinear equations is crucial for understanding most nonlinear physical phenomena. Nonlinear wave phenomena arise in diverse scientific and engineering specializations, such as solid-state physics, chemical physics, and geometry.

Lately, influential and efficient procedures for discovering analytic solutions to nonlinear equations have lured considerable interest from various groups of scientists, such as Semi-inverse variational technique [1], New extended direct algebraic method (NEDAM) [2], Extended rational sine-cosine methods and sinh-cosh methods [3], Multiwave solutions [4], Generalized exponential rational function method (GERFM) [5], Lie symmetry analysis [6–10], Simplified Hirota technique [11], Extended simple equation method [12], Multiple exp-function method [13], Improved auxiliary equation approach [14], Modulation instability [15], Modified Jacobi elliptic expansion method [16], μ-symmetries method [17–20] and so on.

Lie symmetry analysis, which was first studied by S. Lie, is one of the most general and influential strategies for getting exact solutions for NLPDEs. A symmetry group of a differential equation means a transformation that maps (smooth) solutions to solutions. Lie utilized a continuous group of transformations to develop solution strategies for ODEs. ODEs with trivial Lie or no symmetries but possess λ-symmetries can be integrated using the λ-symmetry procedure. λ-symmetry was introduced by Muriel and Romero as a new kind of symmetry [21]. Morando and Gaeta viewed the case of PDEs and extended the λ-symmetries to the μ-symmetries [22–24]. In the event of the $\mu-$symmetries of the Lagrangian, the conservation law is referred to as the conservation law of μ.

The principal purpose of the current investigation is to scrutinize the $\mu-$symmetries, reductions, invariant solutions, and conservation law of μ for the NDMBBME.

***Email addresses and ORCID numbers*: bkopcasz@gmail.com, 0000-0002-6364-3631 (B. Kopçasız), emrullah.yasar@gmail.com, 0000-0003-4732-5753 (E. Yaşar),**
Cite as "B. Kopçasız, E. Yaşar, *μ-symmetries and μ-conservation laws for the nonlinear dispersive modified Benjamin-Bona-Mahony equation*, J. Math. Sci. Model., 6(3) (2023), 87-96"

The study is assembled as follows. Section 2 offers the main concepts of the $\mu-$symmetry and $\mu-$conservation law procedure. We yield the μ-symmetries of the NDMBBME and build the invariant solutions of the model by employing the accepted μ-symmetries in Section 3. We obtain Lagrangian in potential form by using the variational problem method and the Frechet derivative in Section 4. For the NDMBBME, the conservation law of μ is investigated in Section 5. Lastly, in Section 6, conclusions are given.

2. The Principal Vision of the μ-Symmetry and Conservation Law of μ Procedure

2.1. μ-symmetry concept

Surmise that $\mu = \lambda_i dx_i$ be a semi basic one-form on first order jet space $(J^{(1)}\aleph, \pi, \aleph)$, which is compatible, namely, $\wp_j\lambda_i = \wp_i\lambda_j$ [17–20,24]. Here, $\wp_i$ and $\wp_j$ are total derivative with respect to x_i, and λ_i defines from $J^{(1)}\aleph$ to $\mathbb{R}$.
Think that Δ be the sth-order partial differential equation (PDE) as follows

$$\Delta : \bar{h}(x, w^{(s)}) = 0. \tag{2.1}$$

Here $w = w(x) = w(x_1, x_2, ..., x_p)$ and $w^{(s)}$ symbolizes all sth order derivatives of w as to x.
Let Ω be a vector field on $J^{(s)}\aleph$. Then, we describe the Ω as

$$\Omega = \Upsilon + \sum_{|J|=1}^{s} \psi_J \partial w_J, \tag{2.2}$$

in which Υ is a vector field on $\aleph$ and defines as

$$\Upsilon = \xi^i(x,w)\frac{\partial}{\partial x^i} + \varphi(x,w)\frac{\partial}{\partial w}. \tag{2.3}$$

Here, (2.2) is the prolongation of μ of (2.3) if its coefficient provides the prolongation formula of μ

$$\psi_{J,i} = (\wp_i + \lambda_i)\psi_J - w_{J,m}(\wp_i + \lambda_i)\xi^m, \tag{2.4}$$

in which $\psi_0 = \varphi$. Let $R \subset J^{(s)}\aleph$ be the solution manifold for Δ. If $\Omega : R \to TR$, it is said that, for Eq. (2.1), (2.3) is a $\mu-$symmetry. To get μ-symmetry of Eq. (2.1), then applies (2.2) to Eq. (2.1), and restrain the got outcomes to the solution manifold $R_\Delta \subset \aleph^{(s)}$ that will be up to ξ, φ, λ_i. If we deem the λ as functions on $\aleph^{(s)}$ and compatibility conditions between the λ_i, a system of all the dependence on w_J form the determining equations [24]. $V = \exp(\int \mu)\Upsilon$ is an exponential vector field if (2.3) is a vector field on $\aleph$.

Theorem 2.1. *Let sth-order PDE defines as $\Delta(x, w^s)$, (2.3) be a vector field on $\aleph$, with invariant surface condition $Q = \varphi - w_i\xi^i$, and Ω be the $\mu-$prolong of order s of Υ. In this case, for Δ, (2.3) is a $\mu-$symmetry, then $\Omega : R_\Upsilon \to TR_\Upsilon$, in which $R_\Upsilon \subset J^{(s)}\aleph$ is the solution manifold for Δ_Υ made of Δ and $\grave{E}_J := \wp_J Q = 0$, $\forall J$ with $|J| = 0, 1, ..., s-1$ [17–20, 24].*

2.2. μ-conservation law

Surmise that $\mu = \lambda_i dx_i$ be a semi-basic one-form and with the compability condition $\wp_j\lambda_i = \wp_i\lambda_j$.
A conservation law of μ is

$$(\wp_i + \lambda_i)P^i = 0.$$

Here, P^i is a conserved vector of μ and this vector is a matrix-valued $\aleph$-vector.
Surmise that $\mathscr{L} = \mathscr{L}(x, w^{(s)})$ depicts the sth order Lagrangian. For $\mathscr{L}$, (2.3) is a $\mu-$symmetry, namely, $\exists\,\aleph$-vector P^i such that $(\wp_i + \lambda_i)P^i = 0$ where the necessary and sufficient condition is $\Omega[\mathscr{L}] = 0$ [22].
Let second-order Lagrangian defines as $\mathscr{L} = \mathscr{L}(x, t, w, w_x, ..., w_{tt})$ and for $\mathscr{L}$, $\Upsilon = \varphi(\frac{\partial}{\partial w})$ be a $\mu-$symmetry. $\aleph-$vector P^i is got as [22]

$$P^i := \varphi\frac{\partial \mathscr{L}}{\partial w_i} + \left[(\wp_j + \lambda_j)\varphi\right]\frac{\partial \mathscr{L}}{\partial w_{ij}} - \varphi\wp_j(\frac{\partial \mathscr{L}}{\partial w_{ij}}). \tag{2.5}$$

Here, $\wp_j$ is the total derivative.
The Frechet derivative $\wp_\Delta$ is self adjoint, namely, $\wp_\Delta^* = \wp_\Delta$ is necessary and sufficient condition in which a system admits a variational formulation [17–20, 25].

Theorem 2.2. *Let $\Delta = 0$ be a system of differential equations. For some variational problem $\pounds = \int L dx$, Δ is the Euler-Lagrange expression, i.e., $\wp_\Delta = \wp_\Delta^*$ if and only if $\Delta = \grave{E}(L)$. Then, by employing the homotopy formula $L[u] = \int_0^1 u\Delta[\lambda u]d\lambda$, a Lagrangian can be found for Δ.*

3. Application of the μ-Symmetry Procedure to NDMBBME

The NDMBBME can be represented as

$$\Delta_w : w_t + w_x - \delta w^2 w_x + w_{xxx} = 0. \tag{3.1}$$

Here, δ is a nonzero and real constant, and $w = w(x,t)$.
The NDMBBME was first used to define an approximation for surface long waves in nonlinear dispersive media. It can also describe the hydromagnetic waves in a cold plasma, acoustic waves in inharmonic crystals, and acoustic gravity waves in compressible fluids [26–28].

Classical Lie symmetry analysis of Eq. (3.1) was also examined in [29] and 3-dimensional Lie algebra was obtained.
Assume that we have a semi-basic one-form $\mu = \lambda_1 dx + \lambda_2 dt$ such that $\wp_t\lambda_1 = \wp_x\lambda_2$ when $w_t + w_x - \delta w^2 w_x + w_{xxx} = 0$.
Let

$$\Upsilon = \xi\frac{\partial}{\partial x} + \tau\frac{\partial}{\partial t} + \varphi\frac{\partial}{\partial w} \tag{3.2}$$

be a vector field on $\aleph$, and ξ, τ, φ based on x, t, w. The third prolongation is given as

$$\Omega = \xi\frac{\partial}{\partial x} + \tau\frac{\partial}{\partial t} + \varphi\frac{\partial}{\partial w} + \psi^x\frac{\partial}{\partial w_x} + \psi^t\frac{\partial}{\partial w_t} + \psi^{xxx}\frac{\partial}{\partial w_{xxx}}.$$

Ω satisfies the following $\mu-$symmetry condition:

$$\psi^t + \psi^x - 2\beta\varphi w_x - \beta u^2\psi^x + \psi^{xxx} \underset{\Delta=0}{|} = 0,$$

where

$$\begin{aligned}
\psi^x &= (\wp_x + \lambda_1)\varphi - w_x(\wp_x + \lambda_1)\xi - w_t(\wp_x + \lambda_1)\tau,\\
\psi^t &= (\wp_t + \lambda_2)\varphi - w_x(\wp_t + \lambda_2)\xi - w_t(\wp_t + \lambda_2)\tau,\\
\psi^{xx} &= (\wp_x + \lambda_1)\psi^x - w_{xx}(\wp_x + \lambda_1)\xi - w_{xt}(\wp_x + \lambda_1)\tau,\\
\psi^{xxx} &= (\wp_x + \lambda_1)\psi^{xx} - w_{xxx}(\wp_x + \lambda_1)\xi - w_{xxt}(\wp_x + \lambda_1)\tau,
\end{aligned}$$

and $\wp_t$, $\wp_i$ denote the total differentiations as to t and x^i:

$$\begin{aligned}
\wp_t &= \frac{\partial}{\partial t} + w_t\frac{\partial}{\partial w} + w_{tt}\frac{\partial}{\partial w_t} + w_{tx^k}\frac{\partial}{\partial w_{x^k}} + \ldots,\\
\wp_i &= \frac{\partial}{\partial x^i} + w_{x^i}\frac{\partial}{\partial w} + w_{tx^i}\frac{\partial}{\partial w_t} + w_{x^ix^k}\frac{\partial}{\partial w_{x^k}} + \ldots.
\end{aligned}$$

By applying Ω to Eq. (3.1) and substituting $-w_t - w_x + \delta w^2 w_x$ for w_{xxx}, we obtain an over-determined system for $\lambda_1, \lambda_2, \tau, \xi, \varphi$

$$-3\tau_{ww} = 0, \quad -6\xi_{ww} = 0,$$

$$-3\tau\lambda_1 - 3\tau_x = 0,$$

$$-6\tau_w\lambda_1 - 3\tau\lambda_{1w} - 6\tau_{xw} = 0,$$

$$-9\xi_w\lambda_1 - 4\xi\lambda_{1w} - 9\xi_{xw} + 3\varphi_{ww} = 0,$$

$$\vdots$$

$$-3\xi_w\lambda_{1w} - \xi\lambda_{1ww} - 3\lambda_1\xi_{ww} + \varphi_{www} - 3\xi_{wwx} = 0,$$

$$-6\tau_{xw}\lambda_1 - 3\tau_w\lambda_{1x} - 3\tau_x\lambda_{1w} - 2\tau\lambda_{1xw} - 3\tau_w\lambda_1^2 + 3\xi_w - 3\lambda_1\tau\lambda_{1w} - 3\tau_{xwx} = 0. \tag{3.3}$$

Surmise that $\lambda_1 = \wp_x[H] + y$ and $\lambda_2 = \wp_t[H] + z$, in which $H = H(x,t)$, $y = y(x)$ and $z = z(t)$ are arbitrary functions, and λ_1, λ_2 satisfy to $\wp_x\lambda_2 = \wp_t\lambda_1$ on solutions to Eq. (3.1).

Case 1: When $y = 0$, $z = 0$, and $H = -\ln(\Xi)$ in the functions of λ_1 and λ_2, then by substituting the functions

$$\lambda_1 = -\frac{\Xi_x}{\Xi}, \quad \lambda_2 = -\frac{\Xi_t}{\Xi}$$

into the system of (3.3) and solving them , we get

$$\xi = \Xi, \quad \tau = 0, \quad \varphi = 0.$$

Then, by inserting the ξ, τ, and φ into (3.2), we obtain

$$\Upsilon_1 = \Xi\frac{\partial}{\partial x}. \tag{3.4}$$

(3.4) is $\mu-$symmetry of Eq. (3.1). Also,

$$\begin{aligned} V &= \exp\left(\int \lambda_1 dx+\lambda_2 dt\right)\Upsilon \\ &= \exp\left(\int (-\frac{\Xi_x}{\Xi})dx+(-\frac{\Xi_t}{\Xi})dt\right)\Upsilon_1. \end{aligned}$$

Thanks to the Theorem 2.1, the order reduction of Eq. (3.1) is

$$\begin{aligned} Q &= \varphi-\xi w_x-\tau w_t \\ &= -\Xi w_x. \end{aligned} \tag{3.5}$$

Case 2: When $y=0$, $z=0$, and $H=-\ln(\Xi)$ in the functions of λ_1 and λ_2, then by placing the functions

$$\lambda_1=-\frac{\Xi_x}{\Xi},\ \ \lambda_2=-\frac{\Xi_t}{\Xi}$$

into the system of (3.3) and solving them, we attain

$$\xi=\frac{2}{3}\Xi,\quad \tau=\Xi,\quad \varphi=0.$$

Then, by substituting the ξ, τ, and φ into (3.2), we reach

$$\Upsilon_2=\Xi\left(\frac{2}{3}\frac{\partial}{\partial x}+\frac{\partial}{\partial t}\right). \tag{3.6}$$

(3.6) is $\mu-$symmetry of Eq. (3.1). Also,

$$V=\exp\left(\int (-\frac{\Xi_x}{\Xi})dx+(-\frac{\Xi_t}{\Xi})dt\right)\Upsilon_2.$$

By using the Theorem 2.1, the order reduction of Eq. (3.1) is

$$\begin{aligned} Q &= \varphi-\xi w_x-\tau w_t \\ &= -\Xi\left(\frac{2}{3}w_x+w_t\right). \end{aligned} \tag{3.7}$$

Case 3: When $y=0$, $z=\frac{C_1}{C_1t-3}$, and $H=-\ln(\Xi)$ in the functions of λ_1 and λ_2, then by inserting the functions

$$\lambda_1=-\frac{\Xi_x}{\Xi},\ \ \lambda_2=\frac{C_1}{C_1t-3}-\frac{\Xi_t}{\Xi}$$

into the system of (3.3) and solving them, we get

$$\xi=\left(\frac{(2t+x)C_1-C_2-6}{3C_1t-9}\right)\Xi,\quad \tau=\Xi,\quad \varphi=0.$$

Then, by substituting the ξ, τ, and φ into the vector field, we obtain

$$\Upsilon_3=\Xi\left(\left(\frac{(2t+x)C_1-C_2-6}{3C_1t-9}\right)\frac{\partial}{\partial x}+\frac{\partial}{\partial t}\right). \tag{3.8}$$

(3.8) is $\mu-$symmetry of Eq. (3.1). Also,

$$V=\exp\left(\int\left(-\frac{\Xi_x}{\Xi}\right)dx+\left(\frac{C_1}{C_1t-3}-\frac{\Xi_t}{\Xi}\right)dt\right)\Upsilon_3.$$

By using the Theorem 2.1, the order reduction of Eq. (3.1) is

$$\begin{aligned} Q &= \varphi-\xi w_x-\tau w_t \\ &= -\Xi\left[\left(\frac{(2t+x)C_1-C_2-6}{3C_1t-9}\right)w_x+w_t\right]. \end{aligned} \tag{3.9}$$

Here, $\Xi=\Xi(x,t)$ is an arbitrary positive function, C_1 and C_2 are arbitrary constants.

3.1. μ-invariant solutions for the NDMBBME

Thanks to the invariant surface condition, the characteristic equation forms are constructed. By solving the characteristic equation form, similarity variables are obtained. Then, thanks to the similarity variables and the original equation, a PDE can be converted to an ODE. Then, by solving the ODE, the invariant solution is obtained.
The characteristic equation corresponding to (3.5) is written as

$$\frac{dx}{-\Xi} = \frac{dt}{0} = \frac{dw}{0}. \tag{3.10}$$

By solving (3.10), we get similarity variables as indicated below

$$\sigma = t, \quad w = \Xi_1(\sigma).$$

After placing w into Eq. (3.1), Eq. (3.1) can be reduced to the ODE

$$\begin{aligned} \frac{d}{d\sigma}\Xi_1 &= 0, \\ \Xi_1(\sigma) &= C. \end{aligned}$$

Therefore, we have an invariant solution

$$w = C.$$

For (3.7), let us consider $\Xi \neq 0$. Then, we have $\frac{2}{3}w_x + w_t = 0$. The characteristic equation corresponding to (3.7) is written as

$$\frac{dx}{\frac{2}{3}} = \frac{dt}{1} = \frac{dw}{0}. \tag{3.11}$$

By solving (3.11), we get similarity variables as indicated below

$$\varpi = t - \frac{3}{2}x, \quad w = \Xi_2(\varpi).$$

After placing w into Eq. (3.1), Eq. (3.1) can be reduced to the ODE as

$$12\zeta\Xi_2^2\left(\frac{d}{d\varpi}\Xi_2\right) - 4\left(\frac{d}{d\varpi}\Xi_2\right) - 27\left(\frac{d^3}{d\varpi^3}\Xi_2\right) = 0.$$

Solving the above ODE, we get an integral form, specifically,

Solution Set-1: letting $C_1 = C_3 = 0, C_2 = 1$, we obtain

$$w(x,t) = -\frac{9\ JacobiSN\left(\frac{1}{9}\sqrt{6+6\sqrt{1-27\delta}}\left(t-\frac{3}{2}x\right), \frac{1}{9}\sqrt{-\frac{3\left(27\delta-2+2\sqrt{1-27\delta}\right)}{\delta}}\right)}{\sqrt{3+3\sqrt{1-27\delta}}}. \tag{3.12}$$

Solution Set-2: Let $C_1 = C_2 = 0, C_3 = 1$, we get

$$w(x,t) = \frac{\sqrt{2}\sqrt{\delta\left(\tan\left(\frac{2\sqrt{3}}{9}\left(t-\frac{3}{2}x+1\right)\right)^2+1\right)}}{\delta\tan\left(\frac{2\sqrt{3}}{9}\left(t-\frac{3}{2}x+1\right)\right)}. \tag{3.13}$$

Solution Set-3: If we choose $C_1 = C_2 = C_3 = 0$, we reach

$$w(x,t) = \frac{\sqrt{2}\sqrt{\delta\left(\tan\left(\frac{2\sqrt{3}}{9}\left(t-\frac{3}{2}x\right)\right)^2+1\right)}}{\delta\tan\left(\frac{2\sqrt{3}}{9}\left(t-\frac{3}{2}x\right)\right)}. \tag{3.14}$$

For (3.9), let $-\Xi \neq 0$. Then we have $\left(\frac{(2t+x)C_1-C_2-6}{3C_1t-9}\right)w_x + w_t = 0$. The characteristic equation corresponding to (3.9) is written as

$$\frac{dx}{\frac{(2t+x)C_1-C_2-6}{3C_1t-9}} = \frac{dt}{1} = \frac{dw}{0}. \tag{3.15}$$

By solving (3.15), we obtain similarity variables as indicated below

$$\rho = -\frac{C_1(t-x)+C_2-3}{C_1(tC_1-3)^{\frac{1}{3}}}, \quad w = \Xi_3(\rho).$$

After placing w into Eq. (3.1), Eq. (3.1) can be reduced to the ODE

$$-(\frac{d}{d\rho}\Xi_3)C_1\rho + 3(\frac{d^3}{d\rho^3}\Xi_3) = 0.$$

Solving the above equation, we have an invariant solution

$$w(x,t) = C_1 + C_2\rho\left(\begin{array}{c} 3\Gamma(\frac{2}{3})^2\rho(-C_1)^{\frac{1}{3}}\,hypergeom\left(\left[\frac{2}{3}\right],\left[\frac{4}{3},\frac{5}{3}\right],\frac{1}{27}C_1\rho^3\right) \\ +4\pi\sqrt{3}hypergeom\left(\left[\frac{1}{3}\right],\left[\frac{2}{3},\frac{4}{3}\right],\frac{1}{27}C_1\rho^3\right)\end{array}\right)$$

$$+C_3\rho\left(\begin{array}{c}\sqrt{3}\Gamma(\frac{2}{3})^2\rho(-C_1)^{\frac{1}{3}}\,hypergeom\left(\left[\frac{2}{3}\right],\left[\frac{4}{3},\frac{5}{3}\right],\frac{1}{27}C_1\rho^3\right) \\ -4hypergeom\left(\left[\frac{1}{3}\right],\left[\frac{2}{3},\frac{4}{3}\right],\frac{1}{27}C_1\rho^3\right)\pi\end{array}\right). \tag{3.16}$$

(3.16) holds the Eq. (3.1) when $\delta = 0$. Here, $\rho = -\frac{C_1(t-x)+C_2-3}{C_1(tC_1-3)^{\frac{1}{3}}}$. Also, *hypergeom* is hypergeometric function.
In particular, we deal with the following case:

$$\Upsilon_{1,2} = \Upsilon_2 + \gamma_1\Upsilon_1.$$

Thus, we have

$$\Upsilon_{1,2} = \Xi\left(\left(\frac{2}{3}+\gamma_1\right)\frac{\partial}{\partial x} + \frac{\partial}{\partial t}\right). \tag{3.17}$$

(3.17) is $\mu-$symmetry of Eq. (3.1). By using the Theorem 2.1, we have

$$\begin{aligned} Q &= \varphi - \xi w_x - \tau w_t. \\ &= -\Xi\left[\left(\frac{2}{3}+\gamma_1\right)w_x + w_t\right]. \end{aligned} \tag{3.18}$$

The characteristic equation corresponding to (3.18) is written as

$$\frac{dx}{(\frac{2}{3}+\gamma_1)} = \frac{dt}{1} = \frac{dw}{0}. \tag{3.19}$$

By solving (3.19), we get similarity variables as indicated below

$$\kappa = \frac{3t\gamma_1 + 2t - 3x}{2+3\gamma_1}, \quad w = \Xi_4(\kappa).$$

After placing w into Eq. (3.1), Eq. (3.1) can be reduced to the ODE

$$27(\frac{d}{d\kappa}\Xi_4)\Xi_4^2\delta\gamma_1^2 + 36(\frac{d}{d\kappa}\Xi_4)\Xi_4^2\delta\gamma_1 + 12\delta\Xi_4^2(\frac{d}{d\kappa}\Xi_4)$$

$$+27(\frac{d}{d\kappa}\Xi_4)\gamma_1^3 + 27(\frac{d}{d\kappa}\Xi_4)\gamma_1^2 - 4(\frac{d}{d\kappa}\Xi_4) - 27(\frac{d^3}{d\kappa^3}\Xi_4) = 0.$$

By solving the above equation, we get an integral form, especially, if we choose $C_1 = C_3 = 0, C_2 = 1$, we attain

$$w(x,t) = -\frac{1}{\sqrt{\begin{array}{c}-81\gamma_1^3 - 81\gamma_1^2 + 12 + 9\sqrt{\begin{array}{c}81\gamma_1^4 + 54\gamma_1^3 - 27\gamma_1^2 - 108\delta \\ -12\gamma_1 + 4\end{array}}\,\gamma_1 + \\ 6\sqrt{81\gamma_1^4 + 54\gamma_1^3 - 27\gamma_1^2 - 108\delta - 12\gamma_1 + 4}\end{array}}} \times$$

$$\left(18\,JacobiSN\left(\begin{array}{c}\frac{1}{18(2+3\gamma_1)}\sqrt{\begin{array}{c}24 - 162\gamma_1^3 + 18\sqrt{\begin{array}{c}81\gamma_1^4 + 54\gamma_1^3 \\ -27\gamma_1^2 - 108\delta - 12\gamma_1 + 4\end{array}}\,\gamma_1 \\ -162\gamma_1^2 + 12\sqrt{\begin{array}{c}81\gamma_1^4 + 54\gamma_1^3 \\ -27\gamma_1^2 - 108\delta - 12\gamma_1 + 4\end{array}}\end{array}}\,(3t\gamma_1 + 2t - 3x), \\ \frac{1}{18}\left(\frac{\sqrt{6}}{\delta}\sqrt{\begin{array}{c}81\gamma_1^4 + 9\sqrt{81\gamma_1^4 + 54\gamma_1^3 - 27\gamma_1^2 - 108\delta - 12\gamma_1 + 4}\,\gamma_1^2 \\ +54\gamma_1^3 + 3\sqrt{81\gamma_1^4 + 54\gamma_1^3 - 27\gamma_1^2 - 108\delta - 12\gamma_1 + 4}\,\gamma_1 \\ -27\gamma_1^2 - 2\sqrt{\begin{array}{c}81\gamma_1^4 + 54\gamma_1^3 - 27\gamma_1^2 - 108\delta \\ -12\gamma_1 + 4\end{array}} - 54\delta - 12\gamma_1 + 4\end{array}}\right)\end{array}\right)\right)$$

4. Lagrangian of the NDMBBME in Potential Form Using the Variational Problem Method

It is crucial that if an equation has odd order, it does not accept a variational problem, but thanks to the potential form Δ_v, this equation accepts a variational problem [18–20].
The NDMBBME

$$\Delta_w : w_t + w_x - \delta w^2 w_x + w_{xxx} = 0$$

is in an odd order. Frechet derivative of Δ_w is

$$\wp_{\Delta_w} : \wp_t + \wp_x - \delta w_x^2 \wp - 2\delta w w_x + \wp_x^3.$$

Note that $\wp_{\Delta_w} \neq \wp^*_{\Delta_w}$. We say that the NDMBBME does not accept a variational problem. The NDMBBME in Δ_v is got by the lustrous differential substitution $w = v_x$,

$$\Delta_v = v_{xt} + v_{xx} - \delta v_x^2 v_{xx} + v_{xxxx} = 0. \tag{4.1}$$

Eq. (4.1) is named "the NDMBBME in the potential form" and its Frechet derivative is

$$\wp_{\Delta_v} = \wp_x \wp_t + \wp_x^2 - \delta v_x^2 \wp_x^2 - 2\delta v_x v_{xx} \wp_x + \wp_x^4. \tag{4.2}$$

Note that Eq. (4.2) is self-adjoint. Thanks to the Theorem 2.2, the NDMBBME in Δ_v has a Lagrangian of the form

$$\begin{aligned} L[v] &= \int_0^1 v\Delta_v[\lambda v]d\lambda \\ &= -\frac{1}{2}v_x v_t - \frac{1}{2}v_x^2 + \frac{\delta}{12}v_x^4 + \frac{1}{2}v_{xx}^2 + DivP. \end{aligned}$$

Thus, we have

$$\mathscr{L}_{\Delta_v}[v] = -\frac{1}{2}(v_x v_t + v_x^2 - \frac{\delta}{6}v_x^4 - v_{xx}^2). \tag{4.3}$$

5. Application of the μ-Conservation Laws of the NDMBBME

In this part, first of all, we will compute the conservation laws of μ for the NDMBBME as Δ_v. Consider the second-order Lagrangian (4.3) for the NDMBBME as Δ_v

$$\begin{aligned} \Delta_v &= v_{xt} + v_{xx} - \delta v_x^2 v_{xx} + v_{xxxx} \\ &= \grave{E}(\mathscr{L}_{\Delta_v}). \end{aligned} \tag{5.1}$$

Surmise that for $\mathscr{L}_{\Delta_v}[v]$, $\Upsilon = \varphi\partial_v$ be a vector field. Let $\mu = \lambda_1 dx + \lambda_2 dt$ be a semi-basic one-form such that $\wp_x\lambda_2 = \wp_t\lambda_1$ when $\Delta_v = 0$. Thanks to the (2.4), Ω and its coefficients are

$$\Omega = \varphi\frac{\partial}{\partial v} + \psi^x\frac{\partial}{\partial v_x} + \psi^t\frac{\partial}{\partial v_t} + \psi^{xx}\frac{\partial}{\partial v_{xx}},$$

$$\psi^x = (\wp_x + \lambda_1)\varphi, \quad \psi^t = (\wp_t + \lambda_2)\varphi, \quad \psi^{xx} = (\wp_x + \lambda_1)\psi^x.$$

By applying the $\mu-$prolongation Ω to Eq. (5.1) and substituting $\frac{1}{v_x}(-v_x^2 + \frac{\delta}{6}v_x^4 + v_{xx}^2)$ for v_t, we get

$$\lambda_1\varphi + \varphi_x = 0, \quad -2\varphi_{vv} = 0,$$

$$-\frac{\delta}{3}\varphi_v = 0, \quad -\frac{\delta}{2}(\lambda_1\varphi + \varphi_x) = 0,$$

$$\varphi_x + \varphi_t + \lambda_2\varphi + \lambda_1\varphi = 0,$$

$$-2\lambda_{1v}\varphi - 4\lambda_1\varphi_v - 4\varphi_{vx} = 0,$$

$$-2\varphi_{xx} - 2\lambda_1^2\varphi - 4\lambda_1\varphi_x - 2\lambda_{1x}\varphi = 0. \tag{5.2}$$

Consider $\varphi = \Xi$, and $\mathscr{L}_{\Delta_v}[v] = 0$. A particular solution of the system (5.2) is given by

$$\lambda_1 = -\frac{\Xi_x}{\Xi}, \quad \lambda_2 = -\frac{\Xi_t}{\Xi}.$$

Therefore, for $\mathscr{L}_{\Delta_v}[v]$, $\Upsilon = \Xi\frac{\partial}{\partial v}$ is a $\mu-$symmetry. Then, by using Theorem 2.2, there exists an $\aleph$-vector P^i which is conservation law of μ, that is, $(\wp_t + \lambda_i)P^i = 0$. Then, by of (2.5), the $\aleph$-vector P^i for $\mathscr{L}_{\Delta_v}[v]$ is got

$$P^1 = -\Xi(\frac{1}{2}v_t + v_x - \frac{\delta}{3}v_x^3 + v_{xxx}),$$

$$P^2 = -\frac{v_x}{2}\Xi. \tag{5.3}$$

So, for $\mathscr{L}_{\Delta_v}[v]$, conservation law of μ is the form $\wp_x P^1 + \wp_t P^2 + \lambda_1 P^1 + \lambda_2 P^2 = 0$.

Corollary 5.1. *Conservation law of μ for the NDMBBME in $\Delta_v = \grave{E}(\mathscr{L}_{\Delta_v})$ is as*

$$\wp_x P^1 + \wp_t P^2 + \lambda_1 P^1 + \lambda_2 P^2 = 0,$$

where P^1 and P^2 are the $\aleph$-vector P^i of (5.3).

Remark 5.2. *Conservation law of μ for the NDMBBME in Δ_v, satisfying to the Noether's Theorem for $\mu-$symmetry, that is to say*

$$\begin{aligned}(\wp_i + \lambda_i)P^i &= -\Xi(v_{xt} + v_{xx} - \delta v_x^2 v_{xx} + v_{xxxx}) \\ &= Q\grave{E}(\mathscr{L}_{\Delta_v}).\end{aligned}$$

Secondly, let us consider the NDMBBME as Δ_v

$$\Delta_v = v_{xt} + v_{xx} - \delta v_x^2 v_{xx} + v_{xxxx} = 0. \tag{5.4}$$

Eq. (5.4) corresponds to

$$\wp_x(v_t + v_x - \frac{\delta}{3}v_x^3 + v_{xxx}) = 0,$$

or equivalently

$$v_t + v_x - \frac{\delta}{3}v_x^3 + v_{xxx} = \Theta_1(t),$$

where $\Theta_1(t) = \Theta_1$ is an arbitrary function. If we put

$$\Theta_1 - v_x + \frac{\delta}{3}v_x^3 - v_{xxx}$$

for v_t and substitute w for v_x in the $\aleph$-vector P^i of (5.3), then, we get the $\aleph$-vectors P^1 and P^2 as:

$$P^1 = -\Xi(\frac{1}{2}\Theta_1 + \frac{1}{2}w - \frac{\delta}{6}w^3 + \frac{1}{2}w_{xx}),$$

$$P^2 = -\frac{w}{2}\Xi. \tag{5.5}$$

Corollary 5.3. *Conservation law of μ for the NDMBBME Δ_w is*

$$\wp_x P^1 + \wp_t P^2 + \lambda_1 P^1 + \lambda_2 P^2 = 0,$$

where P^1 and P^2 are the $\aleph$-vector P^i of (5.5).

Remark 5.4. *The NDMBBME Δ_w satisfies the characteristic form, that is to say*

$$\begin{aligned}(\wp_i + \lambda_i)P^i &= -\Xi(w_x + w_t - \delta w^2 w_x + w_{xxx}) \\ &= Q\Delta_w.\end{aligned}$$

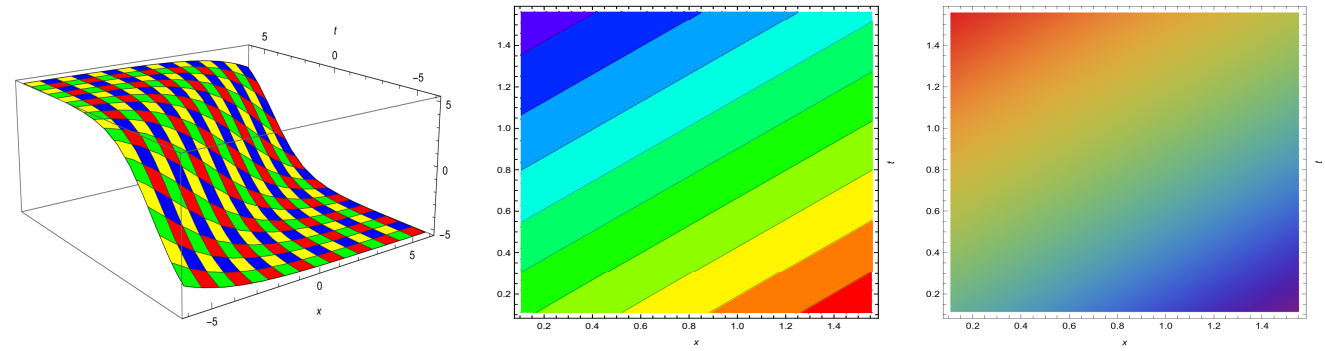

Figure 5.1: The 3−dimensional, contour and density figures of $w(x,t)$ in (3.12)

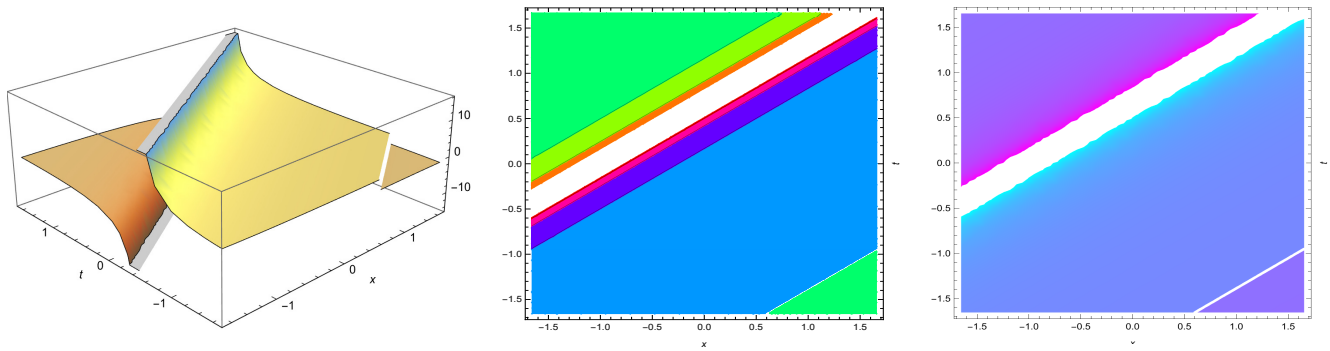

Figure 5.2: The 3−dimensional, contour and density figures of $w(x,t)$ in (3.13)

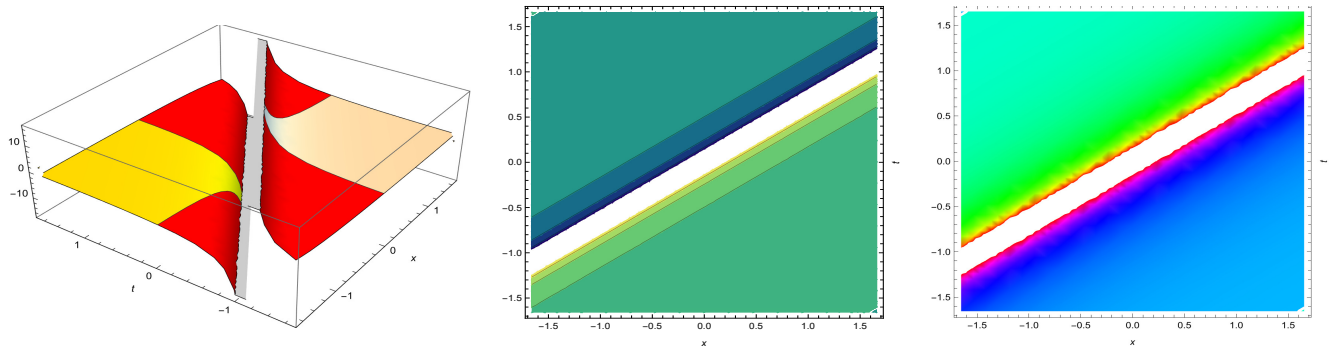

Figure 5.3: The 3−dimensional, contour and density figures of $w(x,t)$ in (3.14)

6. Conclusions

In this study, we considered the NDMBBME to scrutinize the $\mu-$symmetries, symmetry reductions, invariant solutions, and conservation laws. To begin with, some essential properties of the $\mu-$symmetries and conservation law were given. The vital situation in this approach is a semi-basic one-form $\mu = \lambda_i dx_i$, which must satisfy compatibility conditions. Then we demonstrated that the approach of the $\mu-$symmetry reduction can also be analyzed in terms of the formulation of the Noether theorem when $\mu-$symmetries were regarded to discover the invariant solutions of PDEs, which are named the $\mu-$invariant solutions. Moreover, we obtained Lagrangian in potential by using the variational problem method and the Frechet derivative. In this context, the equation must have Lagrangian necessary and sufficient condition its Frechet derivative is self-adjoint. Finally, the conservation law of μ was investigated. The main novelty of this paper is NDMBBM equation is first studied using the $\mu-$symmetry method and conservation law of μ. The 3d, contour, and density figures of the reached solutions were drawn with the aid of Mathematica. The accuracy of the solutions acquired was tested and proved in Maple.

Article Information

Acknowledgements: The authors would like to express their sincere thanks to the editor and the anonymous reviewers for their helpful comments and suggestions.

Author's contributions: All authors contributed equally to the writing of this paper. All authors read and approved the final manuscript.

Conflict of Interest Disclosure: No potential conflict of interest was declared by the author.

Copyright Statement: Authors own the copyright of their work published in the journal and their work is published under the CC BY-NC 4.0 license.

Supporting/Supporting Organizations: No grants were received from any public, private or non-profit organizations for this research.

Ethical Approval and Participant Consent: It is declared that during the preparation process of this study, scientific and ethical principles were followed and all the studies benefited from are stated in the bibliography.

Plagiarism Statement: This article was scanned by the plagiarism program. No plagiarism detected.

Availability of data and materials: Not applicable.

References

[1] B. Kopçasız, A.R. Seadawy, E. Yaşar, *Highly dispersive optical soliton molecules to dual-mode nonlinear Schrödinger wave equation in cubic law media,* Opt. Quantum Electron., **54**(3) (2022), 1-21.
[2] B. Kopçasız, E. Yaşar, *Novel exact solutions and bifurcation analysis to dual-mode nonlinear Schrödinger equation*, J. Ocean Eng. Sci., (2022).
[3] B. Kopçasız, E. Yaşar, *The investigation of unique optical soliton solutions for dual-mode nonlinear Schrödinger's equation with new mechanisms*, J. Opt., (2022),1-15.
[4] E. Yaşar, B. Kopçasız, *Novel multi-wave solutions for the fractional order dual-mode nonlinear Schrödinger equation*, Annals Math. Computat. Sci., **16** (2023), 100-111.
[5] B. Kopçasız, E. Yaşar, *Analytical soliton solutions of the fractional order dual-mode nonlinear Schrödinger equation with time-space conformable sense by some procedures,* Opt. Quantum Electron., **55**(7) (2023), 629.
[6] B. Kopçasız, E. Yaşar, *Dual-mode nonlinear Schrödinger equation (DMNLSE): Lie group analysis, group invariant solutions, and conservation laws*, Internat. J. Modern Phys. B, (2023) 2450020, 26 pages.
[7] Y. Zhang, *Lie symmetry analysis and exact solutions of the Sawada-Kotera equation*, Turkish J. Math., **41**(1) (2017), 158-167.
[8] D. Kaya, G. Iskandarova, *Lie group analysis for initial and boundary value problem of time-fractional nonlinear generalized KdV partial differential equation*, Turkish J. Math., **43**(3) (2019), 1263-1275.
[9] E. Yaşar, T. Özer, *On symmetries, conservation laws, and invariant solutions of the foam-drainage equation*, Int. J. Nonlinear. Mech., **46**(2) (2011), 357-362.
[10] Ö. Orhan, M. Torrisi, R. Tracinà, *Group methods applied to a reaction-diffusion system generalizing Proteus Mirabilis models,* Commun. Nonlinear Sci. Numer. Simul., **70** (2019), 223-233.
[11] S. Kumar, B. Mohan, R. Kumar, *Lump, soliton, and interaction solutions to a generalized two-mode higher-order nonlinear evolution equation in plasma physics*, Nonlinear Dyn., **110**(1) (2022), 693-704.
[12] E.H. Zahran, A. Bekir, *New unexpected soliton solutions to the generalized (2+1) Schrödinger equation with its four-mixing waves*, Int. J. Mod. Phys. B, **36**(25) (2022), 2250166.
[13] T.S. Moretlo, A.R. Adem, B. Muatjetjeja, *A generalized (1+2)-dimensional Bogoyavlenskii–Kadomtsev–Petviashvili (BKP) equation: Multiple exp-function algorithm; conservation laws; similarity solutions*, Commun. Nonlinear Sci. Numer. Simul., **106** (2022), 106072.
[14] M. Islam, F.A. Abdullah, J.F. Gómez-Aguilar, *A variety of solitons and other wave solutions of a nonlinear Schrödinger model relating to ultra-short pulses in optical fibers*, Opt. Quantum Electron., **54**(12) (2022), 1-21.
[15] M. Khater, M. Inc, K.U. Tariq, F. Tchier, H. Ilyas, D. Baleanu, *On some novel optical solitons to the cubic–quintic nonlinear Helmholtz model*, Opt. Quantum Electron., **54**(12) (2022), 1-13.
[16] K. Hosseini, E. Hincal, S. Salahshour, M. Mirzazadeh, K. Dehigia, B.J. Nath, *On the dynamics of soliton waves in a generalized nonlinear Schrödinger equation*, Optik, **272** (2022), 170215.
[17] Y.S. Bai, J.T. Pei, W.X. Ma, λ*-symmetry and* μ*-symmetry reductions and invariant solutions of four nonlinear differential equations*, Mathematics, **8**(7) (2020), 1138.
[18] K. Goodarzi, *Order reduction,* μ*-symmetry and* μ*-conservation law of the generalized mKdV equation with constant-coefficients and variable-coefficients*, Int. J. Ind. Math., **14**(4) (2022), 433-444.
[19] H. Jafari, K. Goodarzi, M. Khorshidi, V. Parvaneh, Z. Hammouch, *Lie symmetry and* μ*-symmetry methods for nonlinear generalized Camassa–Holm equation*, Adv. Differ. Equ., **2021**(1) (2021), 1-12.
[20] Ö. Orhan, T. Özer, *On* μ*-symmetries,* μ*-reductions, and* μ*-conservation laws of Gardner equation*, J. Math. Phys., **26**(1) (2019), 69-90.
[21] C. Muriel, J.L. Romero, *New methods of reduction for ordinary differential equations*, IMA J. App. Math., **66**(2) (2001), 111-125.
[22] G. Cicogna, G. Gaeta, *Noether theorem for* μ*-symmetries*, J.Phys. A: Math Theor., **40**(39) (2007), 11899–11921.
[23] G. Cicogna, G. Gaeta, P. Morando, *On the relation between standard and* μ*-symmetries for PDEs*. J. Phys. A, **37**(40) (2004), 9467–9486.
[24] G. Gaeta, P. Morando, *On the geometry of lambda-symmetries and PDE reduction*, J.Phys. A: Math Gen., **37**(27) (2004), 6955-6975.
[25] P.J. Olver, *Application of Lie Groups to Differential Equations*, New York, Springer-Verlag, 1986.
[26] K. Khan, M.A. Akbar, S.M. Islam, *Exact solutions for (1+1)-dimensional nonlinear dispersive modified Benjamin-Bona-Mahony equation and coupled Klein-Gordon equations*, SpringerPlus, **3**(1) (2014), 1-8.
[27] E. Yusufoğlu, *New solitonary solutions for the MBBM equations using Exp-function method*, Phys. Lett. A, **372**(4) (2008), 442-446.
[28] E.M.E Zayed, S. Al-Joudi, *Applications of an extended* (G'/G)*-expansion method to find exact solutions of nonlinear PDEs in mathematical physics*, Math. Prob Eng., **2010** (2010), 1-19.
[29] M. Khorshidi, M. Nadjafikhah, H. Jafari, M. Al Qurashi, *Reductions and conservation laws for BBM and modified BBM equations*, Open Maths., **14**(1) (2016), 1138-1148.

Journal of Mathematical Sciences and Modelling, 6 (3) (2023) 97-104
Research Article

Journal of Mathematical Sciences and Modelling

Journal Homepage: www.dergipark.gov.tr/jmsm
ISSN 2636-8692
DOI: http://dx.doi.org/ 10.33187/jmsm.1194487

An Application of Infinite Programming on Desirability Functions

Başak Akteke Öztürk

Department of Industrial Engineering, METU, Ankara, Turkey

Article Info

Keywords: *Desirability functions, Multi-response optimization*
2010 AMS: *90C11, 90C90*
Received: *25 October 2022*
Accepted: *14 July 2023*
Available online: *28 July 2023*

Abstract

When assessing the quality of a system or product, it is necessary to take all responses into account and optimize them in a concurrent manner to find the factor levels that satisfy the overall system, process, or product properties to solve the robust design problem. This problem can be solved as a multi-response optimization problem. There are many methods suggested to solve this problem based on different disciplines like multi-objective optimization. In this study, we improve the theory of nondifferentiable desirability functions' optimization for which the so-called gradient-based methods are not useful. In this study, we propose an infinite programming approach for nondifferentiable desirability functions including more than one nondifferentiable point. We employed DNLP model of GAMS/BARON which is a nondifferentiable solver, however, the solution of more than one nondifferentiable point problem is resulted as infeasible. We also tested MATLAB/NOMAD which is a derivative-free solver for MINLP problems, however, MATLAB/NOMAD also did not succeed and could not solve this nondifferentiable problem. Lastly, we use a genetic algorithm that is implemented under MATLAB and it also cannot find a feasible solution. We use an example that is solved by different desirability functions approaches before and show that the desirability functions approach with more than one nondifferentiable point is a good alternative to the ones in the literature. We present the conclusion and future studies at the end of the paper.

1. Introduction

During 1980s, Taguchi introduced the notion of robust design to the quality engineering world [1, 2]. Robust design methodology finds the control factors that give the best setting of responses which corresponds to and aims at variance reduction and insensitivity to noise factors [3]. In this study, we are interested in static systems with multiple responses where the target information of the responses are static [4–8]. From the design of the experiment, the quality data are used to obtain response models and then optimized concurrently by means of desirability functions [9]. Although other multi-objective optimization methods based on utility functions with normed distances are possible to solve a multi-response optimization problem, desirability functions are highly preferred because of their simplicity and ease of implementation with less mathematical and statistical knowledge [10, 11]. Desirability functions are improved in the literature, to solve the dynamic robust design problems which is an advantage of them over methods like loss functions and response surface methodology [4, 12].

Desirability functions first introduced by [13] in 1965, have the disadvantage of lack of shape flexibility. Derringer and Suich suggested new desirability functions with more shape alternatives, however, have the disadvantage of being nondifferentiable when the two-sided individual desirability are included in the problem [14, 15]. Castillo et. al. [16] suggested smoothing the nondifferentiable points by polynomial approximations and then combine them to have an objective function that is differentiable. This method is reported to have the disadvantage of requiring considerable algebra [16]. There are other desirability functions examples in the literature all reported to have disadvantages related with producing global optimal, requiring sophisticated algebra knowledge for being able to use and less shape flexibility. In this study, we improve the method of [16] and propose a method that is easy to use and has shape flexibility which make it implement successfully.

Email address and ORCID number: bozturk@metu.edu.tr, 0000-0003-3058-5882
Cite as "B. Öztürk, *An application of infinite programming on desirability functions*, J. Math. Sci. Model., 6(3) (2023), 97-104."

In [17], we explained the topological structure of desirability functions which give rise to different forms of desirability functions in the literature. We combine this knowledge with the model we present in [18], and propose infinite programming to use in modeling individual desirability functions with infinitely many nondifferentiable points. We propose to have an infinite number of nondifferentiable point in an individual desirability function to have a smooth individual desirability function instead of using powers over desirability functions to have a flexible desirability function. Since we need the constraints of each individual desirability functions being between 0 and 1 in our optimization problem, we face infinity both in the objective and the constraint. This makes the problem infinite programming problem. We employ binary integer variables to represent the function pieces that lie in between the nondifferentiable points. This makes the problem nondifferentiable MINLP in which the number of function pieces can be chosen as infinite. In [17], we explained that these function pieces are min-type continuous selection functions and can be selected either linear or nonlinear. In this study, we choose linear min-type functions for computational purposes, however, it is possible to choose them quadratic or other nonlinear forms.

To solve this infinite programming problem, we employ DNLP model of GAMS/BARON [19, 20] and MINLP model [21] with MATLAB/NOMAD [22] and genetic algorithm of MATLAB [23]. GAMS/BARON finds no feasible solution and MATLAB/NOMAD produce the exceeded iterations output. However, genetic algorithm of MATLAB finds an alternative solution to the solution reported in the literature. We understand that this highly nondifferentiable problem can not be solved by two well-known nondifferentiable solver but only genetic algorithm of MATLAB. We show our implementation on a well-known example from the multi-response optimization literature.

In Section 2, we present our optimization model that enables the user to choose any shape of a desirability function by employing necessary number of nondifferentiable points. In Section 3, we solve a problem including two-sided desirability functions which [16] used and solved. Lastly, we present outlook and future work of the study.

2. Infinite Programming For Desirability Functions

We have studied nondifferentiable individual desirability functions in [9]. All the formulations and classical desirability functions are based on [14]. In this study, we take the binary variables that represent individual desirability functions over finite pieces of the function in the numerical example. Here, it is possible to employ an infinite number of function pieces in obtaining individual desirability function $d_j^Y(\mathbf{x},\mathbf{z}_j)$. We calculate each of the function pieces by using the method given in [16]:

$$d(Y(\mathbf{x})) = a_\zeta + b_\zeta Y \qquad y_\zeta < Y \leq y_{\zeta+1} \qquad (\zeta = 1,2,\ldots,\zeta_j)$$

where $b_\zeta = (d_{\zeta+1} - d_\zeta)/(y_{\zeta+1} - y_\zeta)$ and $a_\zeta = d_{\zeta+1} - b_\zeta y_{\zeta+1}$.

An individual DF $d_j^Y(\mathbf{x},\mathbf{z}_j)$ including $\zeta_j - 1$ many nondifferentiable points can be expressed as follows for $\mathbf{z}_j = (z_{j1}, z_{j2}, \ldots, z_{j\zeta_j})^T$ with $\sum_{\zeta=1}^{\zeta_j} z_{j\zeta} = 1$ $(\zeta = 1,2,\ldots,\zeta_j;\ j = 1,2,\ldots,m)$:

$$d_j^Y(\mathbf{x},\mathbf{z}_j) = \sum_{\zeta=1}^{\zeta_j} z_{j\zeta} d_{j\zeta}^Y(\mathbf{x}) \quad (j = 1,2,\ldots,m).$$

Hence, the overall problem $(\mathscr{P})$ turns into a minimization problem:

$$\begin{aligned}
\text{maximize} \quad & (\prod_{j=1}^{m} d_j^{Y,}(\mathbf{x},\mathbf{z}_j))^{(1/m)} \\
\text{subject to} \quad & \mathbf{x} \in [\mathbf{l}_x, \mathbf{u}_x], \\
& 0 \leq d_j^{Y,}(\mathbf{x},\mathbf{z}_j) \leq 1 \quad (\zeta = 1,2\ldots\zeta_j; j = 1,2,\ldots,m), \\
& \sum_{\zeta=1}^{\zeta_j} z_{j\zeta} = 1 \ (\zeta = 1,2,\ldots,\zeta_j;\ j = 1,2,\ldots,m), \\
& z_{j\zeta} \in \{0,1\} \quad (\zeta = 1,2\ldots\zeta_j; j = 1,2,\ldots,m)
\end{aligned} \tag{2.1}$$

where weights of the desirability functions are given equal $(w_j \geq 0\ (j = 1,2,\ldots,m))$ and $\sum_{j=1}^{m} w_j = 1$ in the problem. We note that each function $d_{j\zeta}^Y : \mathbb{R}^n \to \mathbb{R}$ is assumed to be a C^2-function. Here, $z_{j\zeta}$ is the binary variables for $d_{j\zeta}^Y$ of d_j^Y. In this problem, we assume $\zeta_j \geq 1$ which gives our semi-infinite constraint. Overall desirability function $D^{\mathbf{Y}}(\mathbf{x},\mathbf{z})$ is the geometric mean of the individual desirability functions $d_j^{Y,}(\mathbf{x},\mathbf{z}_j)$.

3. Numerical Example and Results

In this section, we solve wire bonding process optimization problem which is presented in [16] with 3 response models given in [9] according to the proposed method. In this problem, the overall desirability function $D^{\mathbf{Y}}(\mathbf{x},\mathbf{z}) = D(\mathbf{y},\hat{\mathbf{z}}) = D(\mathbf{Y}(\mathbf{x}),\hat{\mathbf{z}})$ with $y_j = Y_j(\mathbf{x})$ $(j = 1,2,3)$ is used. It is obtained by calculating the geometric mean of the individual desirability functions with equal weights. In this study, for achieving the more than one nondifferentiable case, we use three pieces on the left sides of the individual desirability functions and two pieces on the

right. We use the binary variables $z1(j), z2(j), z3(j)$ to show the active piece of the individual desirability functions where the responses of the problem are $\mathbf{Y}(\mathbf{x}) = (Y_1(\mathbf{x}), Y_2(\mathbf{x}), Y_3(\mathbf{x}))$ and all the desirability functions of the problem are two-sided.

In this study, we choose three solvers for solving our infinite programming model of desirability functions including 3 nondifferentiable points. These solvers are well-known in solving successfully the nonlinear programming problems. Although, we fail to achieve feasible solution, in multi-response optimization this can be acceptable as a deep solution.

We added the nonlinear constraints of individual desirability functions being 0 and 1 to the model on which GAMS/BARON is implemented by using a DNLP model. While implementing this DNLP model under GAMS/BARON, we add the following constraint to the problem (2.1) for defining binary variables $z_{j\zeta}$

$$z_{j\zeta} - (z_{j\zeta})^2 = 0.$$

We give the details of the optimization model in appendix A. This model is resulted as infeasible possibly because the highly nondifferentiability of the model.

We also implemented MATLAB/NOMAD on the same problem as a MINLP model, however, MATLAB/NOMAD produce the exceeded iterations output (see Appendix B) and finds no solution.

Lastly, we run genetic algorithm that is implemented under MATLAB and we there is no feasible solution. The results are given in Table 3.1.

Table 3.1: Optimal solution of the Wire Bonding Process Optimization problem with 3 responses with genetic algorithm with MATLAB [23].

Method	$(x_1^0, x_2^0, x_3^0, x_4^0, x_5^0, x_6^0, x_7^0, x_8^0, x_9^0,)$ $(x_{10}^0, x_{11}^0, x_{12}^0, x_{13}^0, x_{14}^0, x_{15}^0, x_{16}^0, x_{17}^0, x_{18}^0)$		
1	$(0.9999, 0.7611, 0.7288, 0.1193, 0.0371, 0.7690, 0.0262, 0.0484, 0.5051, 0.0947)$ $(0.2157, 0.0430, 0.1415, 0.2029, 0.0903, 0.6877, 0.0123, 0.0067)$		
		$(d_1(y_1^*), d_2(y_2^*), d_3(y_3^*), d_4(y_4^*))$	D^*
	1	$(0.5121, 0.9009, 0.5330)$	0.2459

We give in Figure 3.1 the desirability functions with a number of nonsmooth points.

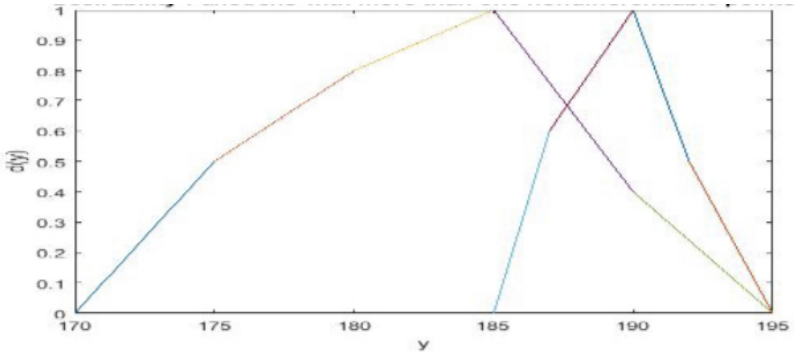

Figure 3.1: Desirability Functions of the example problem.

4. Conclusion and Future Outlook

We show an application of the method for desirability functions including more than one nondifferentiable points. This was suggested in [16] and we achieved this by using infinite programming. We develop the optimization problem with a nondifferentiable model using well-known optimization solvers for this problem. Since our problem is highly nondifferentiable, both solvers, i.e., GAMS/BARON, MATLAB/NOMAD and genetic algorithm of MATLAB fail to find a feasible solution or global but produce a infeasible solution or exceed iterations.

Although the model we develop with infinite programming presents shape alternatives to the users of desirability functions of Derringer and Suich [14, 15], since the current nondifferentiable solvers is not successful on this problem, we suggest to the researchers and scientists to use gradient-based methods in combination with the smoothing technique of [16] for desirability functions with more than one nondifferentiable points or the methodology we suggest with genetic algorithm of MATLAB. However, our study is a theoretical advantage in the field of desirability functions including nondifferentiable points. This suggests to use the modeling of infinite programming and different solvers. Since this study is an emerging field in the multi-response optimization field, it is possible to achieve better results in the future.
In the future, it is possible to use semi-infinite programming approach on this infinitely many nondifferentiable problem study within desirability functions where the objective is based on an infinite number of pieces, however, the constraint given by individual desirability functions of being between 0 and 1 is replaced by the bounds of the responses. Also, exponential desirability functions can be studied with the approach we propose here including infinite programming [25]. We note this highly nondifferentiable optimization problem we present is not signomial optimization problem [24] since the decision variables may take negative values also.

Article Information

Acknowledgements: The authors would like to express their sincere thanks to the editor and the anonymous reviewers for their helpful comments and suggestions.

Author's contributions: The article has a single author. The author has read and approved the final manuscript.

Conflict of interest disclosure: No potential conflict of interest was declared by the author.

Copyright statement: Authors own the copyright of their work published in the journal and their work is published under the CC BY-NC 4.0 license.

Supporting/Supporting organizations: No grants were received from any public, private or non-profit organizations for this research.

Ethical approval and participant consent: It is declared that during the preparation process of this study, scientific and ethical principles were followed and all the studies benefited from are stated in the bibliography.

Plagiarism statement: This article was scanned by the plagiarism program. No plagiarism detected.

Availability of data and materials: All data generated or analysed during this study are included in the published article (and its supplementary information files).

References

[1] G. Taguchi, *Introduction to Quality Engineering: Designing Quality into Products and Processes*, Kraus, White Plains, NY, 1986.
[2] G. Taguchi, *System of Experimental Design: Engineering Methods to Optimize Quality and Minimize Cost*, UNIPUB/Kraus International, White Plains, NY, 1987.
[3] A. I. Khuri, *Multiresponse surface methodology*, Handbook of Statist., **13** (1996), 377–406.
[4] H. H. Chang, *Dynamic multi–response experiments by backpropagation networks and desirability functions*, J. Chin. Inst. Eng., **23**(4) (2010), 280-288.
[5] I. J. Jeong, K. J. Kim, *An interactive desirability function method to multiresponse optimization*, European J. Oper. Res., **195**(2) (2008), 412-426.
[6] I. J. Jeong, K.J. Kim, *D-STEM: a modified step method with desirability function concept*, Comput. Oper. Res., **32** (2005), 3175-3190.
[7] D.H., Lee, K.J. Kim, M. Köksalan, *A posterior preference articulation approach to multiresponse surface optimization* , European J. Oper. Res., **210** (2011), 301-309.
[8] D.H. Lee, K.J. Kim, M. Köksalan, *An interactive method to multiresponse surface optimization based on pairwise comparisons*, IIE Transactions, **44**(1) (2012), 13-26.
[9] B. Akteke Öztürk, G. Köksal, G. W. Weber, *Nonconvex optimization desirability functions*, Qual. Eng., **30**(2) (2017), 293-310.
[10] B. Akteke Öztürk, G. W. Weber, G. Köksal, *Optimization of generalized desirability functions under model uncertainty*, Optimization, **66**(12) (2017), 2157-2169.
[11] R. T. Marler, J. S. Arora, *Survey of multi-objective optimization methods for engineering*, Struct. Multidiscip. Optim., **26**(6) (2004), 369-395.
[12] K. S. Park, K. J. Kim, *Optimizing multi-response surface problems: how to use multi-objective optimization techniques*, IIE Transactions, **37**(6) (2005), 523-532.
[13] E. C. Jr. Harrington, *The desirability function*, Ind. Qual. Control, **21** (1965), 494-498.
[14] G. Derringer, R. Suich, *Simultaneous optimization of several responsevariables*, J. Qual. Technol., **12** (1980), 214-219.
[15] G. Derringer, *A balancing act, optimizing a products properties*, Qual. Prog., **27** (1994), 51-57.
[16] E. Del Castillo, D. C. Montgomery, D. R. Mc Carville, *Modified desirability functions for multiple response optimization*, J. Qual. Technol., **28**(3) (1996), 337-345.
[17] B. Akteke Öztürk, G. W. Weber, G. Köksal, *Generalized desirability functions: a structural and topological analysis of desirability functions*, Optimization, **69**(1) (2019), 115-130.
[18] B. Akteke Öztürk, G. W. Weber, G. Köksal, Desirability functions in multiresponse optimization, Communications in computer and information science, Springer, Cham, (2015), 129–146.
[19] BARON, https://www.gams.com/latest/docs/S_BARON.html, v. 8.1.5, 2010.
[20] GAMS, https://www.gams.com/, v. 23.8.2, 2012.
[21] P. Belotti, C. Kirches, S. Leyffer, J. Linderoth, J. Luedtke, A. Mahajan, *Mixed-integer nonlinear optimization*. Acta Numer., **22** (2013), 1-131.
[22] S. L. Digabel, *Algorithm 909: NOMAD: Nonlinear optimization with the MADS algorithm*, ACM Trans. Math. Software, **37**(4) (2011), 1-15.
[23] S. Sivanandam, S. Deepa, *Genetic Algorithm Implementation Using Matlab. In: Introduction to Genetic Algorithms*. Springer, Berlin, Heidelberg, 2008.
[24] R. Pörn, K.M. Björk, T. Westerlund,*Global solution of optimization problems with signomial parts*, Discrete Optim., **5** (2008), 108-120.
[25] K. Kim, D. Lin, *Simultaneous optimization of multiple responses by maximizing exponential desirability functions*, Appl. Stat., **49**(C) (2000), 311-325.

APPENDIX A

```
$title THE WIRE BONDING PROBLEM - 3 Response

Sets
i index of factors /1*3/
j index of responses /1*3/
l index convex/1*2/;

Variable
x(i)  factors
D     objective function
Y(j)  responses
z11(j)
z12(l)
z21(j)
z22(l)
z31(j)
z32(l);
```

```
z11.lo(j)=0;
z11.up(j)=1;
z12.lo(l)=0;
z12.lo(l)=1;
z21.lo(j)=0;
z21.up(j)=1;
z22.lo(l)=0;
z22.up(l)=1;
z31.lo(j)=0;
z31.up(j)=1;
z32.lo(l)=0;
z32.up(l)=1;

x.lo(i)=-1 ;
x.up(i)=1;

TABLE yDATA(j,*) Response Bounds

          A            B            C          D          E        F          G

   1   174.93333       0.00        23.375    3.625      -19.00    0.00       0.00
   2   154.85714       8.5         30.625    7.875       0.00    -12.85714   11.25
   3   140.23333       5.3438      18.25     19.5938     0.00     0.00       0.00 ;


Equations
COST                 objective function
binarcons11         constraint for binary variable
 binarcons21
binarcons31
mipcons11(j)
mipcons12(l)
mipcons21(j)
mipcons22(l)
mipcons31(j)
mipcons32(l)
subfunc(j)
descons1
descons2
descons3
descons4
descons5
descons6
;

COST.. D=e=((((z11('1'))*((0.5-((0.5/(187-185))*187))+(0.5/(187-185))*Y('1'))
+(z11('2'))*((0.8-(((0.8-0.5)/(188-187))*188))+((0.8-0.5)/(188-187))*Y('1'))
+(z11('3'))*((1-(((1-0.8)/(190-188))*190))+((1-0.8)/(190-188))*Y('1')))
+((z12('1'))*(0.4-(((0.4-1)/(193-190))*193)+((0.4-1)/(193-190))*Y('1'))
+(z12('2'))*((0-(((0-0.4)/(195-193))*195))+((0-0.4)/(195-193)*Y('1')))))
 *(((z21('1'))*((0.5-((0.5/(187-185))*187))+(0.5/(187-185))*Y('2'))
+(z21('2'))*((0.8-(((0.8-0.5)/(188-187))*188))+((0.8-0.5)/(188-187))*Y('2'))
+(z21('3'))*((1-(((1-0.8)/(190-188))*190))+((1-0.8)/(190-188))*Y('2')))
+((z22('1'))*((0.4-(((0.4-1)/(193-190))*193))+((0.4-1)/(193-190))*Y('2'))
+(z22('2'))*((0-(((0-0.4)/(195-193))*195))+((0-0.4)/(195-193)*Y('2')))))
 *(((z31('1'))*((0.5-(((0.5/(175-170)))*175))+(0.5/(175-170))*Y('3'))
+(z31('2'))*((0.8-(((0.8-0.5)/(180-175))*180))+((0.8-0.5)/(180-175))*Y('3'))
+(z31('3'))*((1-(((1-0.8)/(185-180))*185))+((1-0.8)/(185-180))*Y('3')))
+((z32('1'))*((0.4-(((0.4-1)/(190-185))*190))+((0.4-1)/(190-185))*Y('3'))
+(z32('2'))*((0-(((0-0.4)/(195-190)))*195)+((0-0.4)/(195-190)*Y('3'))))))**(1/3);

binarcons11..  sum((j),(z11(j)))+sum((l),(z12(l))) =e= 1 ;
binarcons21..  sum(j,(z21(j)))+sum(l,(z22(l))) =e= 1 ;
binarcons31..  sum((j),(z31(j)))+sum(l,(z32(l))) =e= 1 ;
```

```
mipcons11(j)..(z11(j)-sqr(z11(j)))=e=0;
mipcons12(l)..(z12(l)-sqr(z12(l)))=e=0;
mipcons21(j)..(z21(j)-sqr(z21(j)))=e=0;
mipcons22(l)..(z22(l)-sqr(z22(l)))=e=0;
mipcons31(j)..(z31(j)-sqr(z31(j)))=e=0;
mipcons32(l)..(z32(l)-sqr(z32(l)))=e=0;

subfunc(j)..  (yDATA(j,'A')+yDATA(j,'B')*x('1')+yDATA(j,'C')*x('2')
+yDATA(j,'D')*x('3')+yDATA(j,'E')*x('2')*x('3')+
yDATA(j,'F')*x('1')*x('1')+yDATA(j,'G')*x('1')*x('2')) =e= Y(j);

descons1..((z11('1'))*((0.5-(0.5/(187-185))*187)+(0.5/(187-185))*Y('1'))
+(z11('2'))*((0.8-((0.8-0.5)/(188-187))*188)+((0.8-0.5)/(188-187))*Y('1'))
+(z11('3'))*((1-((1-0.8)/(190-188))*190)+((1-0.8)/(190-188))*Y('1')))
+((z12('1'))*(0.4-((0.4-1)/(193-190))*193+((0.4-1)/(193-190))*Y('1'))
+(z12('2'))*((0-((0-0.4)/(195-193))*195)+((0-0.4)/(195-193)*Y('1'))))=l=1;

descons2.. ((z21('1'))*((0.5-(0.5/(187-185))*187)+(0.5/(187-185))*Y('2'))
+(z21('2'))*((0.8-((0.8-0.5)/(188-187))*188)+((0.8-0.5)/(188-187))*Y('2'))
+(z21('3'))*((1-((1-0.8)/(190-188))*190)+((1-0.8)/(190-188))*Y('2')))
+((z22('1'))*(0.4-((0.4-1)/(193-190))*193+((0.4-1)/(193-190))*Y('2'))
+(z22('2'))*((0-((0-0.4)/(195-193))*195)+((0-0.4)/(195-193)*Y('2'))))=l=1;

descons3..((z31('1'))*((0.5-(0.5/(175-170))*175)+(0.5/(175-170))*Y('3'))
+(z31('2'))*((0.8-((0.8-0.5)/(180-175))*180)+((0.8-0.5)/(180-175))*Y('3'))
+(z31('3'))*((1-((1-0.8)/(185-180))*185)+((1-0.8)/(185-180))*Y('3')))
+((z32('1'))*(0.4-((0.4-1)/(190-185))*190+((0.4-1)/(190-185))*Y('3'))
+(z32('2'))*((0-((0-0.4)/(195-190))*195)+((0-0.4)/(195-190)*Y('3'))))=l=1;

descons4..((z11('1'))*((0.5-(0.5/(187-185))*187)+(0.5/(187-185))*Y('1'))
+(z11('2'))*((0.8-((0.8-0.5)/(188-187))*188)+((0.8-0.5)/(188-187))*Y('1'))
+(z11('3'))*((1-((1-0.8)/(190-188))*190)+((1-0.8)/(190-188))*Y('1')))
+((z12('1'))*(0.4-((0.4-1)/(193-190))*193+((0.4-1)/(193-190))*Y('1'))
+(z12('2'))*((0-((0-0.4)/(195-193))*195)+((0-0.4)/(195-193)*Y('1'))))=g=0;

descons5..  ((z21('1'))*((0.5-(0.5/(187-185))*187)+(0.5/(187-185))*Y('2'))
+(z21('2'))*((0.8-((0.8-0.5)/(188-187))*188)+((0.8-0.5)/(188-187))*Y('2'))
+(z21('3'))*((1-((1-0.8)/(190-188))*190)+((1-0.8)/(190-188))*Y('2')))
+((z22('1'))*(0.4-((0.4-1)/(193-190))*193+((0.4-1)/(193-190))*Y('2'))
+(z22('2'))*((0-((0-0.4)/(195-193))*195)+((0-0.4)/(195-193)*Y('2'))))=g=0;

descons6..((z31('1'))*((0.5-(0.5/(175-170))*175)+(0.5/(175-170))*Y('3'))
+(z31('2'))*((0.8-((0.8-0.5)/(180-175))*180)+((0.8-0.5)/(180-175))*Y('3'))
+(z31('3'))*((1-((1-0.8)/(185-180))*185)+((1-0.8)/(185-180))*Y('3')))
+((z32('1'))*(0.4-((0.4-1)/(190-185))*190+((0.4-1)/(190-185))*Y('3'))
+(z32('2'))*((0-((0-0.4)/(195-190))*195)+((0-0.4)/(195-190)*Y('3'))))=g=0;

MODEL xz /ALL/;

*option domlim=10;
option dnlp=baron;

SOLVE xz USING dnlp MAXIMIZING D;

DISPLAY x.l,Y.l,z11.l,z12.l,z21.l,z22.l,z31.l,z32.l,D.l;
```

APPENDIX B

```
clc
fun=@(x)-((((x(4))*((0.5-((0.5/(187-185))*187))+(0.5/(187-185))...
*(174.9333+23.3750*x(2)+3.6250*x(3)-19.0000*x(2)*x(3)))...
+(x(5))*((0.8-(((0.8-0.5)/(188-187))*188))+...
((0.8-0.5)/(188-187))*(174.9333+23.3750*x(2)+3.6250*x(3)-19.0000*x(2)*x(3)))...
+(x(6))*((1-(((1-0.8)/(190-188))*190))...
+((1-0.8)/(190-188))*(174.9333+23.3750*x(2)+3.6250*x(3)-19.0000*x(2)*x(3))))...
```

```
+(((x(7))*(0.4-(((0.4-1)/(193-190))*193)...
+((0.4-1)/(193-190))*(174.9333+23.3750*x(2)+3.6250*x(3)-19.0000*x(2)*x(3)))...
+(x(8))*((0-(((0-0.4)/(195-193))*195))...
+((0-0.4)/(195-193)*(174.9333+23.3750*x(2)+3.6250*x(3)-19.0000*x(2)*x(3)))))))...
 *(((x(9))*((0.5-((0.5/(187-185))*187))...
+(0.5/(187-185))*(154.8571+8.5000*x(1)+30.6250*x(2)+...
7.8750*x(3)-12.8571*x(1)^2+11.2500*x(1)*x(2)))...
+(x(10))*((0.8-(((0.8-0.5)/(188-187))*188))...
+((0.8-0.5)/(188-187))*(154.8571+8.5000*x(1)+30.6250*x(2)...
+7.8750*x(3)-12.8571*x(1)^2+11.2500*x(1)*x(2)))...
+(x(11))*((1-(((1-0.8)/(190-188))*190))...
+((1-0.8)/(190-188))*(154.8571+8.5000*x(1)+30.6250*x(2)...
+7.8750*x(3)-12.8571*x(1)^2+11.2500*x(1)*x(2))))...
+((x(12))*((0.4-(((0.4-1)/(193-190))*193))+...
((0.4-1)/(193-190))*(154.8571+8.5000*x(1)+30.6250*x(2)+...
7.8750*x(3)-12.8571*x(1)^2+11.2500*x(1)*x(2)))...
+(x(13))*((0-(((0-0.4)/(195-193))*195))+...
((0-0.4)/(195-193)*(154.8571+8.5000*x(1)+30.6250*x(2)...
+7.8750*x(3)-12.8571*x(1)^2+11.2500*x(1)*x(2))))))...
 *(((x(14))*((0.5-(((0.5/(175-170)))*175))+...
(0.5/(175-170))*(140.2333+ 5.3437*x(1)+18.2500*x(2)+19.5938*x(3)))...
+(x(15))*((0.8-(((0.8-0.5)/(180-175))*180))+...
((0.8-0.5)/(180-175))*(140.2333+ 5.3437*x(1)+18.2500*x(2)+19.5938*x(3)))...
+(x(16))*((1-(((1-0.8)/(185-180))*185))+...
((1-0.8)/(185-180))*(140.2333+ 5.3437*x(1)+18.2500*x(2)+19.5938*x(3))))...
+(((x(17))*((0.4-(((0.4-1)/(190-185))*190))+...
((0.4-1)/(190-185))*(140.2333+ 5.3437*x(1)+18.2500*x(2)+19.5938*x(3)))...
+(x(18))*((0-(((0-0.4)/(195-190)))*195)...
+((0-0.4)/(195-190)*(140.2333+ 5.3437*x(1)+18.2500*x(2)+19.5938*x(3)))))))^(1/3);

%x0 = [0.0920 1.0000 0.8170 1 1 1];
x0 = [-1 -1 -1 1 1 1 1 1 1 1 1 1 1 1 1 1 1];
%x0 = [0 0 0 0 0 0];
lb = [-1;-1;-1;-1;-1;-1;-1;-1;-1;-1;-1;-1;-1;-1;-1;-1;-1];
ub = [1;1;1;1;1;1;1;1;1;1;1;1;1;1;1;1;1];

nlcon = @(x)[(((x(4))*((0.5-((0.5/(187-185))*187))...
+(0.5/(187-185))*(174.9333+23.3750*x(2)+3.6250*x(3)-19.0000*x(2)*x(3)))...
+(x(5))*((0.8-(((0.8-0.5)/(188-187))*188))...
+((0.8-0.5)/(188-187))*(174.9333+23.3750*x(2)+3.6250*x(3)-19.0000*x(2)*x(3)))...
+(x(6))*((1-(((1-0.8)/(190-188))*190))+((1-0.8)/(190-188))*...
(174.9333+23.3750*x(2)+3.6250*x(3)-19.0000*x(2)*x(3))))...
+((x(7))*(0.4-(((0.4-1)/(193-190))*193)+((0.4-1)/(193-190)))...
*(174.9333+23.3750*x(2)+3.6250*x(3)-19.0000*x(2)*x(3)))...
+(x(8))*((0-(((0-0.4)/(195-193))*195))+((0-0.4)/(195-193)*...
(174.9333+23.3750*x(2)+3.6250*x(3)-19.0000*x(2)*x(3))))))...

(((x(9))*((0.5-((0.5/(187-185))*187))+(0.5/(187-185))*...
(154.8571+8.5000*x(1)+30.6250*x(2)+7.8750*x(3)-12.8571*x(1)^2+11.2500*x(1)*x(2)))...
+(x(10))*((0.8-(((0.8-0.5)/(188-187))*188))+((0.8-0.5)/(188-187))*...
(154.8571+8.5000*x(1)+30.6250*x(2)+7.8750*x(3)-12.8571*x(1)^2+11.2500*x(1)*x(2)))...
+(x(11))*((1-(((1-0.8)/(190-188))*190))+((1-0.8)/(190-188))*...
(154.8571+8.5000*x(1)+30.6250*x(2)+7.8750*x(3)-12.8571*x(1)^2+11.2500*x(1)*x(2))))...
+(((x(12))*((0.4-(((0.4-1)/(193-190))*193))+((0.4-1)/(193-190))*...
(154.8571+8.5000*x(1)+30.6250*x(2)+7.8750*x(3)-12.8571*x(1)^2+11.2500*x(1)*x(2)))...
+(x(13))*((0-(((0-0.4)/(195-193))*195))+((0-0.4)/(195-193)*...
(154.8571+8.5000*x(1)+30.6250*x(2)+7.8750*x(3)-12.8571*x(1)^2+11.2500*x(1)*x(2)))))))...

 (((x(14))*((0.5-(((0.5/(175-170)))*175))+(0.5/(175-170))*...
(140.2333+ 5.3437*x(1)+18.2500*x(2)+19.5938*x(3)))...
+(x(15))*((0.8-(((0.8-0.5)/(180-175))*180))+((0.8-0.5)/(180-175))*...
(140.2333+ 5.3437*x(1)+18.2500*x(2)+19.5938*x(3)))...
+(x(16))*((1-(((1-0.8)/(185-180))*185))+((1-0.8)/(185-180))*...
(140.2333+ 5.3437*x(1)+18.2500*x(2)+19.5938*x(3))))...
+((x(17))*((0.4-(((0.4-1)/(190-185))*190))+((0.4-1)/(190-185))*...
(140.2333+ 5.3437*x(1)+18.2500*x(2)+19.5938*x(3)))...
```

```
+(x(18))*((0-(((0-0.4)/(195-190)))*195)+((0-0.4)/(195-190)*...
(140.2333+ 5.3437*x(1)+18.2500*x(2)+19.5938*x(3))))))

x(4)+x(5)+x(6)+x(7)+x(8)
x(9)+x(10)+x(11)+x(12)+x(13)
x(14)+x(15)+x(16)+x(17)+x(18)];

cl=[0 0 0 0 0 0 0 0 0];
cu=[1 1 1 1 1 1 1 1 1];

xtype='CCCBBBBBBBBBBBBBB';
opts=optiset('solver','nomad','display','iter')
Opt=opti('fun',fun,'bounds',lb,ub,'nl',nlcon,cl,cu,'xtype',xtype,'options',opts)
[x,fval,exitflag,info] = solve(Opt,x0)
```

Journal of Mathematical Sciences and Modelling, 6(3) (2023) 105-119
Research Article

Journal of Mathematical Sciences and Modelling

Journal Homepage: www.dergipark.gov.tr/jmsm
ISSN 2636-8692
DOI: http://dx.doi.org/10.33187/jmsm.1126660

Implementation of the Hybrid ADI-FDTD Scheme to Maxwell Equation for Mathematical Modeling of Breast Tumor

Ümmü Şahin Şener

Department of Mathematics, Faculty of Science and Arts, Kırklareli University, Kırklareli, Türkiye

Article Info

Keywords: *ADI-FDTD, Breast tumor, FDTD, Mathematical modeling, Maxwell equations, Scattered field*
2010 AMS: *35L05, 35-04*
Received: *6 June 2022*
Accepted: *9 June 2023*
Available online: *31 July 2023*

Abstract

Breast cancer is the most common cancer in women, and non-destructive detection of the tumor is vital. The interaction of electromagnetic waves with breast tissue and the behavior of waves after interaction are used to model tumor detection mathematically. The behavior of electromagnetic waves in a medium is described using Maxwell's equations. Electromagnetic waves propagate according to the electrical properties of a medium. Since the electrical properties of tumor tissue are different from those of normal breast tissue, it is assumed that the tumor is a lossy dielectric sphere, and the breast is a lossy dielectric medium. Under this assumption, Maxwell's equations are used to calculate the scattered field from the tumor. The field scattered by the tumor is different from other tissues because their dielectric properties are different. The location and size of the tumor can be determined by utilizing the difference in scattering from the tissues. While the scattering field from the tumor in spherical geometric form is analytically calculated, it is not analytically possible to calculate the scattering field from the tumor in different geometric shapes. In addition to non-destructive detection of the tumor, an efficient numerical method, the finite difference time domain method (FDTD), is used to simulate the field distribution. After the location of the tumor is determined, the Alternating Direction Implicit (ADI) FDTD method, which gives simulation results by dividing the computation domain into smaller sub-intervals, can be used. Scattered fields are calculated analytically in the geometry where the tumor is in the form of a smooth sphere, and in more complex geometry, the field distributions are successfully obtained with the help of MATLAB using FDTD and ADI-FDTD algorithms.

1. Introduction

According to 2019 World Health Organization (WHO) estimates, cancer is the first or second leading cause of death before age 70 in 112 of 183 countries and is the most important factor negatively affecting longevity and healthy living [1–3]. Among the cancer cases detected, breast cancer is the most common cancer. In 2020, 2.3 million new cases of breast cancer will be detected. This number represents 11.7% of all cancer cases [4], and it is estimated that the risk of cancer will increase in the coming years. As with many other types of cancer, breast cancer does not show symptoms in its early stages, but early diagnosis and treatment prolongs the survival of patients, reduces recurrences, and increases the patient's life expectancy [5–7]. Therefore, detection of breast cancer at the initial stage is important for the success of the treatment. X-ray mammography, ultrasound scanning, and magnetic resonance imaging (MRI) are clinical imaging modalities commonly used in breast cancer detection [8–10].

X-ray mammography has some limitations, especially in young women with particularly dense breast tissue who have never had breast cancer. Other disadvantages of X-ray mammography can be listed as increasing the possibility of getting cancer due to the use of ionizing radiation, discomfort, and pain due to the presence of breast compression and causing concern in patients due to false negative and false positive results [11–13]. The ultrasound method uses sound waves that are converted into pulses by means of a transducer. In cases where a certain feature of the tissue is different in the waves sent to the breast tissue, reflections called echoes occur between tissues with different

Email address and ORCID number: **ummusahin@klu.edu.tr, 0000-0001-9055-8734**
Cite as "Ü. Şahin Şener, *Implementation of the hybrid ADI-FDTD scheme to Maxwell equation for mathematical modeling of breast tumor*, J. Math. Sci. Model., 6(3) (2023), 105-119"

characteristics and form ultrasound images. This method is more costly than X-ray mammography, and the images obtained are also low resolution. Although the MRI technique is more expensive than the ultrasound method and X-ray mammography and cannot determine the exact location of the tumors, it can be used in patients with dense breast tissue and can detect even small tumors [14].
In order to overcome the limitations and disadvantages of MRI imaging, ultrasound method and X-ray method, microwave imaging technique, which uses data obtained from the interaction of electromagnetic waves and tissues, is used. The microwave imaging method has advantages such as using non-ionized waves, not damaging the tissues, inexpensive, and comfortable of use [15]. Normal breast tissue and malignant tissues have different dielectric properties, and this method takes advantage of the dielectric contrast between these tissues. When breast tissue interacts with microwaves, weaker responses from benign lesions are expected, while stronger responses from malignancies are expected during imaging [16–21].
Assuming that the tumor in the breast tissue is spherical, our problem turns into the problem of scattering of electromagnetic waves by a dielectric sphere. The scattering and propagation of the electromagnetic wave from the dielectric sphere can be solved analytically [22, 23]. However, since the tumor is not always be in the shape of a regular sphere, it is not possible to solve the electromagnetic field distribution analytically in a complex geometry. In this case, it is necessary to solve the problem numerically. The modeling of the interaction between electromagnetic waves at microwave frequencies and breast tissue can be done by the numerical solution of Maxwell's equations [24, 25]. Since the FDTD method is one of the most commonly used methods in algorithms for simulating breast imaging at microwave frequencies, the time-dependent Maxwell equations are solved using this method [26].
Although the FDTD method is a commonly used method for solving electromagnetic simulation problems, the maximum time step size should not exceed the minimum cell size in the computational domain (Courant-Friedrich-Levy (CFL) condition), since the traditional FDTD method is an open finite difference algorithm. The maximum size of the time step should be limited by the maximum propagation velocity and the minimum cell size in the computation domain [27]. When the computational domain is transformed into a fine geometry, i.e., when the cell size becomes smaller, it becomes difficult to satisfy the stability condition in the traditional FDTD method. Therefore, a solution can be found using the alternative directionally implicit finite difference time domain method (ADI-FDTD), which is one of the unconditionally stable FDTD methods [28–32].
Since electromagnetic wave propagation and scattering problems are open problems and the FDTD algorithm must be terminated after a certain step, the computation domain is truncated after sufficient interaction with the breast tissue is achieved. Boundary conditions are used where the computation domain is truncated [33, 34]. Boundary conditions should be determined established to prevent waves from returning to the computation domain when they reach the boundary by propagating in the breast tissue. Since the equivalent for open problems in numerical computations is an infinite computation domain, the real infinity of space can be modeled by truncating the computation domain somewhere and applying Absorbing Boundary Conditions (ABC). ABCs are obtained by using absorber lossy media. The use of absorber materials as absorber boundary conditions started with the use of classical lossy and nondispersive materials. The perfectly matched layer developed by Berenger is the strongest ABC compared to other methods. The perfectly matched layer (PML) is a lossy material boundary layer with a thickness of a few cells that surrounds the computational domain from the truncated region. The PML boundary layer matches up with perfectly to the computational domain [35]. PML uses artificial structural parameters to establish the wave impedance matching condition, regardless of the frequency and angle of the incident wave. In our study, it is assumed that the computation domain is surrounded by the PML [36].
In this study, first of all, since the tumor in the breast tissue is considered to be spherical and the spherical structure is a regular geometric shape, an analytical examination of the interaction of electromagnetic wave and a lossy dielectric sphere will be given. Secondly, two different breast simulation geometries will be created, and numerical solution will be made in the geometry where it is not possible to analyze the electromagnetic wave-tissue interaction analytically using the traditional FDTD method. The last but not least it is planned to obtain a better simulation result by simulating with the traditional FDTD method and dividing the part determined to be a tumor into smaller cells and applying the ADI-FDTD algorithm to the area where the smaller cells are located.

2. Material and Methods

2.1. Analytical study

Suppose that the electric field of a uniform plane wave propagating along the z-axis and polarized in the x-direction, as shown in Figure 2.1a and Figure 2.1b, the electric field and magnetic field of the incident wave on a sphere can be expressed as follows:

$$\mathbf{E}^i = \hat{\mathbf{a}}xEx^i = \hat{\mathbf{a}}xE0e^{-j\beta z} = \hat{\mathbf{a}}xE0e^{-j\beta r\cos\theta} \tag{2.1}$$

$$\mathbf{H}^i = \hat{\mathbf{a}}_y H_y^i = \hat{\mathbf{a}}_y H_0 e^{-j\beta z} = \hat{\mathbf{a}}_y H_0 e^{-j\beta r\cos\theta}$$

By transforming from rectangular coordinate components to spherical coordinate components using the equality as follows: By transforming from rectangular coordinate components to spherical coordinate components using the equality as follows:

$$x = r\sin\theta\cos\phi,\ y = r\sin\theta\sin\phi,\ z = r\cos\theta \tag{2.2}$$

Using Eq. (2.2), the relationship between rectangular and spherical components can be written as:

$$\begin{aligned} A_r &= A_x\sin\theta\cos\phi + A_y\sin\theta\sin\phi + A_z\cos\theta \\ A_\theta &= A_x\cos\theta\cos\phi + A_y\cos\theta\sin\phi - A_z\sin\theta \\ A_\phi &= -A_x\sin\phi + A_y\cos\phi \end{aligned} \tag{2.3}$$

Using the system (2.3) the x-component of the Eq. (2.1) can be express in spherical components to

$$\mathbf{E}^i = \hat{\mathbf{a}}_r E_r^i + \hat{\mathbf{a}}_\theta E_\theta^i + \hat{\mathbf{a}}_\phi E_\phi^i$$

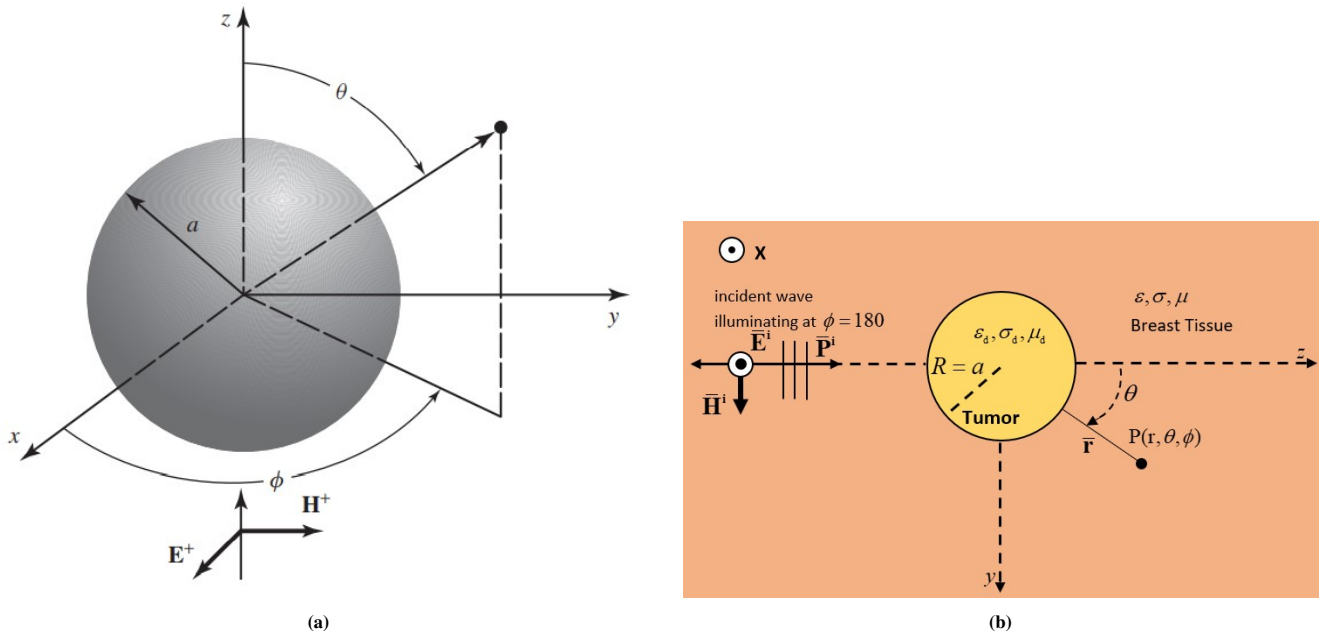

Figure 2.1: (a) Uniform plane wave incident on a sphere [22] **(b)** The state of the electromagnetic wave that incident on a lossy and dispersive dielectric tumor in a lossy and dispersed breast tissue [23]

$$\begin{aligned} E_r^i &= E_x^i \sin\theta\cos\phi = E_0 \sin\theta\cos\phi e^{-j\beta r\cos\theta} = E_0 \frac{\cos\phi}{j\beta r}\frac{\partial}{\partial\theta}\left(e^{-j\beta r\cos\theta}\right) \\ E_\theta^i &= E_x^i \cos\theta\cos\phi = E_0 \cos\theta\cos\phi e^{-j\beta r\cos\theta} \\ E_\phi^i &= -E_x^i \sin\phi = -E_0 \sin\phi e^{-j\beta r\cos\theta} \end{aligned}$$

All of the spherical components of the incident electric field can be expressed using the $E_x^+ = e^{-j\beta z} = e^{-j\beta r\cos\theta} = \sum_{n=0}^{\infty} a_n j_n(\beta r) P_n(\cos\theta)$ equality. In this equality $a_n = j^{-n}(2n+1)$.

$$\begin{aligned} E_r^i &= E_0 \frac{\cos\phi}{j\beta r}\sum_{n=0}^{\infty} j^{-n}(2n+1)\, j_n(\beta r)\frac{\partial}{\partial\theta}\left(P_n(\cos\theta)\right) \\ E_\theta^i &= E_0 \cos\theta\cos\phi \sum_{n=0}^{\infty} j^{-n}(2n+1)\, j_n(\beta r) P_n(\cos\theta) \\ E_\phi^i &= -E_0 \sin\phi \sum_{n=0}^{\infty} j^{-n}(2n+1)\, j_n(\beta r) P_n(\cos\theta) \end{aligned} \tag{2.4}$$

The following Eq. (2.5) can be written between the Bessel and Legendre functions.

$$\begin{aligned} j_n(\beta r) &= \frac{1}{\beta r}\hat{J}_n(\beta r) \\ \frac{\partial P_n}{\partial\theta} &= P_n^1(\cos\theta) \\ P_0^1 &= 0 \end{aligned} \tag{2.5}$$

The Eq. (2.4) can be written as in Eq. (2.6) using the Eq. (2.5)

$$\begin{aligned} E_r^i &= -jE_0 \frac{\cos\phi}{(\beta r)^2}\sum_{n=1}^{\infty} j^{-n}(2n+1)\hat{J}_n(\beta r) P_n^1(\cos\theta) \\ E_\theta^i &= E_0 \frac{\cos\theta\cos\phi}{\beta r}\sum_{n=0}^{\infty} j^{-n}(2n+1)\hat{J}_n(\beta r) P_n^0(\cos\theta) \\ E_r^i &= -E_0 \frac{\sin\phi}{\beta r}\sum_{n=0}^{\infty} j^{-n}(2n+1)\hat{J}_n(\beta r) P_n^0(\cos\theta) \end{aligned} \tag{2.6}$$

Using the vector potential A_i^r the incident electric field can be written as in the Eq. (2.7).

$$E_r^i = \frac{1}{j\omega\mu\varepsilon}\left(\frac{\partial^2}{\partial r^2} + \beta^2\right) A_r^i \tag{2.7}$$

By equating Eq. (2.7) with Eq. (2.6), the following equation can be written for A_r^i.

$$E_r^i = \frac{1}{j\omega\mu\varepsilon}\left(\frac{\partial^2}{\partial r^2}+\beta^2\right)A_r^i$$

TE and TM (with respect to r) fields are formed by vector potentials $\mathbf{A}$ and $\mathbf{F}$. TE mode fields are produced by taking $\mathbf{A}=0$, $\mathbf{F}=\hat{\mathbf{a}}_r F_r(r,\theta,\phi)$, and TM mode fields are produced by writing $\mathbf{A}=\hat{\mathbf{a}}_r A_r(r,\theta,\phi)$, $\mathbf{F}=0$. In addition, the incident and scattered fields by the sphere can be expressed as a superposition of TE and TM [22]. Studies on the scattering and propagation of fields by a lossy dielectric sphere have emerged from the investigation of the interaction of the perfect electric conductor (PEC) sphere and waves. In the lossy dielectric sphere, unlike the PEC sphere, waves penetrate the sphere. Boundary conditions are used to establish a relationship between the fields outside and inside the sphere. Tangential electric and magnetic fields are continuous in a lossy dielectric sphere. To develop the governing equations for the lossy dielectric sphere the geometry is used given in Figure 2.1b. It is accepted that the medium outside the sphere is free space and wave number is β_0, the inside of the sphere is lossy dielectric medium and wave number is $\dot{\beta}_0$. The relative complex permittivity of the dielectric medium $\dot{\varepsilon}_r\,(\dot{\varepsilon}_r=\varepsilon_r{}'-j\varepsilon_r{}'')$ and complex permeability $\dot{\mu}_r\,(\dot{\mu}_r=\mu_r{}'-j\mu_r{}'')$.
The total, incident and scattered fields outside the sphere can be represented by the vector potentials in terms of series expansion given by the follows:

$$\begin{aligned}
A_r^{t+} &= A_r^i + A_r^s = E_0\frac{\cos\phi}{\omega}\sum_{n=1}^{\infty}\left[a_n\hat{J}_n(\beta r)+b_n\hat{H}_n^{(2)}(\beta r)\right]P_n^1(\cos\theta)\\
F_r^{t+} &= F_r^i + F_r^s = E_0\frac{\sin\phi}{\omega\eta}\sum_{n=1}^{\infty}\left[a_n\hat{J}_n(\beta r)+c_n\hat{H}_n^{(2)}(\beta r)\right]P_n^1(\cos\theta)\\
a_n &= j^{-n}\frac{(2n+1)}{n(n+1)}
\end{aligned}$$

The corresponding electric field and magnetic fields to these potentials are given below.

$$\begin{aligned}
E_r^t &= \frac{1}{j\omega\mu\varepsilon}\left(\frac{\partial^2}{\partial r^2}+\beta^2\right)A_r^t\\
E_\theta^t &= \frac{1}{j\omega\mu\varepsilon}\frac{1}{r}\frac{\partial^2 A_r^t}{\partial r\partial\theta}-\frac{1}{\varepsilon}\frac{1}{r\sin\theta}\frac{\partial F_r^t}{\partial\phi}\\
E_\phi^t &= \frac{1}{j\omega\mu\varepsilon}\frac{1}{r\sin\theta}\frac{\partial^2 A_r^t}{\partial r\partial\phi}+\frac{1}{\varepsilon}\frac{1}{r}\frac{\partial F_r^t}{\partial\theta}
\end{aligned}$$

$$\begin{aligned}
H_r^t &= \frac{1}{j\omega\mu\varepsilon}\left(\frac{\partial^2}{\partial r^2}+\beta^2\right)F_r^t\\
H_\theta^t &= \frac{1}{\mu}\frac{1}{r\sin\theta}\frac{\partial A_r^t}{\partial\phi}+\frac{1}{j\omega\mu\varepsilon}\frac{1}{r}\frac{\partial^2 F_r^t}{\partial r\partial\theta}\\
H_\phi^t &= -\frac{1}{\mu}\frac{1}{r}\frac{\partial A_r^t}{\partial\theta}+\frac{1}{j\omega\mu\varepsilon}\frac{1}{r\sin\theta}\frac{\partial^2 F_r^t}{\partial r\partial\phi}
\end{aligned}$$

Although the vector potentials inside and outside the sphere are similar, waves propagating outside the sphere are used, while standing waves in the radial direction are used inside the sphere. Consequently, the vector potentials for the total fields inside the sphere can be written as:

$$\begin{aligned}
A_r^{t-} &= E_0\frac{\cos\phi}{\omega}\sum_{n=1}^{\infty}d_n\hat{J}_n\left(\dot{\beta}_d r\right)P_n^{(1)}(\cos\theta)\\
F_r^{t-} &= E_0\frac{\sin\phi}{\omega\dot{\eta}}\sum_{n=1}^{\infty}e_n\hat{J}_n\left(\dot{\beta}_d r\right)P_n^{(1)}(\cos\theta)
\end{aligned}$$

b_n, c_n coefficients for the fields outside the sphere and d_n, e_n for the fields inside the sphere can be obtained by applying the boundary conditions. In the case of $(r\le a)$, the vector potentials on and inside the sphere are considered, and (-) superscript is used, while $(r\ge a)$ the (+) symbol is used on the potentials, taking into account the vector potentials on and outside the sphere and the fields associated with these potentials [22]. By using boundary conditions given the equations below, the coefficients b_n, c_n, d_n and e_n depending on a_n can be obtained as follows:

$$\begin{aligned}
E_\theta^{t-}(r=a,0\le\theta\le\pi,0\le\phi\le2\pi) &= E_\theta^{t+}(r=a,0\le\theta\le\pi,0\le\phi\le2\pi)\\
E_\phi^{t-}(r=a,0\le\theta\le\pi,0\le\phi\le2\pi) &= E_\phi^{t+}(r=a,0\le\theta\le\pi,0\le\phi\le2\pi)\\
H_\theta^{t-}(r=a,0\le\theta\le\pi,0\le\phi\le2\pi) &= H_\theta^{t+}(r=a,0\le\theta\le\pi,0\le\phi\le2\pi)\\
H_\phi^{t-}(r=a,0\le\theta\le\pi,0\le\phi\le2\pi) &= H_\phi^{t+}(r=a,0\le\theta\le\pi,0\le\phi\le2\pi)
\end{aligned}$$

$$
\begin{aligned}
b_n &= \frac{-\sqrt{\dot{\varepsilon}_r}\hat{J}_n'(\beta_0 a)\hat{J}_n\left(\dot{\beta}_d a\right)+\sqrt{\dot{\mu}_r}\hat{J}_n(\beta_0 a)\hat{J}_n'\left(\dot{\beta}_d a\right)}{\sqrt{\dot{\varepsilon}_r}H_n^{(2)'}(\beta_0 a)\hat{J}_n\left(\dot{\beta}_d a\right)+\sqrt{\dot{\mu}_r}H_n^{(2)}(\beta_0 a)\hat{J}_n'\left(\dot{\beta}_d a\right)}a_n \\
c_n &= \frac{-\sqrt{\dot{\varepsilon}_r}\hat{J}_n(\beta_0 a)\hat{J}_n'\left(\dot{\beta}_d a\right)+\sqrt{\dot{\mu}_r}\hat{J}_n'(\beta_0 a)\hat{J}_n\left(\dot{\beta}_d a\right)}{\sqrt{\dot{\varepsilon}_r}H_n^{(2)}(\beta_0 a)\hat{J}_n'\left(\dot{\beta}_d a\right)-\sqrt{\dot{\mu}_r}H_n^{(2)'}(\beta_0 a)\hat{J}_n\left(\dot{\beta}_d a\right)}a_n \\
d_n &= -j\frac{\dot{\mu}_r\sqrt{\dot{\varepsilon}_r}}{\sqrt{\dot{\varepsilon}_r}H_n^{(2)'}(\beta_0 a)\hat{J}_n\left(\dot{\beta}_d a\right)-\sqrt{\dot{\mu}_r}H_n^{(2)}(\beta_0 a)\hat{J}_n'\left(\dot{\beta}_d a\right)}a_n \\
e_n &= j\frac{\dot{\mu}_r\sqrt{\dot{\varepsilon}_r}}{\sqrt{\dot{\varepsilon}_r}H_n^{(2)}(\beta_0 a)\hat{J}_n'\left(\dot{\beta}_d a\right)-\sqrt{\dot{\mu}_r}H_n^{(2)'}(\beta_0 a)\hat{J}_n'\left(\dot{\beta}_d a\right)}a_n
\end{aligned}
$$

2.2. Maxwell's curl equations

Microwaves or radar signals can be expressed by Maxwell's equations, which relate the electric and magnetic field values at a certain point in space and at a certain time. The differential Maxwell equations for the time-domain, which are necessary to determine the behaviour in the time-domain can be written as follows:

$$
\begin{aligned}
\nabla\times\mathbf{H} &= \frac{\partial\mathbf{D}}{\partial t}+\mathbf{J} \\
\nabla\times\mathbf{E} &= -\frac{\partial\mathbf{B}}{\partial t}-\mathbf{M} \\
\nabla.\mathbf{D} &= \rho_e \\
\nabla.\mathbf{B} &= \rho_m
\end{aligned}
\tag{2.8}
$$

where **H** is the magnetic field strength (Amperes/m or A/m), **D** is the electric displacement (Coulombs/m2 or C/m2), **E** is the electric field strength (Volts/m or V/m), **B** is the magnetic flux density (webers/ m2), **J** is the electric current density (Amperes/ m2), **M** is the magnetic current density (V/ m2), ρ_e is the electric charge density (C/m3), ρ_m is the magnetic charge density (webers/m3). The quantities given here are real functions of positions and time. In order to characterize the medium in which the electromagnetic wave interacts and to supplement Maxwell's equations, it is necessary to define the constitutive relations. The constitutive relations for isotropic, non-dispersive, and linear media can be defined as follows:

$$
\begin{aligned}
\mathbf{D} &= \varepsilon\mathbf{E}=\varepsilon_0\varepsilon_r\mathbf{E} \\
\mathbf{B} &= \mu\mathbf{H}=\mu_0\mu_r\mathbf{H}
\end{aligned}
\tag{2.9}
$$

where ε is the electric permittivity of the medium (farads/m or F/m), $\varepsilon_0 = 8.8542\times10^{-12}$(F/m) is the permittivity of free space and ε_r is the relative permittivity of the medium, μ is the magnetic permeability of the medium (henrys/m or H/m), $\mu_0 = 4\pi\times10^{-7}$(H/m) is the permeability of free space and μ_r is the relative permeability of the medium. **J** electric current density is the sum of the $\mathbf{J}_c=\sigma\mathbf{E}$ conduction current density and $\mathbf{J}_{source}$ source current density ($\mathbf{J}=\mathbf{J}_{source}+\mathbf{J}_c$). Similarly, $\mathbf{M}=\mathbf{M}_c+\mathbf{M}_{source}$ magnetic current density is the sum of $\mathbf{M}_c=\sigma^*\mathbf{H}$ and $\mathbf{M}_{source}$. σ is electric conductivity (siemens/meter), σ^* is equivalent magnetic loss (ohms/meter). Finally, by substituting the Eq. (2.9) in the Eq. (2.8) respectively and rearranging the equations, Maxwell's curl equations for lossy, linear, nondispersive, and isotropic materials can be obtained as follows:

$$
\begin{aligned}
\frac{\partial\mathbf{H}}{\partial t} &= -\frac{1}{\mu}\nabla\times\mathbf{E}-\frac{1}{\mu}\left(\mathbf{M}_{source}+\sigma^*\mathbf{H}\right) \\
\frac{\partial\mathbf{E}}{\partial t} &= \frac{1}{\varepsilon}\nabla\times\mathbf{H}-\frac{1}{\varepsilon}\left(\mathbf{J}_{source}+\sigma\mathbf{E}\right)
\end{aligned}
\tag{2.10}
$$

Six scalar equations can be obtained by writing out the vector components of Eq. (2.10) for E_x, E_y, E_z, H_x, H_y and H_z in the Cartesian coordinate system. Since Eq. (2.9) equations showing electric and magnetic charges are a direct result of curl equations, they do not need to be used in the FDTD algorithm. In other words, since both divergence equations can be obtained from curl equations and initial boundary conditions, the starting point of the FDTD algorithm is Maxwell's curl equations [24].

$$
\begin{aligned}
\frac{\partial H_x}{\partial t} &= \frac{1}{\mu}\left[\frac{\partial E_y}{\partial z}-\frac{\partial E_z}{\partial y}-\left(M_{source_x}+\sigma^*H_x\right)\right] \\
\frac{\partial H_y}{\partial t} &= \frac{1}{\mu}\left[\frac{\partial E_z}{\partial x}-\frac{\partial E_x}{\partial z}-\left(M_{source_y}+\sigma^*H_y\right)\right] \\
\frac{\partial H_z}{\partial t} &= \frac{1}{\mu}\left[\frac{\partial E_x}{\partial y}-\frac{\partial E_y}{\partial x}-\left(M_{source_z}+\sigma^*H_z\right)\right]
\end{aligned}
\tag{2.11}
$$

$$\begin{aligned}\frac{\partial E_x}{\partial t} &= \frac{1}{\varepsilon}\left[\frac{\partial H_z}{\partial y}-\frac{\partial H_y}{\partial z}-\left(J_{source_x}+\sigma E_x\right)\right]\\ \frac{\partial E_y}{\partial t} &= \frac{1}{\varepsilon}\left[\frac{\partial H_x}{\partial z}-\frac{\partial H_z}{\partial x}-\left(J_{source_y}+\sigma E_y\right)\right]\\ \frac{\partial E_z}{\partial t} &= \frac{1}{\varepsilon}\left[\frac{\partial H_y}{\partial x}-\frac{\partial H_x}{\partial y}-\left(J_{source_z}+\sigma^* E_z\right)\right]\end{aligned} \tag{2.12}$$

From the six equations, which are the scalar components of these rotational equations, two main groups of equations that can be evaluated independently of each other are obtained. The group containing E_x, E_y and H_z components is called the transverse electric (TE) mode, and the group containing H_x, H_y and E_z is called the transverse magnetic (TM) mode. EM waves operating in TE mode are called TE waves and EM waves operating in TM mode are called TM waves [25].

2.3. Finite difference time domain method (FDTD)

Analytical methods may not be sufficient to investigate the interaction of electromagnetic wave with an object. As stated in Analytical Study Section, it is analytically possible to examine the scattering or propagation of electromagnetic waves from a smooth surface structure such as a sphere but using numerical methods in cases where the geometry is not smooth allows us to make inferences about the wave-structure interaction. Simulating the interaction of EM waves with a structure whose material properties and geometric shapes are known is a forward problem and this forward problem can be solved using the FDTD technique. The FDTD technique can be used to obtain numerical solutions of Maxwell's equations, which can be written in differential form. In the first step, the FDTD algorithm decomposes the problem geometry into a spatial grid in which the electric and magnetic field components are placed at certain separate locations in space. In the second step, Maxwell's equations are solved in discrete time steps over time. A rectangular grid is used for the discretization because it offers advantages such as ease of use and simplicity. To satisfy Maxwell's divergence equations, the fields are first assumed to be zero throughout the computation domain. As in analytical solutions, boundary conditions apply to the outer boundary of the computational field on all dielectric and conductive surfaces. Electric and magnetic fields are continuous at the interfaces between dielectric materials. Electric and magnetic fields are calculated as a function of time in a leap-frog manner at each gridded point of the computation domain. First the electric field and then the magnetic field are calculated sequentially, and this calculation is repeated at each time step [25,26].
Somewhat surprisingly, since the transverse field representations are best understood in two dimensions [27], Maxwell's equations will be studied by transforming them into two sets of two-dimensional scalar equations. Assuming that the two-dimensional medium is the xy-plane, the problem is independent of the z-dimension, so the derivative terms for the z-dimension are vanished. By using the field distributions and the problem geometry invariance in one of the dimensions in Eq. (2.11) and Eq. (2.12), the following equations for TEz mode (given in Eq. (2.13) and TMz mode (given in Eq. (2.14)) can be obtained respectively:

$$\begin{aligned}\frac{\partial E_x}{\partial t} &= \frac{1}{\varepsilon}\left[\frac{\partial H_z}{\partial y}-\left(J_{source_x}+\sigma E_x\right)\right]\\ \frac{\partial E_y}{\partial t} &= \frac{1}{\varepsilon}\left[-\frac{\partial H_z}{\partial x}-\left(J_{source_y}+\sigma E_y\right)\right]\\ \frac{\partial H_z}{\partial t} &= \frac{1}{\mu}\left[\frac{\partial E_x}{\partial y}-\frac{\partial E_y}{\partial x}\left(M_{source_z}+\sigma^* H_z\right)\right]\end{aligned} \tag{2.13}$$

$$\begin{aligned}\frac{\partial H_x}{\partial t} &= \frac{1}{\mu}\left[-\frac{\partial E_z}{\partial y}-\left(M_{source_x}+\sigma^* H_x\right)\right]\\ \frac{\partial H_y}{\partial t} &= \frac{1}{\mu}\left[\frac{\partial E_z}{\partial x}-\left(M_{source_y}+\sigma^* H_y\right)\right]\\ \frac{\partial E_z}{\partial t} &= \frac{1}{\varepsilon}\left[\frac{\partial H_y}{\partial x}-\frac{\partial H_x}{\partial y}\left(J_{source_z}+\sigma E_z\right)\right]\end{aligned} \tag{2.14}$$

The two-dimensional, time-dependent Maxwell equations described above can be expressed discretely in space and time using the second-order exact central difference formula. The electric and magnetic field components are sampled in discrete position in space and time. In order to create a grid with the FDTD algorithm, the problem geometry is divided into cells called Yee cells. Electric field components are sampled at $0,\Delta t,2\Delta t,...,n\Delta t...$ time steps, with Δt being the time sampling period, while magnetic field components are sampled at $1/2\Delta t,(1+1/2\Delta t),...,(n+1/2\Delta t),...$ time steps. Derivatives in Eq. (2.13) can be approximated using the central difference formula, assuming the center point of the central difference formula in space, $E_x(i,j+1/2)$, and using the center point in the time instant $(n+1/2\Delta t)$.

$$\frac{E_x|_{i+1/2,j}^{n+1}-E_x|_{i+1/2,j}^{n}}{\Delta t}=\frac{1}{\varepsilon_{i+1/2,j}}\left(\frac{H_z|_{i+1/2,j+1/2}^{n+1/2}-H_z|_{i+1/2,j-1/2}^{n+1/2}}{\Delta y}-\left(J_{source_x}|_{i+1/2,j}^{n+1/2}-\sigma_{i+1/2,j}\;E_x|_{i+1/2,j+1/2}^{n+1/2}\right)\right)$$

The $E_x|_{i+1/2,j}^{n+1/2}$ term can be written as the average of the electric fields at the $(n+1)\Delta t$ and $n\Delta t$ time steps as follows:

$$E_x|_{i+1/2,j+1/2}^{n+1/2}=\frac{E_x|_{i+1/2,j+1/2}^{n+1}+E_x|_{i+1/2,j+1/2}^{n}}{2}$$

$$E_x|_{i+1/2\,,j}^{n+1} - E_x|_{i+1/2\,,j}^{n} = \frac{\Delta t}{\varepsilon_{i,j+1/2}}\left(\frac{H_z|_{i+1/2\,,j+1/2}^{n+1/2} - H_z|_{i+1/2\,,j-1/2}^{n+1/2}}{\Delta y} - \left(J_{source_x}|_{i+1/2\,,j}^{n+1/2} - \sigma_{i+1/2\,,j}\left(\frac{E_x|_{i+1/2\,,j+1/2}^{n+1} + E_x|_{i+1/2\,,j+1/2}^{n}}{2}\right)\right)\right) \quad (2.15)$$

When the terms with the same index are collected to the same side and the Eq. (2.15) can be written according to $E_x|_{i+1/2\,,j}^{n+1}$ as Eq. (2.16).

$$\left(1 + \frac{\sigma_{i+1/2\,,j}\Delta t}{2\varepsilon_{i+1/2\,,j}}\right) E_x|_{i+1/2\,,j}^{n+1} = \left(1 - \frac{\sigma_{i+1/2\,,j}\Delta t}{2\varepsilon_{i+1/2\,,j}}\right) E_x|_{i+1/2\,,j}^{n} + \frac{\Delta t}{\varepsilon_{i+1/2\,,j}}\left(\frac{H_z|_{i+1/2\,,j+1/2}^{n+1/2} - H_z|_{i+1/2\,,j-1/2}^{n+1/2}}{\Delta y} - J_{source_x}|_{i+1/2\,,j}^{n+1/2}\right) \quad (2.16)$$

Dividing both sides of the Eq. (2.16) by $\left(1 + \sigma_{i,j+1/2}\,\Delta t/2\varepsilon_{i,j+1/2}\right)$ explicit update equation for $E_x|_{i,j+1/2}^{n+1}$ can be obtained as Eq. (2.17):

$$\begin{aligned} E_x|_{i+1/2\,,j}^{n+1} &= \left(\frac{2\varepsilon_{i+1/2,j} - \sigma_{i+1/2\,,j}\Delta t}{2\varepsilon_{i+1/2\,,j} + \sigma_{i+1/2,j}\,\Delta t}\right) E_x|_{i+1/2\,,j}^{n} \\ &+ \left(\frac{2\Delta t}{\left(2\varepsilon_{i+1/2,j} + \sigma_{i+1/2\,,j}\Delta t\right)\Delta y}\right)\left(H_z|_{i+1/2\,,j+1/2}^{n+1/2} - H_z|_{i+1/2\,,j-1/2}^{n+1/2}\right) \\ &- \left(\frac{2\Delta t}{2\varepsilon_{i+1/2,j} + \sigma_{i+1/2\,,j}\Delta t}\right) J_{source_x}|_{i+1/2\,,j}^{n+1/2} \end{aligned} \quad (2.17)$$

Similarly, the explicit update equations for $E_y|_{i,j+1/2}^{n+1}$ and $H_z|_{i+1/2\,,j+1/2}^{n+1/2}$ can also be obtained as in Eq. (2.18) and Eq. (2.19), respectively.

$$\begin{aligned} E_y|_{i,j+1/2}^{n+1} &= \left(\frac{2\varepsilon_{i,j+1/2} - \sigma_{i,j+1/2}\,\Delta t}{2\varepsilon_{i,j+1/2} + \sigma_{i,j+1/2}\,\Delta t}\right) E_y|_{i,j+1/2}^{n} \\ &+ \left(\frac{2\Delta t}{\left(2\varepsilon_{i,j+1/2} + \sigma_{i,j+1/2}\,\Delta t\right)\Delta x}\right)\left(H_z|_{i-1/2\,j+1/2}^{n+1/2} - H_z|_{i+1/2\,,j+1/2}^{n+1/2}\right) \\ &- \left(\frac{2\Delta t}{2\varepsilon_{i,j+1/2} + \sigma_{i,j+1/2}\,\Delta t}\right) J_{source_y}|_{i,j+1/2}^{n+1/2} \end{aligned} \quad (2.18)$$

$$\begin{aligned} H_z|_{i+1/2\,,j+1/2}^{n+1/2} &= \left(\frac{2\mu_{i+1/2\,,j+1/2} - \sigma_{i+1/2\,,j+1/2}\,\Delta t}{2\mu_{i+1/2\,,j+1/2} + \sigma_{i+1/2\,,j+1/2}\,\Delta t}\right) H_z|_{i+1/2\,,j+1/2}^{n-1/2} \\ &+ \left(\frac{2\Delta t}{\left(2\mu_{i+1/2\,,j+1/2} + \sigma_{i+1/2\,,j+1/2}\,\Delta t\right)\Delta y}\right)\left(E_x|_{i+1/2\,,j+1}^{n} - E_x|_{i+1/2\,,j}^{n}\right) \\ &- \left(\frac{2\Delta t}{\left(2\mu_{i+1/2\,,j+1/2} + \sigma_{i+1/2\,,j+1/2}\,\Delta t\right)\Delta x}\right)\left(E_y|_{i+1,j+1/2}^{n} - E_y|_{i,j+1/2}^{n}\right) \\ &- \left(\frac{2\Delta t}{2\mu_{i+1/2\,,j+1/2} + \sigma_{i+1/2\,,j+1/2}\,\Delta t}\right) M_{source_z}|_{i+1/2\,,j+1/2}^{n} \end{aligned} \quad (2.19)$$

In here, the FDTD update equations of the field components of the TEz mode are obtained, and the update equations of the field components of the TMz mode can be calculated in a similar way.

2.4. Alternating direct implicit- FDTD (ADI-FDTD)

In this study, subgrids that use finer spatial resolution can be used in the numerical modeling of breast tissue and electromagnetic wave interaction, especially in parts with tumors. By using these subgrids, certain regions of the computational field with high dielectric constant can be modeled in detail and the propagation of short wavelength waves can be better represented. By combining the standard FDTD method with the unconditionally stable ADI-FDTD technique, a finer grid and thus more effective simulation results can be obtained in a certain region of the FDTD computation domain. ADI-FDTD is unconditionally stable so that by setting the time step to any value, FDTD can be used in parts with low dielectric value and ADI-FDTD in places with high dielectric value in the same computation region without using a time interpolation scheme. Since the standard FDTD method is an explicit finite difference algorithm, the Courant–Friedrich–Levy (CFL) stability condition must be satisfied. According to CFL condition, a small-time step size results in a significant increase in computation time when using a smaller cell size compared to the wavelength, since the size of the time step should not exceed the minimum cell size in the computation domain. The constraint of the CFL condition can be overcome with the ADI-FDTD algorithm applied to the Yee algorithm to solve Maxwell's equations. The numerical formulation of the ADI-FDTD method for a 2-D TE wave is presented in Eq. (2.20)-(2.22), and the electromagnetic field components are arranged on the cells as in the standard FDTD method. The reason why both standard FDTD and ADI-FDTD algorithms are used together is to obtain a better simulation result by using a finer grid to the computation domain corresponding to the tumor tissue whose location is determined by the FDTD method. The smaller cell is not used in the entire ADI-FDTD calculation

region. The standard FDTD algorithm and cell size are used in the healthy breast tissue portion of the computation domain. Electric fields at the main grid-local grid (the area with smaller cells) are calculated by interpolating the fields in the main grid, and the fields in the local grid are calculated with the ADI-FDTD algorithm. The ADI-FDTD update equations for a 2-D TE wave are arranged on cells as in the standard FDTD method and presented below:

$$\begin{aligned} E_x|_{i+1/2,j}^{n+1/2} &= \left(\frac{2\varepsilon_{i+1/2,j} - \sigma_{i+1/2,j}\Delta t}{2\varepsilon_{i+1/2,j} + \sigma_{i+1/2,j}\Delta t}\right) E_x|_{i+1/2,j}^{n} \\ &+ \left(\frac{2\Delta t}{\left(2\varepsilon_{i+1/2,j} + \sigma_{i+1/2,j}\Delta t\right)\Delta y}\right)\left(H_z|_{i+1/2,j+1/2}^{n} - H_z|_{i+1/2,j-1/2}^{n}\right) \\ &- \left(\frac{2\Delta t}{2\varepsilon_{i+1/2,j} + \sigma_{i+1/2,j}\Delta t}\right) J_{source_x}|_{i+1/2,j}^{n} + \end{aligned} \tag{2.20}$$

$$\begin{aligned} E_y|_{i,j+1/2}^{n+1/2} &= \left(\frac{2\varepsilon_{i,j+1/2} - \sigma_{i,j+1/2}\Delta t}{2\varepsilon_{i,j+1/2} + \sigma_{i,j+1/2}\Delta t}\right) E_y|_{i,j+1/2}^{n} \\ &+ \left(\frac{2\Delta t}{\left(2\varepsilon_{i,j+1/2} + \sigma_{i,j+1/2}\Delta t\right)\Delta x}\right)\left(H_z|_{i-1/2\,j+1/2}^{n+1/2} - H_z|_{i+1/2,j+1/2}^{n+1/2}\right) \\ &- \left(\frac{2\Delta t}{2\varepsilon_{i,j+1/2} + \sigma_{i,j+1/2}\Delta t}\right) J_{source_y}|_{i,j+1/2}^{n} + \end{aligned} \tag{2.21}$$

$$\begin{aligned} H_z|_{i+1/2,j+1/2}^{n+1/2} &= \left(\frac{2\mu_{i+1/2,j+1/2} - \sigma_{i+1/2,j+1/2}\Delta t}{2\mu_{i+1/2,j+1/2} + \sigma_{i+1/2,j+1/2}\Delta t}\right) H_z|_{i+1/2,j+1/2}^{n} \\ &+ \left(\frac{2\Delta t}{\left(2\mu_{i+1/2,j+1/2} + \sigma_{i+1/2,j+1/2}\Delta t\right)\Delta y}\right)\left(E_x|_{i+1/2,j+1}^{n} - E_x|_{i+1/2,j}^{n}\right) \\ &- \left(\frac{2\Delta t}{2\mu_{i+1/2,j+1/2} + \sigma_{i+1/2,j+1/2}\Delta t}\right)\left(E_y|_{i+1,j+1/2}^{n+1/2} - E_y|_{i,j+1/2}^{n+1/2}\right) \\ &- \left(\frac{2\Delta t}{2\mu_{i+1/2,j+1/2} + \sigma_{i+1/2,j+1/2}\Delta t}\right) M_{source_z}|_{i+1/2,j+1/2}^{n} + \end{aligned} \tag{2.22}$$

The set of Eq. (2.17)-(2.19) applies to a coarse grid region, while the set of Eq. (2.20)-(2.22) applies to a finer grid region. For the interface between the two regions, an interpolation scheme required only in space is applied, since the same time step is used in both thick and thin meshes.

2.5. Dielectric properties of breast tissues

Microwave imaging is a technique that uses microwaves to detect objects embedded or hidden in a medium. The main argument for this technique is the significant difference in the dielectric properties of cancerous tumors compared to healthy tissues. Field distribution imaging using microwaves is based on the variation of dielectric properties between normal breast tissue and tumor tissue at microwave frequencies. In order to understand the interaction between microwaves and breast tissue, it is necessary to know the dielectric properties of breast tissues [37, 38]. Studies have been carried out to measure the dielectric properties of cancerous tissues in various tissue types in the radio and microwave frequency ranges in the 10 Hz-20 GHz frequency range, and it has been observed that the dielectric properties of cancerous tissues are different from healthy tissues. The dielectric properties of breast tissues are represented by a complex relative permittivity. $\varepsilon = \varepsilon' - j\varepsilon''$. The real part of this complex number representing the ability of the material to store microwave energy, while the imaginary part indicates the ability of the material to absorb microwave energy and is also called the loss factor. σ is the electrical conductivity of the sample, ω is the angular frequency of the field, ε_0 is the permittivity of free space and $\varepsilon'' = \sigma/\omega\varepsilon_0$.
Measurements in the radio and microwave range have shown that the dielectric properties of healthy breast tissue differ significantly in the vicinity of malignant breast tissues. The results obtained as a result of the measurements vary depending on the number of samples used, the detection volume and depth, the frequency range, and the size of the tissue [39, 40]. Although there are $\pm 10^{0}/_{0}$ differences between the measurement values of the dielectric properties of breast tissues at microwave frequencies, the average values are as in Table 2.1.

3. Numerical Results and Discussions

Two different simulation setups have been developed to observe the interaction of electromagnetic waves at microwave frequencies and breast tissue. These simulation setups form the computational domain of our numerical approach, and calculations are made using the FDTD and ADI-FDTD technique. While solving with the FDTD method, the space should be truncated in a certain place where it will be sufficient in terms of interactions. After the computation domain is determined, the PML absorbing boundary condition is used from the truncated region to model the real infinity and it is assumed that the PML layer surrounds all of the computation domain.

Mediums	ε_r	$\sigma_s\,(S/m)$	μ_r
Normal Breast Tissue	9.0	0.4	1.0
Skin	36.0	4.0	1.0
Malignant	50.0	7.0	1.0
Air	1.0	0.0	1.0

Table 2.1: Parameters of the mediums [37]

3.1. Preparation of the simulation setup

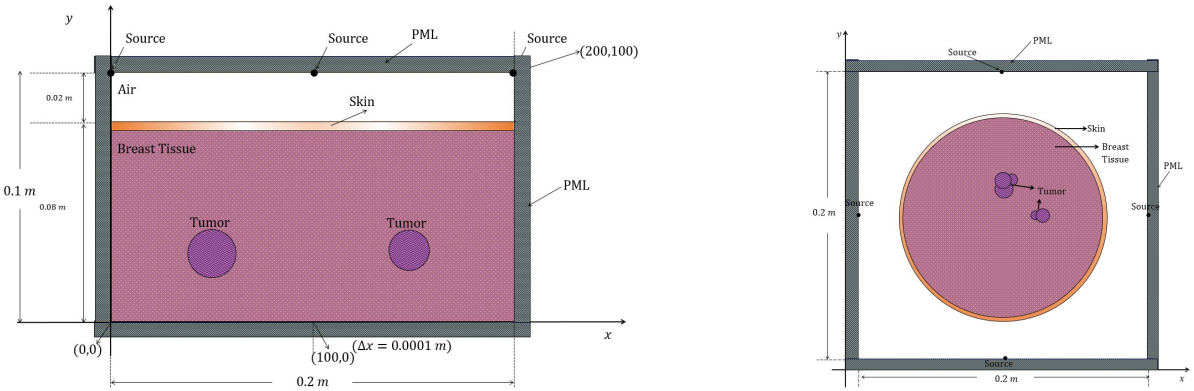

Figure 3.1: **(a)** Rectangular breast model, **(b)** Spherical breast model

In Figure 3.1a a rectangular computational domain is given. The length of the computation region on the x-axis is 0.2 m and the length on the y-axis is 0.1 m. Along the y-axis, 0.076 is breast tissue, 0.004 is skin and 0.02 is air. In the computation domain two tumor tissues in the form of circles with diameters 0.018 m and 0.015 m, which accept the points (0.12, 0.03), (0.16, 0.03) of the computation domain as centers, respectively, are defined. In Figure 3.1b, it is assumed that there is a circular breast tissue inside a square computational domain. The diameter of the circular breast tissue is accepted as 0.16 m and the thickness of the skin layer is taken as 0.004 m, which corresponds to four-unit cells in the FDTD computation space. It is accepted that cancerous tissues are concentrated in two different locations in the circular region and the tumor is expressed using circles whose centers are very close to each other. The first concentration of cancerous tissues is in the upper half of the computation domain, and three circles close to each other are used, and their diameters and coordinates are as follows, respectively: 0.01 m, 0.014 m, 0.016 m and (0.1,0.13), (0.1,0.12), (0.11,0.13). The second concentration of cancerous tissues is in the right side of the computation domain, and two circles close to each other are used, and their diameters and coordinates are as follows, respectively: 0.008 m, 0.012 m, and (0.12,0.1), (0.128,0.1), (0.11,0.13). It is assumed that all cells in the computation domain are the same size The simulation setup and computation domain dimensions are given in Figure 3.1 in detail.

3.2. Simulation results

Sources are the components that initiate the finite difference simulation by activating the electric and magnetic fields as a function of time. Although sources are divided into far field and near field depending on the type of problem being solved, the frequency spectrum of the selected source waveform should be chosen so that all frequencies are considered in the simulations. The frequency range at which valid and accurate simulation results can be obtained is determined by the frequency spectrum of the source waveform. Since frequency and wavelength are inversely proportional, the highest frequency in the source waveform spectrum must be smaller than the highest frequency-wavelength ratio of the cell size. Since the Gaussian waveform can be created to cover all frequencies up to the highest frequency, which depends on the cell size by a factor, the Gaussian waveform is used for the simulations.

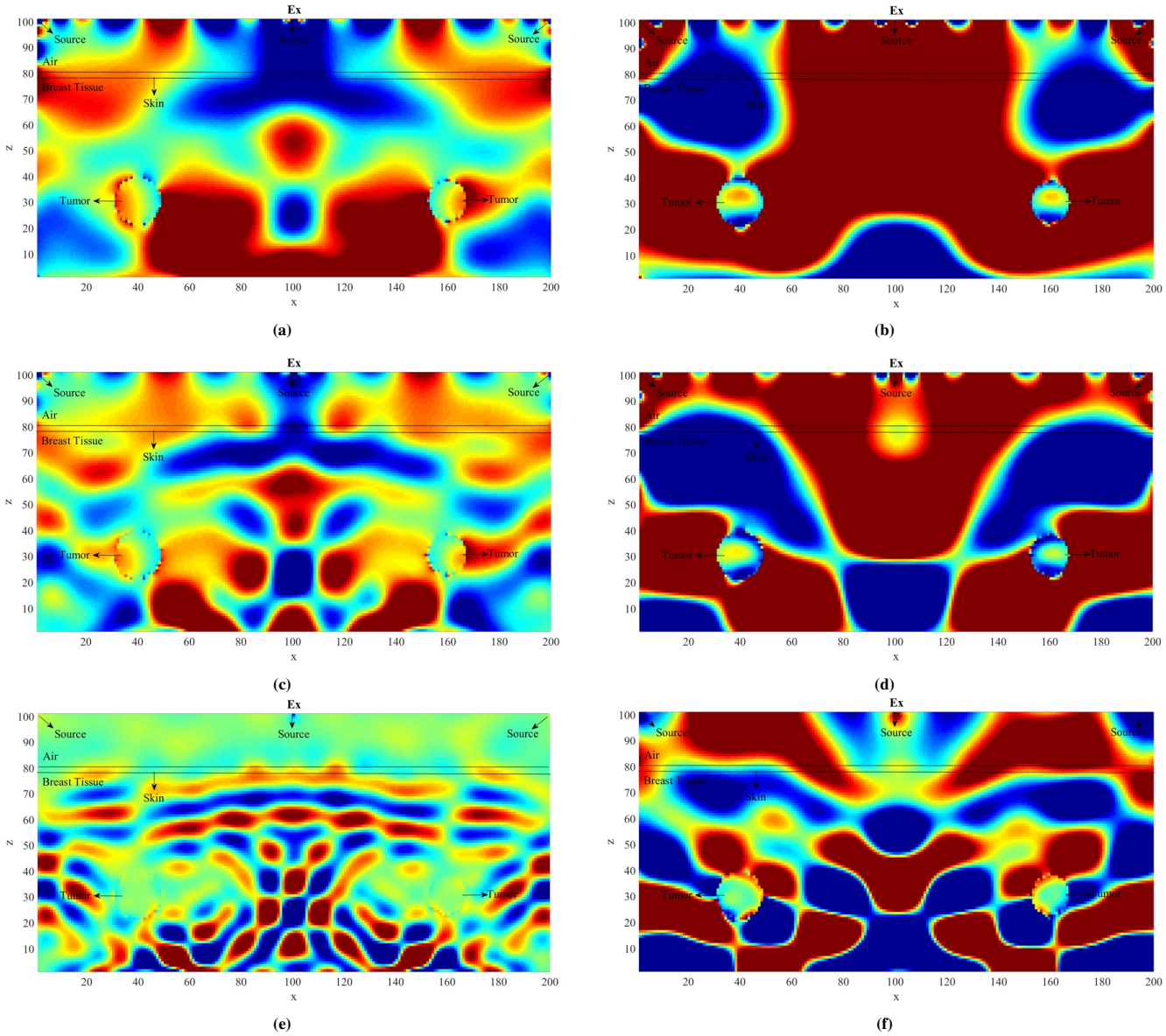

Figure 3.2: Simulation result for rectangular breast model for 650-time step: **(a)** Ex field distribution at 1.5 GHz by FDTD algorithm, **(b)** Ex field distribution at 1.5 GHz by ADI-FDTD algorithm, **(c)** Ex field distribution at 3.0 GHz by FDTD algorithm, **(d)** Ex field distribution at 3.0 GHz by ADI-FDTD algorithm, **(e)** Ex field distribution at 6.0 GHz by FDTD algorithm, **(f)** Ex field distribution at 6.0 GHz by ADI-FDTD algorithm

In Figure 3.2 and Figure 3.3 rectangular simulation setup results are obtained and presented. The Ex-field distributions of the TE mode are presented in using both FDTD and ADI-FDTD algorithms. In the TE wave simulation results obtained using the FDTD algorithm, when the states of the images at different frequencies are compared, better results are obtained at 1.5 GHz frequency. At 3.0 GHz frequency, tumor tissue is less prominent than at 1.5 GHz, and tumor tissue is almost invisible at 6.0 GHz. The Ez-field distributions of the TM mode are presented in Figure 3.3 using both FDTD and ADI-FDTD algorithms. In Figure 3.3, similar to Figure 3.2, 1.5 GHz frequency gives better results in the simulation results obtained using the FDTD algorithm.

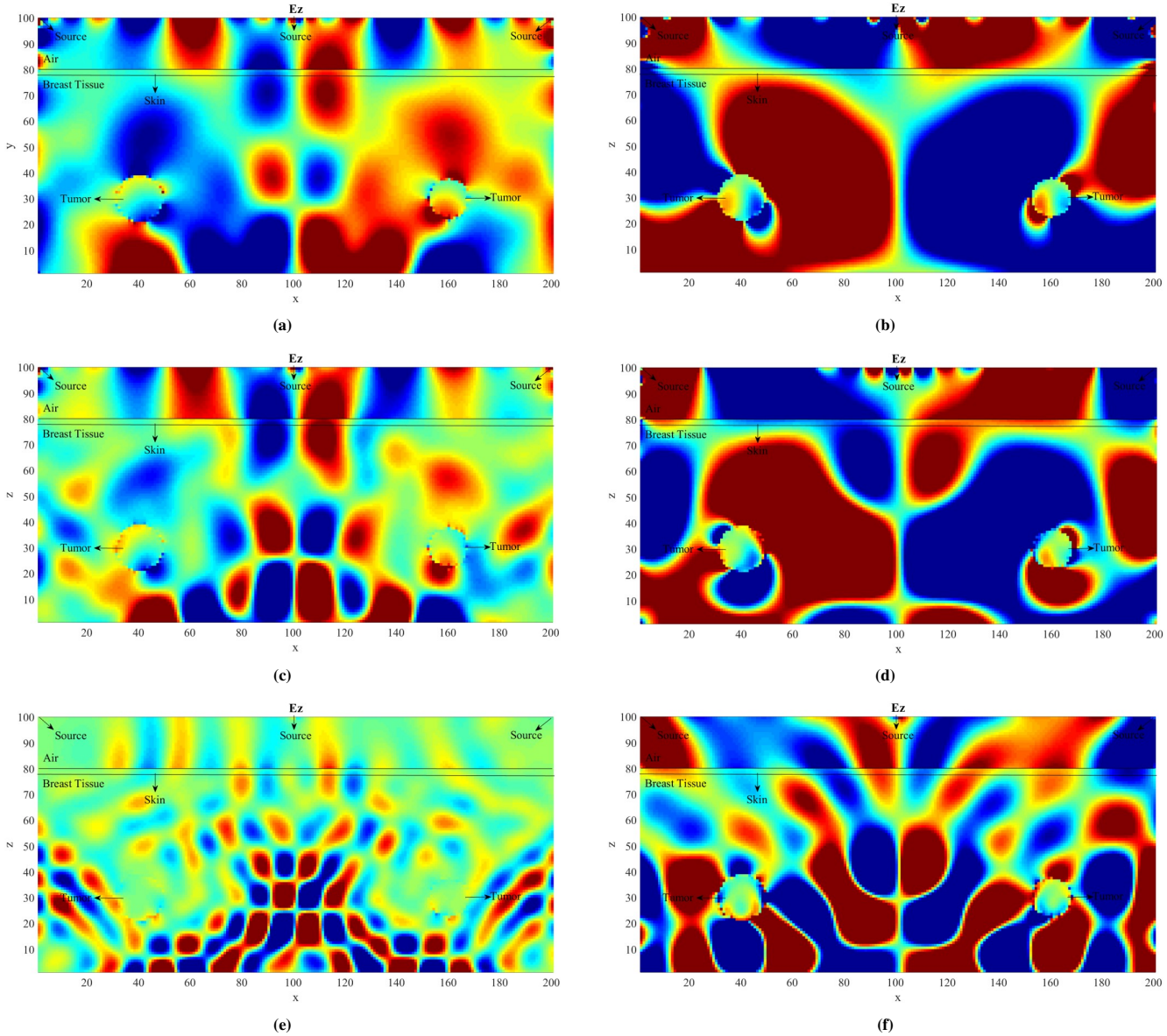

Figure 3.3: Simulation result for rectangular breast model for 650-time step: **(a)** Ez field distribution at 1.5 GHz by FDTD algorithm, **(b)** Ez field distribution at 1.5 GHz by ADI-FDTD algorithm, **(c)** Ez field distribution at 3.0 GHz by FDTD algorithm, **(d)** Ez field distribution at 3.0 GHz by ADI-FDTD algorithm, **(e)** Ez field distribution at 6.0 GHz by FDTD algorithm, **(f)** Ez field distribution at 6.0 GHz by ADI-FDTD algorithm

Circular breast model with massive tumor tissue is modeled in Figure 3.4 and Figure 3.5, Ex field distribution for TE mode and Ez field distribution for TM mode are presented respectively.

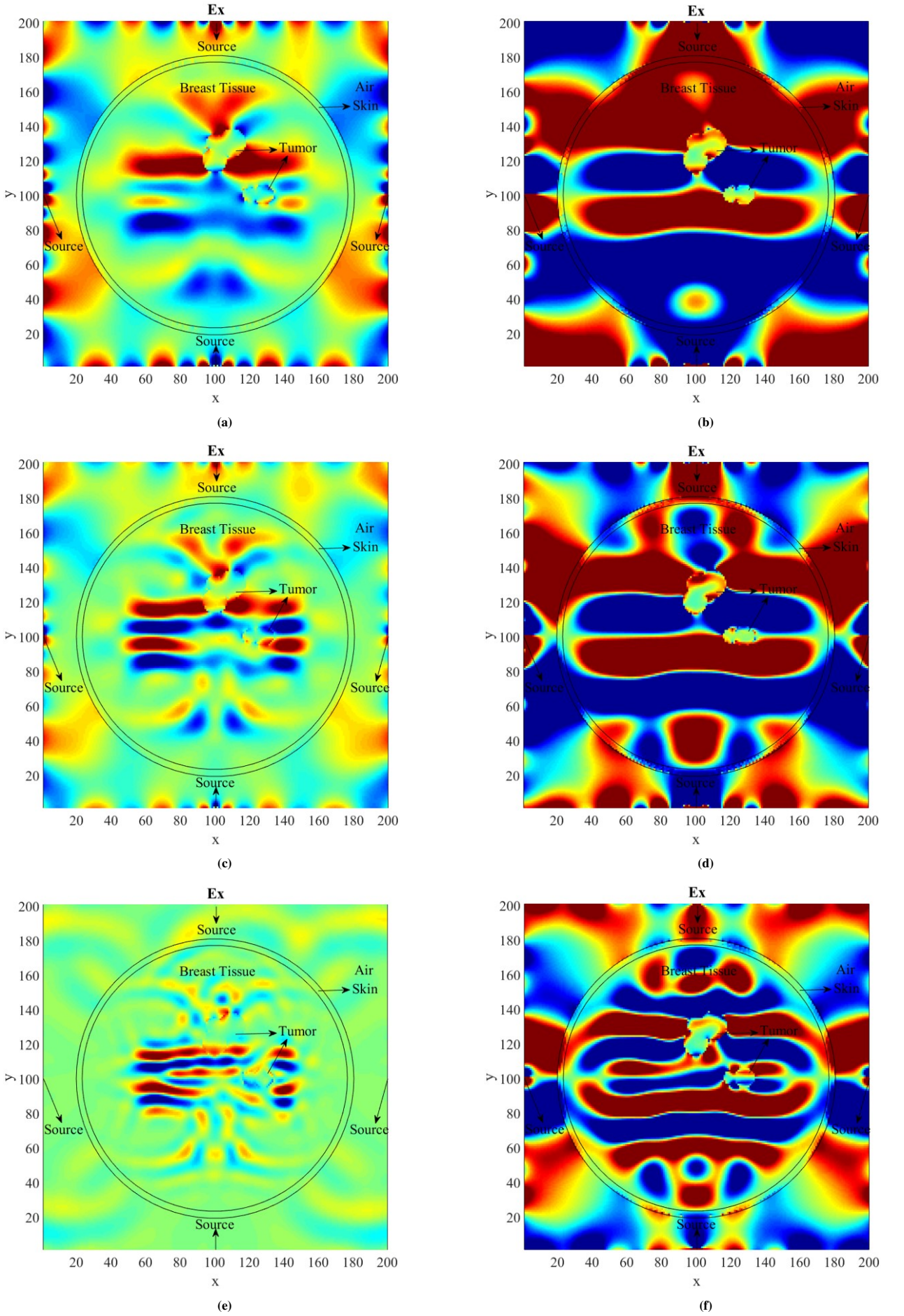

Figure 3.4: Simulation result for spherical breast model for 650-time step: **(a)** Ex field distribution at 1.5 GHz by FDTD algorithm, **(b)** Ex field distribution at 1.5 GHz by ADI-FDTD algorithm, **(c)** Ex field distribution at 3.0 GHz by FDTD algorithm, **(d)** Ex field distribution at 3.0 GHz by ADI-FDTD algorithm, **(e)** Ex field distribution at 6.0 GHz by FDTD algorithm, **(f)** Ex field distribution at 6.0 GHz by ADI-FDTD algorithm

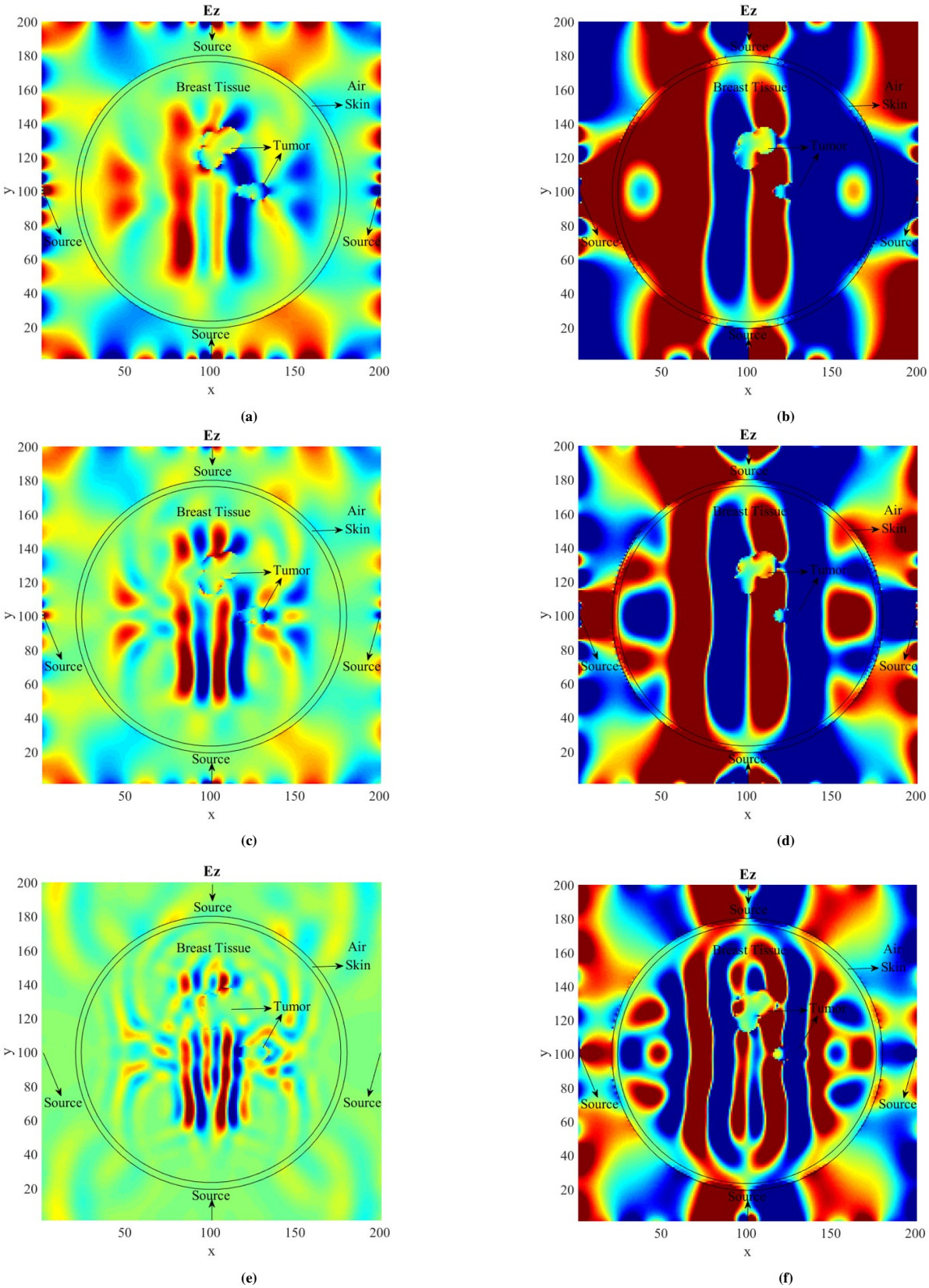

Figure 3.5: Simulation result for spherical breast model for 600-time step: **(a)** Ez field distribution at 1.5 GHz by FDTD algorithm, **(b)** Ez field distribution at 1.5 GHz by ADI-FDTD algorithm, **(c)** Ez field distribution at 3.0 GHz by FDTD algorithm, **(d)** Ez field distribution at 3.0 GHz by ADI-FDTD, **(e)** Ez field distribution at 6.0 GHz by FDTD algorithm, **(f)** Ez field distribution at 6.0 GHz by ADI-FDTD algorithm

Since the geometric structure of the tumor tissue is more complex in the circular model, the boundaries of the tumor tissue are not clear even at the frequency of 3.0 GHz. In the simulation results obtained using the FDTD algorithm, the best result was obtained at the 1.5 GHz frequency. In the results obtained with the help of the ADI-FDTD algorithm, tumor tissue can be observed at all three frequencies. When the Ex and Ez field distributions are compared, since there is more scattering of the wave in the Ez field distribution, the transition of the medium wave to a different medium is observed more clearly.

4. Conclusion

The propagation of electromagnetic waves varies depending on the dielectric properties of the medium. Depending on the dielectric properties of the medium, there may be there may be scattering, lossy propagation, and attenuation may occur. The dielectric properties of cancerous tissue differ significantly from those of healthy tissues. Since the different dielectric properties affect the propagation of the wave, the position and shape of the cancerous breast tissues are modeled mathematically by using the electromagnetic field distribution in the breast tissue. The mathematical modeling of the interaction of waves with mediums can be presented using Maxwell's equations. When the geometry of the interacting medium is smooth, the field distribution in the medium can be calculated analytically. Since cancer tissue is a lossy medium, its shape is assumed to be spherical and the field distribution of electromagnetic waves in the lossy dielectric sphere is calculated analytically. When the medium in which the wave propagates is geometrically complex, the field distribution can be determined by numerical methods. In this study, the shape and location of the tumor are determined using the FDTD method, which is a widely used method for computing the propagation of electromagnetic waves. The propagation of the wave in the breast tissue and the distribution of the fields are simulated with FDTD algorithm. After determining the location of the tumor, better simulation results are obtained by using ADI-FDTD to the location of the tumor and FDTD to the region of healthy tissues. Using both TE and TM waves, the field distributions of waves with different polarizations are compared. In the simulations, both the Ex-field distribution of the TE mode and the Ez field distribution of the TM mode are obtained, and the simulation results obtained at the center frequency of L (1.0-2.0 GHz), S (2.0-4.0 GHz) and C (4.0-8.0 GHz) bands using the FDTD and ADI-FDTD algorithms are compared. In the results obtained using the ADI-FDTD algorithm, tumor tissue is observed more clearly. In the Ez-field distributions, the propagation of the wave from the air medium to the breast tissue can be observed more clearly. Although generally better results are obtained in lower frequency bands, the best results are obtained at 1.5 GHz frequency with the help of ADI-FDTD hybrid algorithm. Using the established mathematical model, it has been shown that the detection of breast cancer can be made with the help of the field distributions obtained as a result of the propagation of electromagnetic waves.

Article Information

Acknowledgements: The authors would like to express their sincere thanks to the editor and the anonymous reviewers for their helpful comments and suggestions.

Author's contributions: The article has a single author. The author has read and approved the final manuscript.

Conflict of interest disclosure: No potential conflict of interest was declared by the author.

Copyright statement: Authors own the copyright of their work published in the journal and their work is published under the CC BY-NC 4.0 license.

Supporting/Supporting organizations: No grants were received from any public, private or non-profit organizations for this research.

Ethical approval and participant consent: It is declared that during the preparation process of this study, scientific and ethical principles were followed and all the studies benefited from are stated in the bibliography.

Plagiarism statement: This article was scanned by the plagiarism program. No plagiarism detected.

Availability of data and materials: Not applicable.

References

[1] F. Bray, M. Laversanne, E. Weiderpass, I. Soerjomataram, *The ever-increasing importance of cancer as a leading cause of premature death worldwide,* Cancer, **127** (16) (2021), 3029-3030.
[2] W. Organization, *Global Health Estimates 2019: deaths by cause, age, sex, by country and by region 2000–2019,* WHO, (2020).
[3] H. Sung, J. Ferlay, R. Siegel, M. Laversanne, I. Soerjomataram, A. Jemal, F. Bray, *Global cancer statistics 2020: GLOBOCAN estimates of incidence and mortality worldwide for 36 cancers in 185 countries,* CA: A Can. J. Clinc., **71** (3) (2021), 209-249 .
[4] M. Lu, X. Xiao, G. Liu, H. Lu, *Microwave breast tumor localization using wavelet feature extraction and genetic algorithm-neural network,* Med. Phys., **48** (10) (2021), 6080-6093.
[5] E. Bond, X. Li, S. Hagness, B. Van Veen, *Microwave imaging via space-time beamforming for early detection of breast cancer,* IEEE Trans. Anten. Prop., **51** (8) (2003), 1690-1705.
[6] M. Lazebnik, M. Okoniewski, J. Booske, S. Hagness, *Highly accurate Debye models for normal and malignant breast tissue dielectric properties at microwave frequencies,* IEEE Mic. Wirel. Comp. Lett., **17** (12) (2007), 822-824.
[7] N. Nikolova, *Microwave imaging for breast cancer,* IEEE Mic. Mag., **12** (7) (2011), 78-94.
[8] R. Conceição, J. Mohr, M. O'Halloran, (Eds.), *An Introduction to Microwave Imaging for Breast Cancer Detection,* Basel, Switzerland, Springer International Publishing, 2016.
[9] S. Kwon, S. Lee, *Recent advances in microwave imaging for breast cancer detection*, Internat. J. Biomed. Imaging, (2016), 1-26.
[10] S. Davis, B. Van Veen, S. Hagness, F Kelcz, *Breast tumor characterization based on ultrawideband microwave backscatter*, IEEE Trans. Biomed. Engrg., **55** (1) (2007), 237-246.
[11] M. Zhao, J. Shea, S. Hagness, D. Weide, B. Van Veen, T. Varghese, *Numerical study of microwave scattering in breast tissue via coupled dielectric and elastic contrasts,* IEEE Anten. Wirer. Prop. Lett., **7** (2008), 247-250.
[12] L. Wang, *Microwave imaging and sensing techniques for breast cancer detection*,Micromachines, **14** (7) (2023), 1462.
[13] R. Torrealba-Meléndez, J. Olvera-Cervantes, A. Corona-Chávez, *UWB microwave radar imaging for detection and discrimination of benign and malignant breast tumors using circularly polarized antennas*, (IEEE WAMICON 2014), (2014), 1-3.
[14] K. Noritake, S. Kidera, Accurate breast surface imaging method with FDTD-based waveform correction for microwave mammography, 2017 International Symposium On Antennas And Propagation (ISAP 2017), (2017), 1-2.
[15] A. Fhager, M. Persson, Reconstrunction strategies for microwave imaging of breast; reconstructions constrained to the breast domain, IEEE MTT-S International Microwave Bio Conference (IMBIOC 2017), (2017), 1-3.
[16] L. Wang, *Microwave sensors for breast cancer detection*, Sensors, **18** (2) (2018), 655.
[17] H. El Misilmani, T. Naous, S. Al Khatib, K. Kabalan, *A survey on antenna designs for breast cancer detection using microwave imaging,* IEEE Access, **8** (2020), 102570-102594.
[18] M. Ahadi, J. Nourinia, C. Ghobadi, *Square monopole antenna application in localization of tumors in three dimensions by confocal microwave imaging for breast cancer detection: experimental measurement*, Wirel. Pers. Commun., **116** (2021), 2391-2409.

[19] B.Moloney, D. O'Loughlin, S. Abd Elwahab, M. Kerin, *Breast cancer detection—A synopsis of conventional modalities and the potential role of microwave imaging*, Diagnostics, **10** (2) (2020), 103.

[20] D. Carvalho, A. Aragão, A. Ferrari, B.Sanches, W. Noije, Software-defined radio assessment for microwave imaging breast cancer detection, 2020 IEEE Nordic Circuits and Systems Conference (NorCAS 2020), (2020), 1-6.

[21] D. Godinho, J. Felicio, C. Fernandes, R. Conceicao, *Experimental evaluation of an axillary microwave imaging system to aid breast cancer staging*, IEEE J. Elect., RF Mic. Med. Biology, **6** (1) (2021), 68-76.

[22] C. Balanis, *Advanced Engineering Electromagnetics*, John Wiley and Sons, 2012.

[23] İ. Ünal, B. Turetken, U. Bulus, C. Canbay, Analysis of the electromagnetic field scattered by a spherical breast tumour model, 2013 International Symposium On Electromagnetic Theory, (2013), 574-577.

[24] A.Taflove, S. Hagness, M. Piket-May, *Computational electromagnetics: the finite-difference time-domain method*, Elec. Eng. Hand., **3** (15) (2005), 629-670.

[25] D. Sullivan, *Electromagnetic Simulation Using the FDTD Method*, John Wiley and Sons, 2013.

[26] K. Kunz, R. Luebbers, *The Finite Difference Time Domain Method for Electromagnetics*, CRC Press,1993.

[27] A. Elsherbeni, V. Demir, *The Finite-Difference Time-Domain Method for Electromagnetics with MATLAB® Simulations*, IET, 2015.

[28] T. Namiki, *A new FDTD algorithm based on alternating-direction implicit method*, IEEE Trans. Mic. Theory Tech., **47** (10) (1999), 2003-2007.

[29] T.Namiki, *3-D ADI-FDTD method-unconditionally stable time-domain algorithm for solving full vector Maxwell's equations*, IEEE Trans. Mic. Theory Tech., **48** (10) (2000), 1743-1748.

[30] X. Wang, J. Gao, Z. Chen, F. Teixeira, *Unconditionally stable one-step leapfrog ADI-FDTD for dispersive media*, IEEE Trans. Antenn. Prop., **67** (4) (2019), 2829-2834.

[31] D. Y. Heh, E. L. Tan, *Unconditionally stable multiple one-dimensional ADI-FDTD method for coupled transmission lines,* IEEE Trans. Antenn. Prop., **66** (12) (2018), 7488-7492.

[32] E. L. Tan, D. Y. Heh, *Multiple 1-D fundamental ADI-FDTD method for coupled transmission lines on mobile devices*, IEEE J. Multisc. Multiph. Comp. Tech., **4** (2019) 198-206.

[33] B. Zou, S. Liu, L. Zhang, S. Ren, *Efficient one-step leapfrog ADI-FDTD for far-field scattering calculation of lossy media*, Mic. Opt. Tech. Lett. 62 (5) (2020), 1876-1881.

[34] G. Mur, *Absorbing boundary conditions for the finite-difference approximation of the time-domain electromagnetic-field equations*, IEEE Trans. Elec. Comput., **4** (1981), 377-382.

[35] J. Berenger, *A perfectly matched layer for the absorption of electromagnetic waves,* J. Comput. Phys., **114** (2) (1994), 185-200.

[36] J. Berenger, *Perfectly matched layer for the FDTD solution of wave-structure interaction problems*, IEEE Trans. Antenn. Prop., **44** (1) (1996), 110-117.

[37] E. Zastrow, S. Davis, M. Lazebnik, F. Kelcz, B. Van Veen, S. Hagness, *Development of anatomically realistic numerical breast phantoms with accurate dielectric properties for modeling microwave interactions with the human breast,* IEEE Trans. Biomed. Engrg., **55** (12) (2008), 2792-2800.

[38] E. Fear, M. Stuchly, *Microwave detection of breast cancer*, IEEE Trans. Mic. Theory Tech., **48** (11) (2000), 1854-1863.

[39] S. Hagness, A. Taflove, J. Bridges, *Three-dimensional FDTD analysis of a pulsed microwave confocal system for breast cancer detection: Design of an antenna-array element*, IEEE Trans. Antenn. Prop., **47** (5) (1999), 783-791.

[40] M. Lazebnik, C. Watkins, S. Hagness, J. Booske, D. Popovic, L. McCartney, M. Okoniewski, M. Lindstrom, T. Breslin, J. Harter, The dielectric properties of normal and malignant breast tissue at microwave frequencies: analysis, conclusions, and implications from the wisconsin/calgary study, 2007 IEEE Antennas And Propagation Society International Symposium (2007), 2172-2175.

Journal of Mathematical Sciences and Modelling, 6 (3) (2023) 120-132
Research Article

Journal of Mathematical Sciences and Modelling

Journal Homepage: www.dergipark.gov.tr/jmsm
ISSN 2636-8692
DOI: http://dx.doi.org/10.33187/jmsm.1241420

DNA Secret Writing With Laplace Transform of Mittag-Leffler Function

Mehmet Çağrı Yılmazer[1], Emrah Yılmaz[2*], Tuba Gülşen[3] and Mikail Et[4]

[1, 2*, 3, 4]*Department of Mathematics, Faculty of Science, Firat University, Elazığ, Türkiye*
[*]*Corresponding author*

Article Info

Keywords: *Cryptology, Data encryption, DNA, Mittag-Leffler function, Laplace transform, Statistical tests*
2010 AMS: *33E12, 44A10, 62P99, 68P25, 92D20, 94A60*
Received: *24 January 2023*
Accepted: *25 August 2023*
Available online: *10 September 2023*

Abstract

In this study, we present a new cryptosystem named Deoxyribose Nucleic Acid (DNA) secret writing with the Laplace transform of the Mittag-Leffler function. The method is proper for encrypting large files. In this technique, we consider the original message as binary sequence. These binary streams corresponding to the plain text is transformed to DNA bases by utilizing DNA encoding, then the DNA codes are transformed to positive integers. We apply the Laplace transform to these numbers which are coefficients of the expansion of the Mittag-Leffler function. To provide multi-stage protection, the outcome coefficients are transformed to binary sequences and other level of encryption with cumulative XOR is applied and equivalent MSBs obtained at every iteration are utilized for building cipher text. Decryption is implemented in the opposite way. We employ monobit test, correlation analysis for measuring the reliability of encryption and Python programming language to obtain secret message, the plain text and computations of statistical tests.

1. Introduction

Cryptography is simply the science of utilizing mathematics for encryption and decryption of information. Its essential aim is to provide two groups, to communicate over a channel that is insecure in the manner that an opponent cannot comprehend the message that is for the intended recipient. Information security is becoming increasingly important in the utilization of electronic telecommunication in financial activities. Cryptography is intended to enable safety services and it has become an important technique in many areas for information protection. Encryption is the procedure of converting an original message called plain text to obscuring form named cipher text. We commonly use it for confidentiality and generally for secret communication [1–3].

A cipher is defined as a method to apply encryption and decryption. As mentioned above, the actual message is regarded as plain text and the enciphered form as cipher text. The encrypted message comprises the entire information of the original message but is not in form decipherable by a person or computer unless an appropriate tool to decrypt it. It must look like nonsense to those not aimed to understand it. We usually parameterize ciphers by using a bit of subsidiary information, named as a key. The encrypting process is diversified based on the key, which modifies the elaborated operation of the method. Unless the key is proper, decryption is not possible.

Several methods for cryptography are presented in [4–11]. The mathematical method utilizing matrices for it are presented in Dhanorkar and Hiwarekar [12], Overbey and others [13], Saeednia [14]. A message is encrypted by means of series expansion of $f(t)$ and its Laplace transform [1, 15, 16]. In [17], Hiwarekar uses the Laplace transform of hyperbolic cosine functions for encryption and decryption. Here, we propose Mittag-Leffler function and its variations for encryption and decryption by Laplace transform in DNA secret codes. First, let's talk about the importance of DNA chains in encryption.

It was stated by Watson and Crick that DNA chains are important in the encryption of information [18]. Although DNA encryption is a new and useful, it is not as useful as the conventional method. We can combine it with current cryptographic systems to enable improved

***Email addresses and ORCID numbers*: m.cagri.yilmazer@gmail.com, 0000-0001-9784-838X (M. Ç. Yılmaze), emrah231983@gmail.com, 0000-0002-7822-9193 (E. Yılmaz), tubagulsen87@hotmail.com, 0000-0002-2288-8050 (T. Gülşen), mikailet68@gmail.com, 0000-0001-8292-7819 (M. Et)**
Cite as "M. Ç. Yılmazer, E. Yılmaz, T. Gülşen, M. Et, *DNA secret writing with Laplace transform of Mittag-Leffler function*, J. Math. Sci. Model., 6(3) (2023), 120-132."

security [19–21]. Adleman's research [22] in DNA computing and Viviana Risca's project on DNA steganography gave rise to new fields of DNA cryptography and stenography [23]. In [24], Sukalyan and Moumita Som presented a new technique for DNA encoding by using Laplace transform. For a better understanding of the subject, let's explain the structure of DNA.

DNA is a long polymer consisting of numerous nucleotides in the shape of a double helix storing genetic information. Each spiral chain composed of sugar phosphate as spine and bases are joined to complemental chain by hydrogen bridges between dual bases Adenine(A), thymine(T), guanine(G) and cytosine(C). Adenine and thymine are joined by two hydrogen bridges while guanine and cytosine are joined by three. It is shown that DNA cryptography is very effective in its initial phase. Nowadays, various DNA computing algorithms can be solutions for cryptanalysis and stenography problems. The idea of DNA computing compounded with areas of cryptography and steganography becomes a new technique for nonbreakable algorithms [25, 26].

There exists two complemental strands in the framework of DNA. Each base in DNA has a sugar constituent connected to a phosphate group at one place, and to a nitrogen comprising nucleotide bounded at another place. The strands in DNA possess the phosphate of one base connected to sugar of the next base to form a chain of consecutive sugars and phosphates with dangling nitrogenous bases, as seen in Figure 1.1.

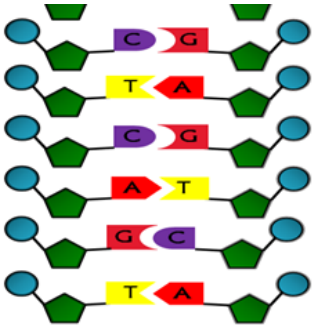

Figure 1.1: Fundamental DNA framework.

DNA includes two such strands, intertwined with each other to constitute a duplex helix with the nucleoids on the inside. Each A on one strand constitutes weak bonds with a T on the other chain, and each C on a chain weakly to a G on the opposite strand. Thus, the two chains are complemental and the sequence in one can be understood from other's sequence. The fundamental DNA framework is illustrated in Figure 1.2.

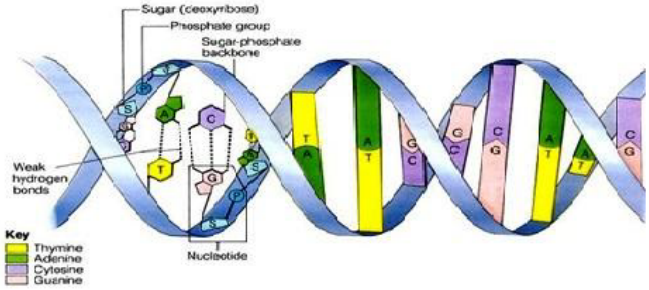

Figure 1.2: Composite of Nucleotide bases in chains.

These complemental chains possess codons as basic components. Codons are essentially triads of nucleotide bases. Table 1 below demonstrates codons building DNA sequences in two complemental chains. As can be observed DNA nucleotide bases are included by codons and are complemented each other. We can utilize these codons for encryption and decryption of the information.

2. Preliminaries

In this section, we provide definitions and some features of the Mittag-Leffler function, Laplace transform, and relations between them which are important in applying our method to cryptography.

Definition 2.1. *Let f be a function defined on the set of positive real numbers. Then, $L\{f(t)\}$ or $F(s)$ which is the Laplace transform of $f(t)$ is defined by*

$$L\{f(t)\} = F(s) = \int_0^\infty e^{-st} f(t)\, dt. \tag{2.1}$$

The domain of $F(s)$ is set of values of s which the above improper integral converges. Furthermore, we can write the formula (2.1) as $f(t) = L^{-1}\{F(s)\}$. In this situation, $f(t)$ is defined as inverse Laplace transform of $F(s)$. We call the symbol L which transforms $f(t)$ into $F(s)$ as the Laplace transform operator. On the other hand, we can define the symbol L^{-1} which transforms $F(s)$ to $f(t)$ as the inverse Laplace operator [27].

The Laplace transform is named in memory of the French mathematician, physicist, and astronomer *Pierre-Simon Marquis de Laplace* (1749-1827), who utilized the transform in his inquiries of probability theory.

Assume that the functions f and g have Laplace transforms for $s > c_1$ and $s > c_2$, respectively. If c represents the maximum of the two numbers c_1 and c_2, then for $s > c$ and constant α and β, following expression holds:

$$\int_0^\infty e^{-st}[\alpha f(t) + \beta g(t)]\,dt = \alpha \int_0^\infty e^{-st} f(t)\,dt + \beta \int_0^\infty e^{-st} g(t)\,dt.$$

That is to say L is a linear transform

$$L\{\alpha f(t) + \beta g(t)\} = \alpha L\{f(t)\} + \beta L\{g(t)\}.$$

Moreover, using the features of the definite integral, the Laplace transform of any finite functions of t is the sum of Laplace transforms of single functions. Likewise, the same is held for inverse Laplace transforms [27].

We give some fundamental Laplace transforms as follows [27]

$$\begin{aligned} L\{t^n\} &= \frac{n!}{s^{n+1}}, \\ L^{-1}\{\frac{1}{s^{n+1}}\} &= \frac{t^n}{n!}. \end{aligned}$$

Before touching on the Laplace transform of the Mittag-Leffler function and its variations, we want to mention about Mittag-Leffler function, its properties, and its history.

The exponential function e^z has a very significant role in the theory of integer-order differential equations. One-parameter generalization of it, the function that is now represented by the following definition [28, 29].

Definition 2.2. *One-parametric Mittag-Leffler function is defined by*

$$E_\alpha(z) = \sum_{j=0}^{\infty} \frac{z^j}{\Gamma(\alpha j + 1)} \ (\alpha \in \mathbb{C}),$$

where Γ *is the gamma function. It was presented by Mittag-Leffler [30–32] and investigated also by Wiman [33, 34].*

The two-parameter form of the Mittag-Leffler function, which plays a critical role in the fractional calculus was presented by Agarwal [29,35]. By using Laplace transform method, Humbert and Agarwal get several relations for this function [29, 36]. It could have been named the Agarwal function. However, Humbert and Agarwal greatheartedly left the same notation as for the one-parameter Mittag-Leffler function, and this is why we call the two-parameter function as the Mittag-Leffler function [28, 29, 37].

Definition 2.3. *By using the series expansion, a two-parameter form of the Mittag-Leffler function can be defined as follows [28, 29]*

$$E_{\alpha,\beta}(z) = \sum_{j=0}^{\infty} \frac{z^j}{\Gamma(\alpha j + \beta)}, \ (\alpha, \beta > 0). \tag{2.2}$$

From the definition, we get

$$E_{1,m}(z) = \frac{1}{z^{m-1}} \left\{ e^z - \sum_{j=0}^{m-2} \frac{z^j}{j!} \right\}.$$

Some of the special conditions for Mittag-Leffler function are the hyperbolic sine and cosine:

$$\begin{aligned} E_{2,1}\left(z^2\right) &= \sum_{j=0}^{\infty} \frac{z^{2j}}{\Gamma(2j+1)} = \sum_{j=0}^{\infty} \frac{z^{2j}}{(2j)!} = \cosh z, \\ E_{2,2}\left(z^2\right) &= \sum_{j=0}^{\infty} \frac{z^{2j}}{\Gamma(2j+2)} = \frac{1}{z} \sum_{j=0}^{\infty} \frac{z^{2j+1}}{(2j+1)!} = \frac{\sinh z}{z}. \end{aligned}$$

For $\beta = 1$, we get one-parameter Mittag-Leffler function as

$$E_{\alpha,1}(z) = \sum_{j=0}^{\infty} \frac{z^j}{\Gamma(\alpha j + 1)} = E_\alpha(z).$$

Using term-by-term derivation, we can build from (2.2) the series expansion of derivatives of the two-parameter Mittag-Leffler function [38]

$$\frac{d^k}{dz^k} E_{\alpha,\beta}(z) = \sum_{j=k}^{\infty} \frac{(j)_k}{\Gamma(\alpha j + \beta)} z^{j-k}, \ k \in \mathbb{N},$$

with $(x)_k$ representing the factorial below

$$(x)_k = x(x-1)\ldots(x-k+1).$$

By modifying the index of the summation, we can derive the following expression of the kth order derivative of two-parameter Mittag-Leffler function by

$$\frac{d^k}{dz^k}E_{\alpha,\beta}(z) = \sum_{j=0}^{\infty}\frac{(j+k)_k}{\Gamma(\alpha j+\alpha k+\beta)}z^j.$$

We give the following Laplace transform of $t^{\alpha k+\beta-1}E^{(k)}_{\alpha,\beta}(\pm at^\alpha)$, which has significant role in our study [29],

$$\begin{aligned} L\{t^{\alpha k+\beta-1}E^{(k)}_{\alpha,\beta}(\pm at^\alpha)\} &= \int_0^\infty e^{-st}t^{\alpha k+\beta-1}E^{(k)}_{\alpha,\beta}(\pm at^\alpha)\,dt \\ &= \frac{k!s^{\alpha-\beta}}{(s^\alpha \mp a)^{k+1}},\ \left(Re(s) > |a|^{\frac{1}{a}}\right). \end{aligned}$$

3. Main Results

For encryption of the message, P, the plain text, is transformed into 8-bit binary codes of ASCII values corresponding to the original text, P_{bin}. Then, we transform P_{bin} into DNA codes, P_{dna} by applying the following assignments

Binary stream	00	01	10	11
DNA Nucleotide Base	A	C	G	T

Table 3.1: DNA Nucleotide bases and their corresponding 2 bit binary stream

where A, T, G, C are DNA nucleotide pairs. Afterwards, P_{dna} is transformed into sequence of integers, P_{int} by utilizing the following table,

A	T	G	C
10	20	30	40

Table 3.2: DNA nucleotide bases and their corresponding decimal values.

we can correspond base pairs to numeric values. Subsequently, every integer in P_{int} can be utilized as the coefficients of the Laplace transform of the function $f(t) = Gt^{\alpha k+\beta-1}E^{(k)}_{\alpha,\beta}(\pm at^\alpha)$, in other words

$$\begin{aligned} L\{Gt^{\alpha k+\beta-1}E^{(k)}_{\alpha,\beta}(\pm at^\alpha)\} &= L\left\{\sum_{j=0}^{\infty}\frac{G_j(j+k)!}{j!}\frac{(\pm a)^j t^{\alpha j+\alpha k+\beta-1}}{\Gamma(\alpha j+\alpha k+\beta)}\right\} \\ &= \sum_{j=0}^{\infty}\frac{G_j(j+k)!(\pm a)^j}{j!}\frac{1}{s^{\alpha j+\alpha k+\beta}}, \end{aligned} \tag{3.1}$$

where $G_j \geq 0$, $\forall j \geq 8$. Thereafter, the coefficients of (3.1) namely, $C_j = \frac{G_j(j+k)!(\pm a)^j}{j!}$ is converted into P_{Lap} by using $C_j \mod 128$. Therefore, we can assign each integer of P_{Lap} to its corresponding 7 binary equivalents and these values are transformed into P_{XOR} by applying cumulative XOR protocol in Figure 3.1. Finally, we can correspond ASCII equivalent of the values in P_{XOR} to letters of encrypted text, E.

For decryption of the secret message, the encrypted text E is transformed into its corresponding ASCII values that is 7 binary equivalent, E_{ASCII}. Afterwards, cumulative XOR protocol is applied and outcome binary sequences are transform back into their corresponding decimal form DE_j, and by using $C_j = 128\cdot key_j + DE_j$, we obtain the coefficients of the Laplace transform again. If inverse Laplace transform is applied to the following

$$G\frac{k!s^{\alpha-\beta}}{(s^\alpha \mp a)^{k+1}} = \sum_{j=0}^{\infty}\frac{C_j}{s^{\alpha j+\alpha k+\beta}},\ C_j = \frac{G_j(j+k)!(\pm a)^j}{j!},$$

we get G_j which is sequence of integers corresponding to DNA nucleotide bases. Subsequently, G_j is transformed back into DNA bases by utilizing Table 3.2 which generate P_{dna}. Then, we can convert the DNA nucleotide bases back to their binary streams i.e. P_{bin} by utilizing Table 3.1. Lastly, the binary sequences in P_{bin} are assigned to their equivalent ASCII values and therefore generating the decrypted text or the plain text, P.

Theorem 3.1. *The plain text string in respect of $G_j, j = 0,1,2,...$ by using the Laplace transform of $Gt^{\alpha k+\beta-1}E^{(k)}_{\alpha,\beta}(\pm at^{\alpha})$ can be transformed to P_{Lap} that is consists of DE_j where*

$$DE_j = C_j - 128 \cdot key_j, \text{ for } j = 0,1,2,\cdots$$

and

$$C_j = \frac{G_j\,(j+k)!\,(\pm a)^j}{j!}, \text{ for } j = 0,1,2,\cdots$$

with private key

$$key_j = \frac{C_j - DE_j}{128}, \text{ for } j = 0,1,2,\cdots.$$

Theorem 3.2. *The encrypted text string in respect of $G_j, j = 0,1,2,...$, with private key $key_j, j = 0,1,2,...$ by using the inverse Laplace transform of*

$$G\frac{k!s^{\alpha-\beta}}{(s^{\alpha} \mp a)^{k+1}} = \sum_{j=0}^{\infty} \frac{G_j\,(j+k)!\,(\pm a)^j}{j!}\frac{1}{s^{\alpha j+\alpha k+\beta}}$$

can be transformed to P_{int} that is consists of G_j, where

$$G_j = \frac{DE_j + 128 \cdot key_j}{\frac{(j+k)!}{j!}(\pm a)^j}, \text{ for } j = 0,1,2,\cdots$$

and

$$C_j = 128 \cdot key_j + DE_j, \text{ for } j = 0,1,2,\cdots.$$

Theorem 3.3. *Encryption of the plain text and decryption of the secret message in terms of (3.1) is independent of the choice of α and β in Mittag-Leffler function.*

Proof. Let us consider the function as follow

$$\begin{aligned} Gt^{\alpha k+\beta-1}E^{(k)}_{\alpha,\beta}(\pm at^{\alpha}) &= \sum_{j=0}^{\infty} \frac{G_j\,(j+k)!}{j!}\frac{(\pm a)^j t^{\alpha j+\alpha k+\beta-1}}{\Gamma(\alpha j+\alpha k+\beta)} \\ &= \frac{G_0\,(0+k)!}{0!}\frac{(\pm a)^0 t^{\alpha\cdot 0+\alpha k+\beta-1}}{\Gamma(\alpha\cdot 0+\alpha k+\beta)} \\ &+ \frac{G_1\,(1+k)!}{1!}\frac{(\pm a)^1 t^{\alpha\cdot 1+\alpha k+\beta-1}}{\Gamma(\alpha\cdot 1+\alpha k+\beta)} \\ &+ \frac{G_2\,(2+k)!}{2!}\frac{(\pm a)^2 t^{\alpha\cdot 2+\alpha k+\beta-1}}{\Gamma(\alpha\cdot 2+\alpha k+\beta)} \\ &+ \cdots + \frac{G_n\,(n+k)!}{n!}\frac{(\pm a)^n t^{\alpha n+\alpha k+\beta-1}}{\Gamma(\alpha n+\alpha k+\beta)} + \cdots. \end{aligned} \tag{3.2}$$

By taking the Laplace transform of (3.2) and using $\Gamma(k+1) = k!$, we have

$$\begin{aligned} G\frac{k!s^{\alpha-\beta}}{(s^{\alpha} \mp a)^{k+1}} &= \frac{G_0\,(0+k)!}{0!}\frac{(\pm a)^0}{(\alpha\cdot 0+\alpha k+\beta-1)!}\frac{(\alpha\cdot 0+\alpha k+\beta-1)!}{s^{\alpha\cdot 0+\alpha k+\beta}} \\ &+ \frac{G_1\,(1+k)!}{1!}\frac{(\pm a)^1}{(\alpha\cdot 1+\alpha k+\beta-1)!}\frac{(\alpha\cdot 1+\alpha k+\beta-1)!}{s^{\alpha\cdot 1+\alpha k+\beta}} \\ &+ \frac{G_2\,(2+k)!}{2!}\frac{(\pm a)^2}{(\alpha\cdot 2+\alpha k+\beta-1)!}\frac{(\alpha\cdot 2+\alpha k+\beta-1)!}{s^{\alpha\cdot 2+\alpha k+\beta}} \\ &+ \cdots + \frac{G_n\,(n+k)!}{n!}\frac{(\pm a)^n}{(\alpha\cdot n+\alpha k+\beta-1)!}\frac{(\alpha\cdot n+\alpha k+\beta-1)!}{s^{\alpha\cdot n+\alpha k+\beta}} + \cdots \\ &= \frac{G_0\,(0+k)!\,(\pm a)^0}{0!}\frac{1}{s^{\alpha\cdot 0+\alpha k+\beta}} + \frac{G_1\,(1+k)!\,(\pm a)^1}{1!}\frac{1}{s^{\alpha\cdot 1+\alpha k+\beta}} \\ &+ \frac{G_2\,(2+k)!\,(\pm a)^2}{2!}\frac{1}{s^{\alpha\cdot 2+\alpha k+\beta}} + \cdots + \frac{G_n\,(n+k)!\,(\pm a)^n}{n!}\frac{1}{s^{\alpha\cdot n+\alpha k+\beta}} + \cdots. \end{aligned}$$

Therefore, the sequence corresponding to numerical values of the encrypted text is obtained as a

$$C_j = \frac{G_j\,(j+k)!\,(\pm a)^j}{j!}, \text{ for } j = 0,1,2,\cdots.$$

This proves the theorem. □

In the following, we provide an example for encryption of the plain text and decryption of the secret message in respect of DNA secret writing with the Laplace transform of the Mittag-Leffler function.

3.1. Encryption

We consider the two-letter word "Go" for demonstrating the algorithm. Here, 71 (01000111) and 111 (01101111) are ASCII values of "G" and "o", respectively. Equivalent binary stream characterization of the word is illustrated as follows.

0	1	0	0	0	1	1	1	0	1	1	0	1	1	1	1

Table 3.3: Binary characterization of ASCII coded "Go"

We code the binary bit utilizing DNA coding exemplified in Table 3.3. Therefore, DNA encoded text transform into CACTCGTT and we apply integer encoding to the script by utilizing Table 3.4. Hence, the equivalent integer encoded text is obtained as follow.

20	10	20	40	20	30	40	40

Table 3.4: Integer encoded script

We implement the Laplace transform taking the above integer codes as following. Let's consider the following expression

$$\begin{aligned} t^{\alpha k+\beta-1}E^{(k)}_{\alpha,\beta}\left(\pm at^{\alpha}\right) &= \sum_{j=0}^{\infty}\frac{(j+k)!}{j!}\frac{(\pm a)^j t^{\alpha j+\alpha k+\beta-1}}{\Gamma(\alpha j+\alpha k+\beta)} \\ &= \frac{(0+k)!}{0!}\frac{(\pm a)^0 t^{\alpha\cdot 0+\alpha k+\beta-1}}{\Gamma(\alpha\cdot 0+\alpha k+\beta)} \\ &+ \frac{(1+k)!}{1!}\frac{(\pm a)^1 t^{\alpha\cdot 1+\alpha k+\beta-1}}{\Gamma(\alpha\cdot 1+\alpha k+\beta)} \\ &+ \frac{(2+k)!}{2!}\frac{(\pm a)^2 t^{\alpha\cdot 2+\alpha k+\beta-1}}{\Gamma(\alpha\cdot 2+\alpha k+\beta)} \\ &+ \cdots+\frac{(n+k)!}{n!}\frac{(\pm a)^n t^{\alpha n+\alpha k+\beta-1}}{\Gamma(\alpha n+\alpha k+\beta)}+\cdots, \end{aligned} \tag{3.3}$$

where $\alpha,\beta>0$ and $a\in\mathbb{R}^+$.

Assume that

$$\begin{aligned} &G_0=20, \quad G_1=10, \quad G_2=20, \\ &G_3=40, \quad G_4=20, \quad G_5=30, \\ &G_6=40, \quad G_7=40, \quad G_n=0, \quad \text{for } n\geq 8. \end{aligned}$$

By choosing $\alpha=2$, $\beta=1$, $k=0$ and $a=2$ in (3.3), we can suppose that,

$$\begin{aligned} f(t)=GE_{2,1}\left(2t^2\right) &= \sum_{k=0}^{\infty}\frac{G_k\cdot\left(2t^2\right)^k}{\Gamma(2k+1)}=\sum_{k=0}^{\infty}\frac{G_k\cdot 2^k t^{2k}}{(2k)!} \\ &= \frac{G_0\cdot 2^0 t^0}{0!}+\frac{G_1\cdot 2^1 t^2}{2!}+\frac{G_2\cdot 2^2 t^4}{4!} \\ &+ \frac{G_3\cdot 2^3 t^3}{3!}+\frac{G_4\cdot 2^4 t^4}{4!}+\frac{G_5\cdot 2^5 t^5}{10!} \\ &+ \frac{G_6\cdot 2^6 t^6}{12!}+\frac{G_7\cdot 2^7 t^7}{14!}+\frac{G_8\cdot 2^8 t^8}{16!}+\cdots \\ &= 15+17\cdot\frac{2t^2}{2!}+14\cdot\frac{2^2t^4}{4!}+5\cdot\frac{2^3t^6}{6!} \\ &+ 4\cdot\frac{2^4t^8}{8!}+18\cdot\frac{2^5t^{10}}{10!}+18\cdot\frac{2^6t^{12}}{12!} \\ &+ 14\cdot\frac{2^7t^{14}}{14!}+17\cdot\frac{2^8t^{16}}{16!}. \end{aligned}$$

By applying Laplace transform to both sides, we get

$$\begin{aligned} L\{f(t)\} &= L\{GE_{2,1}\left(2t^2\right)\} \\ &= L\left\{20+10\cdot\frac{2t^2}{2!}+20\cdot\frac{2^2t^4}{4!}+\cdots+40\cdot\frac{2^7t^{14}}{14!}\right\} \\ &= \frac{20}{s}+\frac{20}{s^3}+\frac{80}{s^5}+\frac{320}{s^7}+\frac{320}{s^9}+\frac{960}{s^{11}}+\frac{2560}{s^{13}}+\frac{5120}{s^{15}}. \end{aligned}$$

By taking modulo 128 on 20, 20, 80, 320, 320, 960, 2560, 5120, we have sequence which consists of 20, 20, 80, 64, 64, 64, 0, 0.

We transform each of these integer into their equivalent ASCII values (7 bit binary) and then apply cumulative XOR operation repetitively until one bit is obtained. The technique is explicated taking binary stream corresponding to 20, i.e. 0010100 on Figure 3.1.

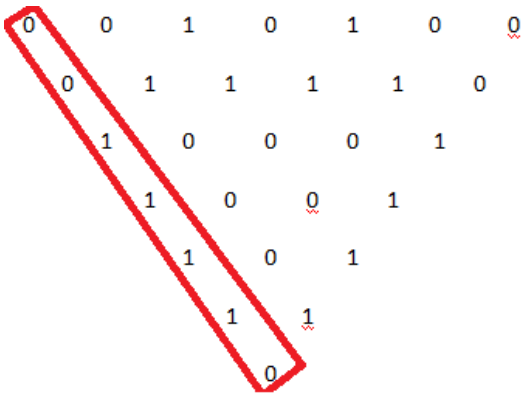

Figure 3.1: Cumulative XOR Method on Binary sequence corresponding to 20 and MSB collection

Hence, the binary version of the encoded cipher character equivalent to 20 is 0011110. By applying similar method to another values, we obtain the following table.

Laplace Coefficients	Binary Equivalents	Cumulative XOR	Cipher Text (ASCII)	Cipher Text (Character)
20	0010100	0011110	30	∧∧
20	0010100	0011110	30	∧∧
80	1010000	1100110	102	*f*
64	0101000	1111111	127	*LeD*
64	0101000	1111111	127	*LeD*
64	0101000	1111111	127	*LeD*
0	0000000	0000000	0	∧@
0	0000000	0000000	0	∧@

Table 3.5: Binary sequences corresponding to Laplace coefficients and their equivalent cipher characters

Therefore, secret message equivalent to ”Go” is ”∧∧∧∧fLeDLeDLeD∧@∧@”.

3.2. Decryption

The encrypted text characters in respect of the ASCII values correspond to 30, 30, 102, 127, 127, 127, 0 and 0. We transform these values into their 7 binary bit streams and apply cumulative XOR operation to them to generate binary sequences corresponding to Laplace coefficients. Therefore, we transform these coefficients back to their decimal values and perform the inverse Laplace transform as follows.

We take into consideration

$$\begin{aligned} G\frac{s}{s^2-2} &= \frac{15}{s}+\frac{34}{s^3}+\frac{56}{s^5}+\frac{40}{s^7}+\frac{64}{s^9}+\frac{576}{s^{11}}+\frac{1152}{s^{13}}+\frac{1792}{s^{15}}+\frac{4352}{s^{17}} \\ &= \sum_{j=0}^{\infty}\frac{q_j}{s^{2j+1}}. \end{aligned} \tag{3.4}$$

By applying inverse Laplace transform to both sides of (3.4), we obtain

$$\begin{aligned} GE_{2,1}\left(2t^2\right) &= 20\cdot 2^0+\frac{10\cdot 2^1\cdot t^2}{2!}+\frac{20\cdot 2^2\cdot t^4}{4!} \\ &+ \frac{40\cdot 2^3\cdot t^6}{6!}+\frac{20\cdot 2^4\cdot t^8}{8!}+\frac{30\cdot 2^5\cdot t^{10}}{10!} \\ &+ \frac{40\cdot 2^6\cdot t^{12}}{12!}+\frac{40\cdot 2^7\cdot t^{14}}{14!}. \end{aligned}$$

Consequently, we get $G_0=20$, $G_1=10$, $G_2=20$, $G_3=40$, $G_4=20$, $G_5=30$, $G_6=40$ and $G_7=40$.

Thus, integer values corresponding to DNA nucleotides are 20, 10, 20, 40, 20, 30, 40 and 40 which are transformed back to their equivalent bases by utilizing Table 3.5.

As a result, the DNA encoded text is coverted to $CACTCGTT$ and utilizing Table 3.1 the binary sequence of original message is transformed to 0100011101101111.

Finally, we decompose the binary sequence into corresponding ASCII equivalent which generates the ASCII values of "G" and "o" are 71 (01000111) and 111 (01101111), respectively. Therefore, the original message "Go" is obtained.

Example 3.1. *Assume the plain text be string 'PROFESSOR'. By applying our results in section 3, we have the following secret messages*

(1) $'\wedge\wedge\wedge J\wedge\wedge"\wedge\wedge\wedge T""'$ *for* $a = 1$, $k = 0$,
(2) $'\wedge\wedge\wedge\wedge <*R4\wedge QLeD'$ *for* $a = 1$, $k = 1$,
(3) $'\wedge\wedge\wedge T4;aF\,];'$ *for* $a = 3$, $k = 0$,
(4) $'Df\,3LeD\,]*LeD\wedge@'$ *for* $a = 3$, $k = 3$,
(5) $'U*U\wedge@LeDLeD\wedge@\wedge@'$ *for* $a = 5$, $k = 5$.

The results in Example 3.1 can be obtained by utilizing the codes below, which we write by the help of Python 3.8.5.

```
import string
import math
import re
string.ascii_lowercase

alph = list(string.ascii_lowercase)

ascii_char_dic = {
        "0":"^@", "1":"^A", "2":"^B", "3":"^C", "4":"^D",
        "5":"^E", "6":"^F", "7":"^G", "8":"^H", "9":"^I",
        "10":"^J", "11":"^K","12":"^L", "13":"^M", "14":"^N",
        "15":"^O", "16":"^P","17":"^Q", "18":"^R", "19":"^S",
        "20":"^T", "21":"^U", "22":"^V", "23":"^W", "24":"^X",
        "25":"^Y", "26":"^Z", "27":"^[", "28":"^'\'", "29":"^]",
        "30":"^^", "31":"^_", "32":" __", "33":"!", "34":" " ",
        "35":"#", "36":"$", "37":"%", "38":"&", "39": "'", "40":"(",
        "41":")", "42":"*", "43":"+", "44":",", "45":"-", "46":".",
        "47":"/", "48":"0", "49":"1", "50":"2", "51":"3", "52":"4",
        "53":"5", "54":"6", "55":"7", "56":"8", "57":"9", "58":":",
        "59":";", "60":"<", "61":"=", "62":">", "63":"?", "64":"@",
        "65":"A", "66":"B", "67":"C", "68":"D", "69":"E", "70":"F",
        "71":"G", "72":"H", "73":"I", "74":"J", "75":"K", "76":"L",
        "77":"M", "78":"N", "79":"O", "80":"P", "81":"Q", "82":"R",
        "83":"S", "84":"T", "85":"U", "86":"V", "87":"W", "88":"X",
        "89":"Y", "90":"Z", "91":"[", "92":"'\'", "93":"]", "94":"^",
        "95":"_", "96":'`', "97":"a", "98":"b", "99":"c", "100":"d",
        "101":"e", "102":"f", "103":"g", "104":"h", "105":"i", "106":"j",
        "107":"k", "108":"l", "109":"m", "110":"n", "111":"o", "112":"p",
        "113":"q", "114":"r", "115":"s", "116":"t", "117":"u", "118":"v",
        "119":"w", "120":"x", "121":"y", "122":"z", "123":"{", "124":"|",
        "125":"}", "126":"~", "127":"LeD"
}

def binary_operator(i):
    list_3 = []
    while i >= 1:
         list_3.append(i % 2)
         i = i // 2
    return list_3[::-1]

def xor(list_z):
    list_ex = []
    for i in range(len(list_z)):
        if i < len(list_z)-1:
            list_ex.append(list_z[i] ^ list_z[i+1])
    return list_ex

def cumulative_xor(list_z):
    list_xor = []
    while len(list_z) > 0:
         list_xor.append(list_z[0])
         list_z = xor(list_z)
    return list_xor
```

```
def cipher_numbers(list_y):
    list_sum = []
    for i in range(len(list_y)):
        list_sum.append((2**(len(list_y)-1-i))*list_y[i])
    return sum(list_sum)

def dna_privatekey_general(list_manipulated, list_mod):
     list_dna_privatekey = [int((i-j) / 128) for i, j in zip(list_manipulated, list_mod)]
     return list_dna_privatekey

def dna_encryption_general(a, n):
    dic_nucleoid_binary = {"00":"A", "01":"C", "10":"G", "11":"T"}
    dic_nucleoid_dec = {"A":10, "C":20, "G":30, "T":40}
    mes = input("Please enter an message for encryption: ")
    mes2 = list(mes)
    ascii_list = [ord(i) for i in mes2]
    list_binary = []
    for i in ascii_list:
        x = [str(j) for j in [0] + binary_operator(i)]
        y = "".join(x)
        list_binary.append(y)
   list_bin = []
   for i in list_binary:
      for j in i:
          list_bin.append(j)
   list_bin_2 = []
   for i in range(0, len(list_bin), 2):
        j = list_bin[i] + list_bin[i+1]
        list_bin_2.append(j)
   list_nucleoid = []
   for i in list_bin_2:
        list_nucleoid.append(dic_nucleoid_binary[i])
   list_coff = []
for i in list_nucleoid:
    list_coff.append(dic_nucleoid_dec[i])
list_manipulated =  [int(list_coff[i]*(math.factorial(i+n)/(math.factorial(i))*(a**i)))
                     for i in range(len(list_coff))]
list_mod = [i % 128 for i in list_manipulated]
 list_bin_3 = []
for i in list_mod:
    list_bin_3.append(binary_operator(i))
list_bin_4 = []
for j in list_bin_3:
   if len(j) < 7:
      if j != []:
           list_bin_4.append((7-len(j))*[0] + j)
       else:
           list_bin_4.append(7*[0] + j)
   else:
       list_bin_4.append(j[0:7])

list_cum_xor = []

for i in list_bin_4:
    list_cum_xor.append(cumulative_xor(i))

list_cipher_numbers = []
for i in list_cum_xor:
    list_cipher_numbers.append(cipher_numbers(i))
list_encrypted = []
for i in list_cipher_numbers:
    list_encrypted.append(ascii_char_dic[str(i)])
list_binary_full = [i for i in list_cum_xor]
list_binary_full_2 = [j for i in list_cum_xor for j in i]
list_binary_plain = [j for i in list_bin_4 for j in i]
```

```
print("*"*114)
print("Your encrypted message is: ", "".join(list_encrypted))
print("*"*114)
print("Your encrypted list is:", list_encrypted)
print("*"*114)
print("Your private key is:", dna_privatekey_general(list_manipulated, list_mod))
print("*"*114)
#print(list_binary)
#print(list_bin)
#print(list_cum_xor)
#print(list_coff)
print("DNA bases:",list_nucleoid)
print("*"*114)
#print(list_binary_full)
#print(list_binary_plain)
print("Results of monobit test:")
print(monobit_test(list_binary_full))
print("*"*114)
print("phi test:", phi_test(list_binary_plain, list_binary_full_2))



def dna_decryption_general(a, n):
    dic_nucleoid_binary = {"00":"A", "01":"C", "10":"G", "11":"T"}
    dic_nucleoid_dec = {"A":10, "C":20, "G":30, "T":40}
    dmes = input("Please enter an secret message for decryption: ")
    dna_privatekey = input("Please enter private key: ").split(", ")
    dna_list_privatekey = [int(i) for i in dna_privatekey]
    #print("dna_list_privatekey",dna_list_privatekey)
    #dmes_list = dmes.split(", ")
    string_list = list(re.findall(r"'(.*?)'", ''.join(dmes)))
    #print(string_list)
    #print("string_list", string_list)
    list_keys = []
    for i in string_list:
        for k, l in ascii_char_dic.items():
            if i == l:
                list_keys.append(k)
    #print("list_keys",list_keys)
    list_keys_num = [int(i) for i in list_keys]
    #print("list_keys_num",list_keys_num)
    list_binary_x = [binary_operator(i) for i in list_keys_num]
    #print("list_binary_x",list_binary_x)
    list_binary_xor = []
    for j in list_binary_x:
       if len(j) < 7:
          if j != []:
              list_binary_xor.append((7-len(j))*[0] + j)
          else:
              list_binary_xor.append(7*[0] + j)
      else:
          list_binary_xor.append(j[0:7])
    #print("list_binary_xor",list_binary_xor)
    list_binary_y = [cumulative_xor(i) for i in list_binary_xor]
    #print("list_binary_y",list_binary_y)
    list_ciphers = [cipher_numbers(i) for i in list_binary_y]
    #print("list_ciphers",list_ciphers)
    list_dec = [i + 128*j for i, j in zip(list_ciphers,  dna_list_privatekey)]
    #print("list_dec",list_dec)
    list_manipulated = [int(list_dec[i] / (math.factorial(i+n)/(math.factorial(i))*(a**i)))
                        for i in range(len(list_dec))]
    #print("list_manipulated",list_manipulated)
    list_dna_nucleoid = []
    for i in list_manipulated:
        for k, l in dic_nucleoid_dec.items():
           if i == l:
```

```
            list_dna_nucleoid.append(k)
#print("list_dna_nucleoid",list_dna_nucleoid)
list_dna_binary = []
for i in list_dna_nucleoid:
    for k, l in dic_nucleoid_binary.items():
        if i == l:
            list_dna_binary.append(k)
#print("list_dna_binary",list_dna_binary)
list_final_bef = []
for i in range(0, len(list_dna_binary), 4):
     list_final_bef.append(list_dna_binary[i:i+4])
#print("list_final_bef",list_final_bef)
list_final = []
for j in list_final_bef:
    list_final.append("".join(j))
#print("list_final",list_final)
list_sum = []
for j in list_final:
    list_num = [int(i) for i in j]
    list_sum.append(cipher_numbers(list_num))
#print("list_sum",list_sum)
list_final_words = []
for i in list_sum:
     for k, l in ascii_char_dic.items():
         if str(i) == k:
            list_final_words.append(l)
print("DNA bases:", list_dna_nucleoid)
print("The original message: " + "".join(list_final_words))
```

Before using phi coefficient test and monobit test for the results above, we want to provide some information on these test.

Numerous studies have been done to examine the reliability of a cryptographic algorithm. Inhomogeneity, frequency distribution, and bit rate are usually utilized reliability techniques. The technique to be performed in this article is the monobit test. The monobit test is utilized to determine whether the frequency of 0's and 1's in bit sequences in the encrypted text. Let and represent the number of 0's and 1's in bit sequences respectively. The calculated value obtained with is compared with the critical of value at 1 degree of freedom. If the calculated values of value is smaller than the critical of value, it means that the bit sequences passed the monobit test. The formula of the Monobit test is denoted by

$$\chi^2 = \frac{(n_0 - n_1)^2}{n},$$

where n_0, n_1 and n represent the number of zeroes, ones, and both of them, respectively [39].

Correlation analysis used in statistics investigates whether there is a relationship between two or more variables. The phi coefficient will be utilized to find the correlation value. The phi coefficient is the coefficient of the relationship between two variables with a binary data structure. The goal is to get a completely different or low relationship between plain text and cipher text. If the obtained phi coefficient approaches 1, there is a strong relationship between them. If the phi coefficient approaches 0, there is a very weak relationship between them [40–42].

By using the table as follows,

	$y=1$	$y=0$	$total$
$x=1$	n_{11}	n_{10}	$n_{1\cdot}$
$x=0$	n_{01}	n_{00}	$n_{0\cdot}$
$total$	$n_{\cdot 1}$	$n_{\cdot 0}$	n

Table 3.6: 2×2 table for two random variables x and y

we get the following phi coefficient formula

$$\phi = \frac{n_{11}n_{00} - n_{10}n_{01}}{\sqrt{n_{\cdot 1}n_{\cdot 0}n_{1\cdot}n_{0\cdot}}},$$

where n_{11}, n_{10}, n_{01} and n_{00} denote the observation frequencies.

By utilizing the monobit test and correlation analysis, we have the following results for cipher texts in Example 3.1.

Cipher Text	Calculated value		Calculated value	
	Phi Coefficient	Monobit Test	Phi Coefficient	Monobit Test
∧∧∧J∧∧”∧∧∧T””	0.464150	2.571428	0.5	3.8415
∧∧∧∧<*R4∧QLeD	0.410720	0.285714	0.5	3.8415
∧∧∧T4;aF];	0.292307	0.285714	0.5	3.8415
Df 3LeD]*LeD∧@	0.083333	1.142857	0.5	3.8415
U∗U∧@LeDLeD∧@∧@	0.203653	0.642857	0.5	3.8415

Table 3.7: Results for Monobit Test and Correlation Analysis

The values of Table 3.7 can be attained by utilizing following codes, which we write by means of Python 3.8.5.

```
def phi_test(list_1, list_2):
    list_3 = [i for i in zip(list_1, list_2)]
    list_oo = [i for i in list_3 if i == (1,1)]
    list_oz = [i for i in list_3 if i == (1,0)]
    list_zz = [i for i in list_3 if i == (0,0)]
    list_zo = [i for i in list_3 if i == (0,1)]
    list_po = [i for i in list_3 if i[1] == 1]
    list_pz = [i for i in list_3 if i[1] == 0]
    list_op = [i for i in list_3 if i[0] == 1]
    list_zp = [i for i in list_3 if i[0] == 0]
    a = (len(list_oo)*len(list_zz)) - (len(list_oz)*len(list_zo))
    b = math.sqrt(len(list_op)*len(list_zp)*len(list_po)*len(list_pz))
    phi = a / b
    return phi

def monobit_test(list_ex):
    list_z = []
    list_zeros = []
    list_ones = []
    for i in list_ex:
        for j in i:
            list_z.append(j)
    for k in list_z:
        if k == 0:
            list_zeros.append(k)
    elif k == 1:
        list_ones.append(k)
    chi = (len(list_zeros) - len(list_ones))**2 / (len(list_zeros) + len(list_ones))
    print("Zeros:",len(list_zeros))
    print("Ones:",len(list_ones))
    print(chi)
```

The computed values of χ^2 and ϕ are less in relation to critical values of them. This implies that these binary streams corresponding to cipher texts pass the Monobit test and correlation analysis in respect of phi coefficient. According to the correlation analysis, it is seen that there is a weak relationship between the first text and the last text. In addition, the values obtained in the Monobit test show the power of the function and transformation used.

4. Conclusions

In this study, a text that was handled by using DNA codes effectively was encrypted using the Mittag-Leffler function and Laplace transform, and a new text with different characters was obtained. Here, the strength of the password created by applying the XOR operation in the method has been increased. The difference of this study is the simultaneous use of the Mittag-Leffler function and the Laplace transform. At the end of the study, the reliability of the encryption technique was checked with the Monobit test. The results obtained are quite good. In addition, with the correlation test, it was examined whether there was a relationship between the first and the last text. As a result of this examination, it was seen that there was an acceptable, weak relationship..

Article Information

Acknowledgements: The authors would like to thank the referees for their contribution to the development of the article.

Author's contributions: The authors have no conflicts of interest to declare. All co-authors have seen and agree with the contents of the manuscript and there is no financial interest to report.

Conflict of interest disclosure: No potential conflict of interest was declared by the author.

Copyright statement: Authors own the copyright of their work published in the journal and their work is published under the CC BY-NC

4.0 license.

Supporting/Supporting organizations: No grants were received from any public, private or non-profit organizations for this research.

Ethical approval and participant consent: It is declared that during the preparation process of this study, scientific and ethical principles were followed and all the studies benefited from are stated in the bibliography.

Plagiarism statement: This article was scanned by the plagiarism program. No plagiarism detected.

Availability of data and materials: Not applicable.

References

[1] G. N. Lakshmi, B.R. Kumar, A.C. Sekhar, *A cryptographic scheme of Laplace transforms*, Int. J. Math. Arch., **2** (12) (2011), 2515-2519.
[2] A. P. Stakhov, *The golden section in the measurement theory*, Comput. Math. Appl., **17** (4-6) (1989), 613–638.
[3] A. P. Stakhov, *The "golden" matrices and a new kind of cryptography*, Chaos, Solit. Fractals, **32** (3) (2007), 1138–1146.
[4] T. H. Barr, *Invitation to Cryptology*, Pearson, Prentice Hall, 2002.
[5] J. A. Buchmann, *Introduction to Cryptography*, New York, Springer, 2009.
[6] E. Cole, R. Krutz, J.W. Conley, *Network Security Bible*, Indianapolis, Wiley Publishing, 2009.
[7] W. Stallings, *Network Security Essentials: Applications and Standards*, Boston, Prentice Hall, 2001.
[8] W. Stallings, *Cryptography and Network Security*, London, Pearson Education Ltd, 2005.
[9] A. Stanoyevitch, *Introduction to Cryptography with Mathematical Foundations and Computer Implementations*, Boca Raton, CRC Press, 2010.
[10] Z. M. Z Muhammad, F. Özkaynak, *Security problems of chaotic image encryption algorithms based on cryptanalysis driven design technique*, IEEE Access, **7** (2019), 99945-99953.
[11] F. Özkaynak, A. B. Özer, *Cryptanalysis of a new image encryption algorithm based on chaos*, Optik, **127** (13) (2016), 5190-5192.
[12] G. A. Dhanorkar, A. P. Hiwarekar, *A generalized Hill cipher using matrix transformation*, Int. J. Math. Sci. Eng. Appl., **5** (4) (2011), 19-23.
[13] J. Overbey, W. Traves, J. Wojdylo, *On the keyspace of the Hill cipher*, Cryptologia, **29** (1) (2005), 59-72.
[14] S. Saeednia, *How to make the Hill cipher secure*, Cryptologia, **24** (4) (2000), 353-360.
[15] A. P. Hiwarekar, *A new method of cryptography using Laplace transform*, Int. J. Math. Arch., **3** (3) (2012), 1193-1197.
[16] A. P. Hiwarekar, *A new method of cryptography using Laplace transform of hyperbolic functions*, Int. J. Math. Arch., **4** (2) (2013), 208-213.
[17] A. P. Hiwarekar, *Application of Laplace transform for cryptographic scheme*, Proc. World Congr. Eng., **1** (2013), 1-6.
[18] J. D. Watson, F.H.C. Crick, *Molecular structure of nucleic acids: a structure for deoxyribose nucleic acid*, Am. J. Psychiatry, **160** (4) (2003), 623-624.
[19] G. Cui, L. Qin, Y. Wang, X. Zhang, *Information security technology based on DNA computing*, ASID, (2007) 288-291.
[20] G. Z. Cui, Y. Liu, X. Zhang, *New direction of data storage: DNA molecular storage technology*, Comput. Eng. Appl., **42** (26) (2006), 29-32.
[21] X. Wang, Q. Zhang, *DNA computing-based cryptography*, Fourth Int. Conf. Bio-Inspired Comput., (2009), 1-3.
[22] L. M. Adleman, *Molecular computation of solutions to combinatorial problems*, Science, **266** (5187) (1994) 1021-1024.
[23] C. T. Clelland, V. Risca, C. Bancroft, *Hiding messages in DNA microdots*, Nature, **399** (6736) (1999), 533-534.
[24] S. Som, M. Som, *DNA secret writing with Laplace transform*, Int. J. Comput. Appl., **975** (8887) (2012), 43-50.
[25] R. J. Lipton, *Using DNA to solve NP-complete problems*. Science, **268** (4) (1995), 542-545.
[26] S. T. Amin, M. Saeb M, S. El-Gindi, *A DNA-based implementation of YAEA encryption algorithm*, Comput. intel., (2006), 120-125.
[27] D. G. Zill, *Advanced Engineering Mathematics, Burlington*, Jones & Bartlett Learning, 2020.
[28] R. P. Boas Jr, *Higher transcendental functions*, Science, **122** (3163) (1955), 290-290.
[29] I. Podlubny, *Fractional Differential Equations*, 198, San Diego, California, USA, Academic Press, 1999.
[30] G. M. Mittag-Leffler, *Sur la nouvelle fonction* $E_\alpha(x)$, C. R. Acad. Sci. Paris, **137** (2) (1903), 554-558.
[31] G.M. Mittag-Leffler, *Sopra la funzione* $E_\alpha(x)$, Rend. Acad. Dei Lincei, **13** (5) (1904), 3-5.
[32] G. M. Mittag-Leffler, *Sur la represention analytique d'une branche uniforme d'une fonction monog´ene*, Acta Math., **29** (1) (1905), 101-181.
[33] A. Wiman, *Über den fundamentalsatz in der teorie der funktionen* $E_a(x)$, Acta Math., **29** (1) (1905), 191-201.
[34] A. Wiman, *Über die nulstellen der funktionen* $E_a(x)$, Acta Math., **29** (1) (1905), 217-234.
[35] R. P. Agarwal, *A propos d'une note de M Pierre Humbert*, C. R. Acad. Sci., **236** (21) (1953), 2031-2032.
[36] P. Humbert, R.P. Agarwal, *Sur la fonction de Mittag-Leffler et quelques-unes de ses g´en´eralisitions*, Bull. des Sci. Math., **77** (2) (1953), 180-185.
[37] M. M. Dzhrbashyan, *Integral Transforms and Representations of Functions in the Complex Domain*, Moscow, Nauka (in Russian), 1966.
[38] R. Garrappa, M. Popolizio, *Computing the matrix Mittag-Leffler function with applications to fractional calculus*, J. Sci. Comput., **77** (1) (2018), 129-153.
[39] A. Ruk, *A statistical test suite for the validation of random number generators and pseudo-random number generators for cryptographic applications*, NIST, 2001.
[40] H. Cramer, *Mathematical Methods of Statistics*, Princeton, Princeton Univ Press, 1946.
[41] G. Nagalakshmi, A.C. Sekhar, N.R. Sankar, K. Venkateswarlu, *Enhancing the data security by using RSA algorithm with application of Laplace transform cryptosystem*, Int. J. Recent Technol. Eng., **8** (2) (2019), 6142-6147.
[42] B. W. Matthews, *Comparison of the predicted and observed secondary structure of T4 phage lysozyme*, Biochim. Biophys. Acta (BBA)-Protein Struct., **405** (2) (1975), 442-451.

Journal of Mathematical Sciences and Modelling, 6(3) (2023) 133-149
Research Article

Journal of Mathematical Sciences and Modelling

Journal Homepage: www.dergipark.gov.tr/jmsm
ISSN 2636-8692
DOI: http://dx.doi.org/10.33187/jmsm.1339842

A mathematical model with fractional order for obesity with positive and negative interactions and its impact on the diagnosis of diabetes

Erick Manuel Delgado Moya[1*], Alain Pietrus[2], Séverine Bernard[2] and Silvère Paul Nuiro[2]

[1]*School of Technology, Universidade Estadual de Campinas (UNICAMP), Brazil*
[2]*Department of Mathematics and Computer Sciences,University of Antilles, France*
[*]*Corresponding author*

Article Info

Keywords: *Diabetes, Caputo sense, Model, Obesity, Overweight*
2010 AMS: *92D30, 26A33, 92C50*
Received: *10 August 2023*
Accepted: *30 November 2023*
Available online: *5 December 2023*

Abstract

Overweight and obesity are current problems humankind faces and have serious health consequences because they contribute to diseases such as heart diseases and diabetes. In this paper, we present a mathematical model for the study of overweight and obesity in a population and its impact on the growth of the number of diabetics. For the construction of the model, we take into account social factors and the interactions between different elements of society. We use fractional-order derivatives in the Caputo sense because of the advantages of this type of technique with respect to the memory effect, and it shows different behaviors depending on the fractional order. We find the basic reproduction number and prove the local and global stability of the disease-free equilibrium points. We study the sensitivity index with respect to the basic reproduction number for parameters associated with weight gain due to social pressure and the rate of diagnosis of diabetes not associated with body weight. To validate the model, we perform computational simulations with data extracted from the literature. We conclude that for higher fractional orders a higher value of the basic reproduction number was reached. We show that at the end of the study for different fractional orders that normal-weight individuals are decreasing, and overweight, obese, and diabetic people are increasing.

1. Introduction

In 2016, more than 1.9 billion adults were overweight, and among them, more than 650 million were obese worldwide. As a result, diseases associated with overweight and obesity have also been on the rise globally [1].
To determine body weight state, we use the body mass index (BMI), which is defined as [2]:

$$BMI = \frac{\text{weight}}{\text{height}^2}.$$

Then, individuals are considered of normal-weight when $BMI \in [18.6, 24.9]$, overweight individuals are when $BMI \in [25, 29.9]$, obese individuals are when $BMI \in [30, 40]$, and in complicated situations over 40. We know that the body mass index can be high in people with high muscle mass but we assume that these cases are not included because before calculating the BMI we do a preliminary analysis. The root cause of obesity and overweight is an energy imbalance between calories consumed and calories expended.
A poorly balanced diet, stress, sedentary lifestyle, and factors such as environmental changes, and lack of sanitation in sectors such as agriculture, environment, processing, distribution, and marketing of food cause an increase in the number of cases of overweight and obesity in the population [1]. We have two types of diabetes and among their differences is that type I diabetes is primarily diagnosed by genetic disorders and usually manifests itself at an early age and type 2 diabetes is mainly related to lifestyle and develops over time. We also have

***Email addresses and ORCID numbers*: erickdelgadomoya@gmail.com, 0000-0001-5937-5374 (E. Moya), alain.pietrus@univ-antilles.fr, 0009-0005-8064-4950 (A. Pietrus), severine.bernard@univ-antilles.fr, 0000-0001-8493-9821 (S. Bernard), paul.nuiro@univ-antilles.fr, 0000-0002-9537-7913 (S. Nuiro)**
Cite as "E. M. Delgado Moya, A. Pietrus, S. Bernard, S. P. Nuiro, *A mathematical model with fractional order for obesity with positive and negative interactions and its impact on the diagnosis of diabetes*, J. Math. Sci. Model., 6(3) (2023), 133-149"

cases where the continuous use of medications can develop diabetes [3, 4]. Among the factors that lead to type 2 diabetes is obesity. The likelihood of developing type 2 diabetes as well as its severity increases with obesity. The risk of developing type 2 diabetes in people with obesity is 7 times higher and in overweight people 3 times higher than in people with normal-weight and a healthy lifestyle [4, 5].
In recent years, the use of mathematical models to study the dynamics of obesity and overweight has increased [6]-[10]. Ejima et al. [6] presented a mathematical model that studies the genetic and non-genetic effects that lead to obesity and among the results they obtained was that homozygous individuals are more susceptible to both the risk of social contagion and the risk of spontaneous weight gain. Kim and So-Yeun Kim [7] with the inclusion of psychological and social factors proposed a mathematical model for the dynamics of obesity. Paudel [8] proposed a model for the dynamics of obesity with a SIR structure and analyzed the effect of the social network on the spread of obesity. Al-Tuwairqi and Matbouli [9] proposed two mathematical models to study the impact of fast food on the increase in obesity and the role of physical activity. Pietrus et al. [10] developed a mathematical model to study the impact of media on the dynamics of obesity in a population. Model proposals for the study of the impact of diabetes on a population have increased in recent decades [11]-[15]. For example, Dubey and Goswami [11] presented a model of diabetes and its complications using a fractional operator. Sandhya and Kumar [12] proposed a mathematical model for the study of diabetes mellitus with the presence of plasma glucose concentration, generalized insulin, and plasma insulin concentration. Anusha and Athithan [13] proposed a mathematical model for type 2 diabetes and stratified the population into susceptible, unbalanced glucose level (IGL), treatment, and restriction. Banzi et al. [14] presented a mathematical model to investigate the behavior of glucose, insulin, glucagon, stored insulin, and labile insulin in diabetics. Delgado et al. [15] presented a deterministic compartmental model that studies overweight, obesity, and diabetes in a population, taking into account the negative impact of an overweight or obese individual on a normal-weight individual, and also the impact of social pressure on the increase of overweight and obese cases and consequently the increase of diabetes diagnosis.
The aim of this work is to present a mathematical model using fractional-order derivatives in the Caputo sense for the study of obesity and, as a consequence, diabetes in a population. This model has as its main center the positive impact of the contact of an individual with normal-weight with an overweight and the inverse negative impact. It also studies the impact of pressure on the increase in cases of overweight and obesity. It allows us to quantify in the dynamics of how overweight and obesity increase the diagnosis of diabetes, also take into account that other factors not associated with body weight can cause new cases of diabetes.
This paper is organized as follows: In Section 2, we present the mathematical definitions used in the paper. In Section 3, we introduce the model, show the basic properties and study the basic reproduction number. Section 4 is devoted to numerical experimentation. We finish the paper with some conclusions in Section 5.

2. Theorical Background

The following definitions are used to formulate and study the fractional-order model.
We assume that $\alpha \in \mathbb{R}_+$, $b > 0$, $f \in AC^n[a,b]$ (absolutely continuous), and $n = [\alpha]$ (entire part of α). We define the left-sided and right-sided fractional integral Riemann-Louville for $f : \mathbb{R}^+ \longrightarrow \mathbb{R}$ and $\alpha > 0$ are:

$$ {}_a\mathbb{I}_t^\alpha f(t) := \frac{1}{\Gamma(\alpha)} \int_a^t \frac{f(s)ds}{(t-s)^{1-\alpha}}, \qquad \text{(Left)} $$

$$ {}_t\mathbb{I}_b^\alpha f(t) := \frac{1}{\Gamma(\alpha)} \int_t^b \frac{f(s)ds}{(s-t)^{1-\alpha}} \qquad \text{(Right)} $$

where Γ is Gamma function, and we define $\mathbb{I}_t^\alpha f(t) = {}_0\mathbb{I}_t^\alpha f(t)$.
The left-sided and right-sided Riemann–Liouville fractional derivatives are defined as [16, 17]:

$$ {}_a\mathbf{D}_t^\alpha f(t) = \frac{d^n}{dt^n}\left(\frac{1}{\Gamma(n-\alpha)} \int_a^t (t-s)^{n-\alpha-1} f(s)ds\right), \qquad \text{(Left)} $$

$$ {}_t\mathbf{D}_b^\alpha f(t) = \frac{d^n}{dt^n}\left(\frac{(-1)^n}{\Gamma(n-\alpha)} \int_t^b (s-t)^{n-\alpha-1} f(s)ds\right) \qquad \text{(Right)} $$

and we denote $\mathbf{D}_t^\alpha f(t) = {}_0\mathbf{D}_t^\alpha f(t)$.
The left-sided and right-sided fractional derivatives proposed by Caputo are given by [16, 17]:

$$ {}_a^c\mathbb{D}_t^\alpha f(t) = \frac{1}{\Gamma(n-\alpha)} \int_a^t (t-s)^{n-1-\alpha} f^{(n)}(s)ds, \qquad \text{(Left)} $$

$$ {}_t^c\mathbb{D}_b^\alpha f(t) = \frac{(-1)^n}{\Gamma(n-\alpha)} \int_t^b (s-t)^{n-1-\alpha} f^{(n)}(s)ds \qquad \text{(Right)} $$

and we define ${}^c\mathbb{D}_t^\alpha f(t) = {}_0^c\mathbb{D}_t^\alpha f(t)$.
In the order-fractional derivatives, we find the memory effect which is an important factor in epidemic modeling [18]-[20].
In recent decades, works have been presented where models with fractional orders are used and compared with real data and it has been obtained that they can capture real behaviors, see [21]-[24].

3. Model Formulation

The body mass index is a hasty diagnosis of overweight and obesity but we assume that we have a previous evaluation for the diagnosis of patients with these physical conditions. Then, based on the body mass index, we define the compartments of our model as: normal-weight individuals, S, overweight individuals, O_w, obese individuals, O_b and diabetic individuals, D.
We define the negative impact rate as

$$ \lambda_O = (\alpha^*)^\alpha \frac{(O_w + \varepsilon O_b)}{N}, $$

and positive impact rate as

$$\lambda_S = \frac{(\beta^*)^\alpha S}{N},$$

where α^* and β^* are the effective contact rate and N is the total population ($N = S + O_w + O_b + D$). These rates will represent the negative influence that an overweight or obese person has on a person with normal-weight, leading this person to increase his body weight and leave the compartment, and the positive influence that a person with normal-weight has on an overweight or obese person, who with an improvement in his lifestyle, decreases his body weight and passes through the different compartments. Let us assume that the effective contact rate in the negative effect (α^*) is greater than the effective contact rate in the positive effect (β^*). This means that leading a nutritionally disordered and/or sedentary life is easier than leading a nutritionally healthy life in addition to other elements such as physical exercise.

We assume that the impact of overweight and obese on a person with normal-weight is different, for this, we use the modification parameter ε such that $\varepsilon > 1$. The rates M_S and M_D represent the entry of individuals with normal-weight and diabetes respectively.

The mortality rate from natural causes in the population is defined as μ and we assume that it is the same from any compartment. We define d as the mortality rate associated with diseases related to increased body weight, mainly cardiac ones, and t_H represents the modification parameter for the obese and t_D for diabetics.

The rate α_1 characterizes cases diagnosed with diabetes due to causes that are not directly associated with weight gain including genetic, racial, hereditary, and other factors. Parameters α_2 and α_3 are the rates of diabetes diagnoses associated with overweight and obesity, respectively. The rate of death associated with diabetes is denoted by μ_D.

The rate δ characterize individuals who are overweight but improve to normal-weight and η is for obese individuals who become overweight. These two parameters are not related to the interaction with a normal-weight individual. Individuals who increase in body weight from overweight to obese are defined by the rate γ. The rate β_1 represents the social pressure that causes an individual with normal-weight to become obese. This rate is characterized by stress, lack of time for healthy eating and physical exercise, sedentary lifestyle, etc. The fractional derivative operator in the Caputo sense, ${}^c\mathbb{D}_t^\alpha$ has a dimension α, then on the right-hand side of the model all parameters will have power dimension α except the modification parameter [25]. So, the model that relates obesity to diabetes in a population using fractional derivatives in the Caputo sense is:

$$\begin{aligned}
{}^c\mathbb{D}_t^\alpha S &= M_S^\alpha + (\delta^\alpha + \lambda_S)O_w - (\mu^\alpha + \alpha_1^\alpha + \beta_1^\alpha + \lambda_O)S,\\
{}^c\mathbb{D}_t^\alpha O_w &= (\lambda_O + \beta_1^\alpha)S + \eta^\alpha O_b - (\lambda_S + \gamma^\alpha + \mu^\alpha + d^\alpha + \delta^\alpha + \alpha_2^\alpha)O_w,\\
{}^c\mathbb{D}_t^\alpha O_b &= \gamma^\alpha O_w - (\eta^\alpha + \mu^\alpha + t_H d^\alpha + \alpha_3^\alpha)O_b,\\
{}^c\mathbb{D}_t^\alpha D &= M_D^\alpha + \alpha_1^\alpha S + \alpha_2^\alpha O_w + \alpha_3^\alpha O_b - (\mu_d^\alpha + \mu^\alpha + t_D d^\alpha)D,
\end{aligned} \tag{3.1}$$

with initial condition

$$S(0) = S_0 \geq 0, O_w(0) = O_{w0} \geq 0, O_b(0) = O_{b0} \geq 0, D(0) = D_0 \geq 0 \text{ and with } \alpha \in (0,1].$$

Variable	Description
S	normal-weight individuals
O_W	Overweight individuals
O_b	Obese individuals
D	Diabetic individuals
Parameter	**Description**
M_S, M_D	Recruitment rates for normal-weight and diabetic individuals
α^*, β^*	Effective contact rates
d	death rate associated with weight gain
μ	Natural death rate
μ_d	Diabetes death rate
η	Rate of weight reduction from obese to overweight
γ	Rate of weight gain from overweight to obese
δ	Rate of weight reduction from overweight to normal-weight
α_1	Rate of diagnosis of diabetes not associated with body weight
α_2	Rate of diabetes diagnosis in overweight individuals
α_3	Rate of diagnosis of diabetes in obese individuals
β_1	Rate of weight gain associated with social factors
ε, t_D, t_H	Modification parameters

Table 3.1: Description of variables and parameters of model (3.1).

Basic properties of model (3.1)

Now, let us prove the existence and positivity of the solution of Model (3.1), and let's find the biologically feasible region. The following results and their proofs can be found in [26].

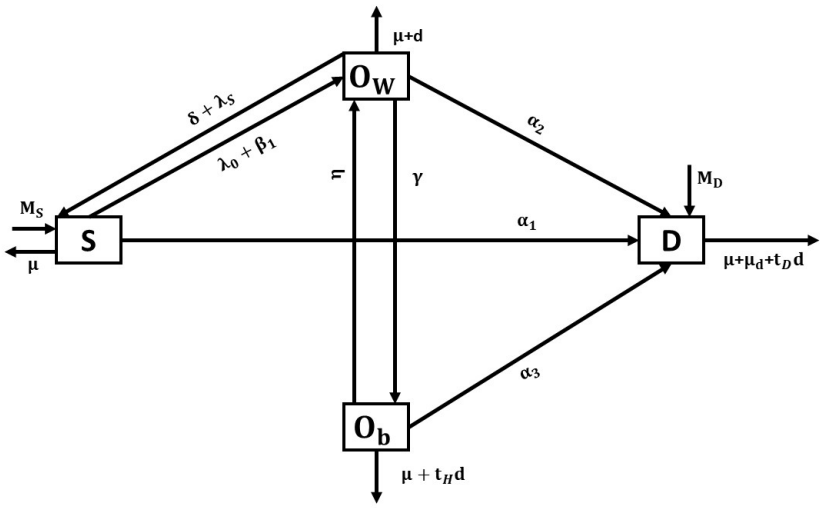

Figure 3.1: Flow chart of Model (3.1).

Existence and non-negativity of solutions

Let's denominate

$$\Omega = \{x = (S, O_w, O_b, D) : S, O_w, O_b, D \geq 0\}.$$

The following lemma and corollary will be used in the proof of Theorem (3.3) and can be found in [27]-[30].

Lemma 3.1. *(Generalized mean value theorem) Suppose that $f \in C[a,b]$ ($C[a,b]$ is the set of continuous functions on the interval $[a,b]$) and ${}^c\mathbb{D}_t^\alpha f \in C[a,b]$, for $\alpha \in (0,1]$. Then, for all $t \in (a,b]$, it exists $\varepsilon \in [a,t]$, such that*

$$f(t) = f(a) + \frac{1}{\Gamma(\alpha)}({}^c\mathbb{D}_t^\alpha f)(\varepsilon)(t-a)^\alpha.$$

Corollary 3.2. *Consider that $f \in C[a,b]$ and ${}^c\mathbb{D}_t^\alpha f \in C[a,b]$, for $\alpha \in (0,1]$. Then if*

- ${}^c\mathbb{D}_t^\alpha f(t) \geq 0$, $\forall t \in (a,b)$, *then $f(t)$ is non-decreasing for each $t \in [a,b]$,*
- ${}^c\mathbb{D}_t^\alpha f(t) \leq 0$, $\forall t \in (a,b)$, *then $f(t)$ is non-increasing for each $t \in [a,b]$.*

Theorem 3.3. *There is an unique solution $x = (S, O_w, O_b, D)^T$ of Model (3.1) for $t \geq 0$ and the solution will remain in Ω.*

Proof. By Theorem 3.1 and Remark 3.2 of [30], we have that the solution in $(0,\infty)$ of the initial value problem (3.1) exists and is unique. Now, we will prove the positivity of the solution of Model (3.1). In order to do this, we need to prove that for every hyperplane bounding the nonnegative orthant, the vector field points to Ω. From Model (3.1), we have:

$$\begin{aligned}
{}^c\mathbb{D}_t^\alpha S\big|_{S=0} &= M_S^\alpha + \delta^\alpha O_w > 0,\\
{}^c\mathbb{D}_t^\alpha O_w\big|_{O_w=0} &= \left(\frac{\varepsilon(\alpha^*)^\alpha O_b}{N} + \beta_1^\alpha\right)S + \eta^\alpha O_b \geq 0,\\
{}^c\mathbb{D}_t^\alpha O_b\big|_{O_b=0} &= \gamma^\alpha O_w \geq 0,\\
{}^c\mathbb{D}_t^\alpha D\big|_{D=0} &= M_D^\alpha + \alpha_1^\alpha S + \alpha_2^\alpha O_w + \alpha_3^\alpha O_b > 0.
\end{aligned}$$

Using Corollary 3.2, we have that the solution will remain in Ω. □

Biologically feasible region

Now, let's prove that Ω_α is the biologically feasible region for Model (3.1).

Lemma 3.4. *The closed set $\Omega_\alpha = \left\{(S, O_w, O_b, D) \in \mathbb{R}_+^4 : N \leq \frac{M_S^\alpha + M_D^\alpha}{\mu^\alpha}\right\}$ is positively invariant with respect to model (3.1).*

Proof. The fractional derivative in the Caputo sense of the total population is

$${}^c\mathbb{D}_t^\alpha N(t) = {}^c\mathbb{D}_t^\alpha S(t) + {}^c\mathbb{D}_t^\alpha O_w(t) + {}^c\mathbb{D}_t^\alpha O_b(t) + {}^c\mathbb{D}_t^\alpha D(t) = M_S^\alpha + M_D^\alpha - \mu^\alpha N(t) - d^\alpha(O_w(t) + t_H O_b(t) + t_D D(t)) - \mu_d^\alpha D(t),$$

and we have

$${}^c\mathbb{D}_t^\alpha N(t) + \mu^\alpha N(t) \leq M_S^\alpha + M_D^\alpha.$$

To continue the proof we use the following definitions:

Definition 3.5. *The Laplace transform of the Caputo fractional derivatives of the function $\phi(t)$ with order $\alpha > 0$ is defined as*

$$\mathscr{L}\left[{}^{c}\mathbb{D}_{t}^{\alpha}\phi(t)\right] = s^{\alpha}\phi(s) - \sum_{v=0}^{n-1}\phi^{(v)}(0)s^{\alpha-v-1}. \tag{3.2}$$

Definition 3.6. *The Laplace transform of the function $t^{\alpha_1-1}\mathbb{E}_{\alpha,\alpha_1}(\pm\lambda t^{\alpha})$ is defined as*

$$\mathscr{L}\left[t^{\alpha_1-1}\mathbb{E}_{\alpha,\alpha_1}(\pm\lambda t^{\alpha})\right] = \frac{s^{\alpha-\alpha_1}}{s^{\alpha}\mp\lambda}, \tag{3.3}$$

where $\mathbb{E}_{\alpha,\alpha_1}$ is two-parameters Mittag-Leffler function $\alpha,\alpha_1 > 0$. Further, the Mittag-Leffler function satisfies the following equation:

$$\mathbb{E}_{\alpha,\alpha_1}(f) = f\mathbb{E}_{\alpha,\alpha+1}(f) + \frac{1}{\Gamma(\alpha_1)}. \tag{3.4}$$

Applying the Laplace transform to (3.2), we have

$$s^{\alpha}\phi(N) - s^{\alpha-1}\phi(0) \leq \frac{M_S^{\alpha}+M_D^{\alpha}}{s} - \mu^{\alpha}\phi(N),$$

which further gives

$$N(t) \leq \frac{M_S^{\alpha}+M_D^{\alpha}}{s(s^{\alpha}+\mu^{\alpha})} + \frac{s^{\alpha-1}}{s^{\alpha}+\mu^{\alpha}}N(0).$$

Using the equations (3.2)-(3.4), we assumed that $(S(0),O_w(0),O_b(0),D(0)) \in \mathbb{R}_+^4$, then

$$N(t) \leq (M_S^{\alpha}+M_D^{\alpha})t^{\alpha}\mathbb{E}_{\alpha,\alpha+1}(-\mu^{\alpha}t^{\alpha}) + N(0)\mathbb{E}_{\alpha,1}(-\mu t^{\alpha}).$$

Using the asymptotic behavior of the Mittag-Leffler function, we can observe that $N(t) \to \dfrac{M_S^{\alpha}+M_D^{\alpha}}{\mu^{\alpha}}$ as $t \to \infty$.

The Ω_{α} region is well established and the solution with initial value that belongs to Ω_{α} remains in Ω_{α} for each time $t > 0$. □

4. Basic Reproduction Number Study

The objective of this section is to calculate the basic reproduction number, using the next-generation matrix method that uses the equilibrium point without obesity, overweight, and diabetes. As a consequence of using this equilibrium as part of the method used, we study its stability and the direct effect on the basic reproduction number of the parameter associated with weight gain due to social pressure.

In a population composed only of susceptible individuals, the average number of infections caused by an infected individual is defined as basic reproduction number $\Re_0$. If $0 < \Re_0 < 1$, the infection will die out in the long run and if $\Re_0 > 1$, the infection will be able to spread in a population [31]. The higher the $\Re_0$ the more difficult it is to control the epidemic. The $\Re_0$ can be affected by several factors, such as the duration of infectivity of the affected patients, the infectivity of the organism and the degree of contact between the susceptible and infected populations.

The study of our basic reproduction number is centered on the impact of overweight and obesity, so these compartments are the ones that will be analyzed. We recall that diabetes is included in our study as a consequence of weight gain and furthermore, the body weight of individuals is not differentiated within this compartment. To find the basic reproduction number, we use the next generation-matrix method presented in [31]-[33], where the disease-free equilibrium point of Model (3.1) is $\varepsilon_0 = \left(\dfrac{M_S^{\alpha}}{k_{11}}, 0, 0, 0\right)$ where $k_{11} = \mu^{\alpha} + \alpha_1^{\alpha} + \beta_1^{\alpha}$. For our study, the disease-free equilibrium point refers to overweight and obesity, and then we will have people with normal-weight and diabetics since we may have diagnoses of diabetes that are not associated with body weight.

The transmission and transition matrices are:

$$F = \begin{pmatrix} \dfrac{M_S^{\alpha}\left((\alpha^*)^{\alpha}-(\beta^*)^{\alpha}\right)}{Nk_{11}} & \dfrac{M_S^{\alpha}\varepsilon(\alpha^*)^{\alpha}}{Nk_{11}} \\ 0 & 0 \end{pmatrix},$$

$$V = \begin{pmatrix} k_{12} & -\eta^{\alpha} \\ -\gamma^{\alpha} & k_{13} \end{pmatrix},$$

respectively. Then, for Model (3.1) the basic reproduction number is:

$$\Re_0 = \rho(FV^{-1}) = \frac{M_S^{\alpha}\left(k_{13}\left((\alpha^*)^{\alpha}-(\beta^*)^{\alpha}\right)+\varepsilon(\alpha^*)^{\alpha}\gamma^{\alpha}\right)}{Nk_{11}(k_{12}k_{13}-\eta^{\alpha}\gamma^{\alpha})},$$

where $k_{12} = \gamma^{\alpha}+\mu^{\alpha}+d^{\alpha}+\delta^{\alpha}+\alpha_2^{\alpha}$, $k_{13} = \eta^{\alpha}+\mu^{\alpha}+t_H d^{\alpha}+\alpha_3^{\alpha}$, $k_{14} = \mu_d^{\alpha}+\mu^{\alpha}+t_D d^{\alpha}$, and $\rho(FV^{-1})$ is the spectral radius of the matrix FV^{-1}.

We will study the local and global stability of the equilibrium point without obesity, overweight, and diabetes and without the impact of social pressure ($\beta_1 = 0$). For this parameter, we study its impact on the basic reproduction number and on the compartments.

The local stability of ε_0 can be determined using the following theorem:

Theorem 4.1. *Let $\alpha = \frac{p}{q}$ where $p,q \in \mathbb{Z}_+$ and $gdc(p,q) = 1$. Define $M = q(p = M\alpha)$, then the disease-free equilibrium point ε_0 of model (3.1) is asymptotically stable if $[arg(\lambda)] > \frac{\pi}{2M}$ for all roots λ of the following equation*

$$\det(\lambda^p \mathbb{I}_4 - M_1) = 0,$$

where $\mathbb{I}_4$ is the identity matrix of order 4×4, M_1 is the matrix of the linearization of model (3.1) at ε_0, $arg(\lambda)$ is the argument of λ and $gdc(p,q)$ is greatest common divisor of p and q.

Proof.

$$\det(\lambda^p \mathbb{I}_4 - M_1) = (\lambda^p + k_{11})(\lambda^p + k_{14})(\lambda^{2p} + b\lambda^p + c),$$

where $b = \frac{M_S^\alpha\left((\beta^*)^\alpha - (\alpha^*)^\alpha\right)}{Nk_{11}} + k_{12} + k_{13}$, $c = \frac{M_S^\alpha\left(k_{13}\left((\beta^*)^\alpha - (\alpha^*)^\alpha\right) - \varepsilon(\alpha^*)^\alpha\gamma^\alpha\right)}{Nk_{11}} + k_{12}k_{13} - \eta^\alpha\gamma^\alpha$.
Let's study the case when $c > 0$. Then, $c > 0$ implies that:

$$\frac{M_S^\alpha\left(k_{13}\left((\beta^*)^\alpha - (\alpha^*)^\alpha\right) - \varepsilon(\alpha^*)^\alpha\gamma^\alpha\right)}{Nk_{11}} + k_{12}k_{13} - \eta^\alpha\gamma^\alpha > 0. \tag{4.1}$$

Developing the expression (4.1), we have that $c > 0$ when,

$$\frac{M_S^\alpha\left((k_{13}\left((\alpha^*)^\alpha - (\beta^*)^\alpha\right) + \varepsilon(\alpha^*)^\alpha\gamma^\alpha\right)}{Nk_{11}(k_{12}k_{13} - \eta^\alpha\gamma^\alpha)} = \Re_0 < 1.$$

Using that $c > 0$ if $\Re_0 < 1$, we will prove that $b > 0$. We have:

$$\frac{M_S^\alpha\left((k_{13}\left((\alpha^*)^\alpha - (\beta^*)^\alpha\right) + \varepsilon(\alpha^*)^\alpha\gamma^\alpha\right)}{Nk_{11}} < k_{12}k_{13} - \eta^\alpha\gamma^\alpha,$$

$$\frac{M_S^\alpha(k_{13}\left((\alpha^*)^\alpha - (\beta^*)^\alpha\right)}{Nk_{11}} < k_{12}k_{13} - \eta^\alpha\gamma^\alpha - \frac{\varepsilon(\alpha^*)^\alpha\gamma^\alpha}{Nk_{11}}. \tag{4.2}$$

The elements of the right-hand side of inequality (4.2) are positive, we have that:

$$\frac{M_S^\alpha\left((k_{13}\left((\alpha^*)^\alpha - (\beta^*)^\alpha\right)\right)}{Nk_{11}} < k_{12}k_{13}.$$

First, we divide by k_{13}, which by definition is nonzero (it suffices that μ is nonzero which is the death rate from causes not associated with obesity), and we have that:

$$\frac{M_S^\alpha\left((\alpha^*)^\alpha - (\beta^*)^\alpha\right)}{Nk_{11}} < k_{12}.$$

Now, we add k_{13} which is positive, and obtain the inequality:

$$\frac{M_S^\alpha\left((\alpha^*)^\alpha - (\beta^*)^\alpha\right)}{Nk_{11}} < k_{12} + k_{13}.$$

We can conclude that:

$$b = \frac{M_S^\alpha\left((\beta^*)^\alpha - (\alpha^*)^\alpha\right)}{Nk_{11}} + k_{12} + k_{13} > 0.$$

Authors in [34], showed that the Routh-Hurwitz criteria, $b, c > 0$, are necessary and sufficient for $[arg(\lambda)] > \frac{\pi}{2}$. It is clear that all of the eigenvalues are negative ($[arg(\lambda)] > \frac{\pi}{2}$) if $\Re_0 < 1$. Hence, the disease-free equilibrium ε_0 is locally asymptotically stable for $\alpha \in (0,1]$ if $\Re_0 < 1$. □

This theorem was proved with analogous ideas in references [35]-[37]. From Theorem 2 of [32, 37], we have the following lemma characterizing the instability with the $\Re_0$:

Lemma 4.2. *The disease-free equilibrium point ε_0 of model (3.1) is unstable if $\Re_0 > 1$.*

Now, using an analogous method applied to Model (3.1), we prove the global stability of the disease-free equilibrium point. Following [38], we can rewrite the model (3.1) as

$$\begin{aligned} {}^c\mathbb{D}_t^\alpha X &= F(X,I), \\ {}^c\mathbb{D}_t^\alpha I &= G(X,I), \quad G(X,0) = 0, \end{aligned}$$

where $X \in \mathbb{R}_+^2$ is the vector with diabetics and normal-weight individuals and $I \in \mathbb{R}_+^2$ have the compartment related overweight and obese of Model (3.1).

The disease-free equilibrium point is now denoted by $E_0^\alpha = (X_0, 0)$, $X_0 = \left(\frac{M_S^\alpha}{\mu^\alpha}, 0\right)$.

The conditions (H_1^α) and (H_2^α) below must be satisfied to guarantee the global asymptotic stability of E_0^α.

$$\begin{aligned} (H_1^\alpha): &\quad \text{For} \quad {}^c\mathbb{D}_t^\alpha X = F(X,0), \quad X_0 \quad \text{is globally asymptotically stable,} \\ (H_2^\alpha): &\quad G(X,I) = AI - G^*(X,I), \quad G^*(X,I) \geq 0, \quad \text{for} \quad (X,I) \in \Omega_\alpha, \end{aligned}$$

where $A = D_I G(X_0, 0)$, ($D_I G(X_0,0)$ is the Jacobian of G with respect to I at $(X_0,0)$) is a M-matrix (the off-diagonal elements of A are non-negative) and Ω_α is the biologically feasible region.
The following result shows the global stability of the disease-free equilibrium point.

Theorem 4.3. *The fixed point E_0^α is a globally asymptotically stable equilibrium (G.A.S) of Model (3.1) provided that $\Re_0 < 1$ and that the conditions (H_1^α) and (H_2^α) are satisfied.*

Proof. Let

$$F(X,0) = \begin{pmatrix} M_S^\alpha - k_{11}S \\ M_D^\alpha + \alpha_1^\alpha S - k_{14}D \end{pmatrix}.$$

As $F(X,0)$ is linear, then X_0 is globally stable and (H_1^α) is satisfied. Let

$$A = \begin{pmatrix} -k_{12} + (\alpha^*)^\alpha + \lambda_S & \eta^\alpha + \varepsilon(\alpha^*)^\alpha \\ \gamma^\alpha & -k_{13} \end{pmatrix},$$

$$I = (O_w, O_b),$$

$$G^*(X,I) = AI^T - G(X,I),$$

$$G^*(X,I) = \begin{pmatrix} G_1^*(X,I) \\ G_2^*(X,I) \end{pmatrix} = \begin{pmatrix} (\alpha^*)^\alpha (O_w + \varepsilon O_b)\left(1 - \dfrac{S}{N}\right) \\ 0 \end{pmatrix}.$$

Since $\dfrac{S}{N} \leq 1$ then $1 - \dfrac{S}{N} \geq 0$. Thus $G^*(X,I) \geq 0$ for all $(X,I) \in \Omega_\alpha$. Consequently, E_0^α is globally asymptotically stable. □

Analogous proofs can be found in the bibliographical references [26, 28, 29].

4.1. Sensitive index

In this section, we performed a sensitivity analysis of the $\Re_0$ with respect to the parameters β_1 and α_1, which are related to weight gain associated with social pressure and the diagnosis of diabetes that is associated with factors other than body weight. The sensitivity analysis of the basic reproduction number determines the relative importance of the parameters present in the basic reproduction number, such as the parameters of transmission, resistance, recovery, among others. The sensitivity index can be defined using the partial derivatives, provided that the variable be differentiable with respect to the parameter under study. Sensitivity analysis also helps to identify the vitality of the parameter values in the predictions using the model [39]-[41].

Definition 4.4. *([41]) The normalized forward sensitivity index of a variable v that depends differentiability on a parameter p is defined as:*

$$\Upsilon_p^v := \frac{\partial v}{\partial p} \times \frac{p}{v}.$$

The sensitivity index of $\Re_0$ helps to determine the parameters that have an impact on it.
We can characterize the sensitivity index as follows:

- A positive value of the sensitivity index implies that an increase of the parameter value causes an increase of the basic reproduction number.
- A negative value of the sensitivity index implies that an increase of the parameter value causes a decrease of the basic reproduction number.

Since the $\Re_0$ was calculated with the parameters at the $\alpha-$level, the sensitivity analysis is also performed at this level for consistency of the study. The expressions of the sensitivity indices of the selected parameters are as follows:

$$\Upsilon_{\alpha_1}^{\Re_0} = -\frac{\alpha\alpha_1^\alpha}{k_{11}},$$

$$\Upsilon_{\beta_1}^{\Re_0} = -\frac{\alpha\beta_1^\alpha}{k_{11}}.$$

Parameters α_1 and β_1 have a negative sensitivity index with respect to $\Re_0$, which implies that an increase of these parameters will mean a decrease of $\Re_0$. The social pressure exerted on an individual and the diagnosis of diabetes for causes not associated with body weight independently, a growth in their respective parameters will mean a decrease on $\Re_0$.

5. Numerical Simulations

In this section, we perform computational simulations to validate the proposed model and make a study of the basic reproduction number. The algorithm used to numerically solve nonlinear differential equations of fractional-order system (3.1) is in [42]-[44]. The algorithm has the structure of a PECE (Predict-Evaluate-Correct-Evaluate) method and combines a fractional-order algorithm with a classical method. The approach chosen is Adams-Bashforth-Moulton for both integrators. The key to deriving the method in the fractional variant is to use the trapezoidal quadrature product formula. This algorithm is independent of the $\alpha-$value and behaves very similarly to the classical Adams-Bashforth-Moulton method. The stability properties do not change in the fractional version compared to the classical algorithm. The programming was carried out in Matlab software. The data used for the computational simulations are extracted from the literature or assumed. The parameter values for the computational simulations are $(\alpha^*)^\alpha = 2$ (assumed), $(\beta^*)^\alpha = 0.2$ (assumed), $M_S^\alpha = 667.685$ [28], $M_D^\alpha = 4.1$ (assumed), $\beta_1^\alpha = 0.25$ (assumed), $\varepsilon = 0.007$ [10], $\eta^\alpha = 0.1$ [10], $\gamma^\alpha = 0.0015$ [10], $\delta^\alpha = 0.002$ [10], $\mu^\alpha = \frac{1}{70.5}$ [26], $d^\alpha = 0.07$ (assumed), $t_H = 1.02$ (assumed), $t_D = 1.03$ (assumed), $\mu_d^\alpha = 0.013$ (assumed), $\alpha_1^\alpha = 0.1$ (assumed), $\alpha_2^\alpha = 0.35$ [45, 46], $\alpha_3^\alpha = 0.4$ [45, 46], and $\alpha = 0.3, 0.5, 0.7, 0.9, 1$. The initial conditions are $S = 874.1400$, $O_w = 1.2000$, $O_b = 1.5000$ and $D = 100.0000$ on the scale of 10000 individuals.

5.1. Basic reproduction number

In this section, we study the impact on the basic reproduction number of the parameters $\eta, \gamma, \delta, \beta_1$, and $\alpha_i, i = 1,2,3$ and interpret how joint variations of them affect or not the behavior of $\Re_0$ for different fractional orders. We will study the joint variations of the parameters associated with transitions through the compartments associated with body weight and diabetes as a consequence of weight. The intervals of the parameters are $\eta \in [0.00028, 0.1]$, $\gamma \in [0.00028, 0.0015]$, $\delta \in [0.00035, 0.002]$ (extracted from [10]), $\alpha_2 \in [0.35, 0.49]$ and $\alpha_3 \in [0.3, 0.53]$ (extracted from [45, 46]). The joint variation of the selected parameters provides us with information on how they will influence the $\Re_0$, for different fractional orders. It will allow us to obtain information not only about how they may or may not affect $\Re_0$, but also what happens when we vary the fractional order. This information will help us create future strategies to reduce overweight and obesity.
In the study of the variation of the parameters α_2 and α_3 associated with suffering from diabetes as a consequence of overweight and obesity, we observed that $\Re_0$ increases in value as α increases in the study, see Figures 5.1a-5.1e. For $\alpha = 0.9$, we find values greater and less than unity and for $\alpha = 1$, $\Re_0$ is greater than unity, see Figures 5.1d and 5.1e. This information gives us different possibilities of behavior for different $\alpha-$values which helps in the control proposals. We can notice that when α_3 increases it has a strong influence on the basic reproduction number.
In the joint variation of η and γ that are associated with the cases that go from obese to overweight (positive situation) and those that go from overweight to obese (adverse situation), it happens that $\Re_0$ increases as $\alpha-$values increases, see Figures 5.2a-5.2e. For $\alpha = 0.9$, we have that $\Re_0$ remains close to unity (≤ 0.95) and exceeds it, see Figure 5.2d. For $\alpha = 1$, $\Re_0$ exceeds unity reaching values greater than two, see Figure 5.2e. The higher $\Re_0$ the more difficult is the control.
An analogous behavior occurs for the variation of η and δ (positive situation because these are the ones that go from overweight to reach a normal-weight), see Figures 5.3a-5.3e. These variations show the influence that N has on the dynamics.
In the variation of γ and δ together in $\Re_0$, unlike the two previous ones, the unit is only exceeded when $\alpha = 1$ (for the $\alpha-$values studied) and it is lower than the variations of η and γ, and η and δ, see Figures 5.4a-5.4e.
We can conclude that with greater fractional order the $\Re_0$ in all the variations studied will be greater, even reaching values greater than unity. The higher the $\Re_0$, the more difficult the design of strategies to control overweight and obesity and, as a consequence, diabetes. Furthermore, with selected parameters, it shows us that we must control more than one compartment in the dynamics.

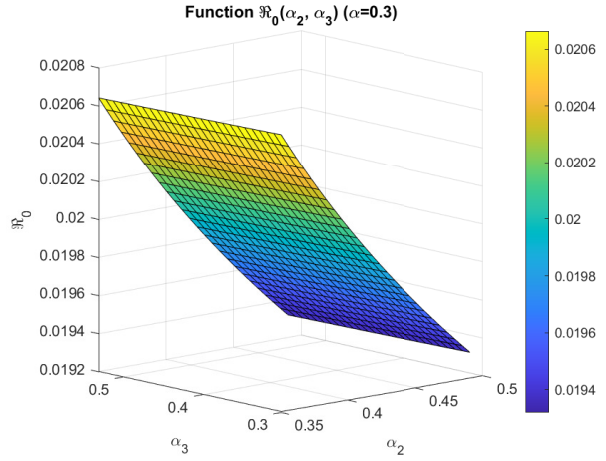

(a) $\Re_0(\alpha_2, \alpha_3)$ for $\alpha = 0.3$

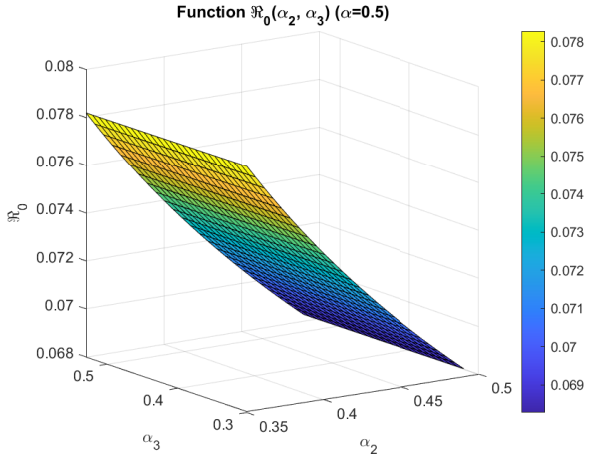

(b) $\Re_0(\alpha_2, \alpha_3)$ for $\alpha = 0.5$

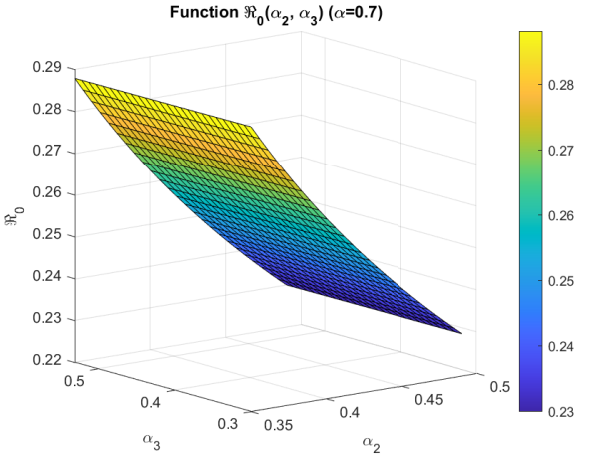

(c) $\Re_0(\alpha_2, \alpha_3)$ for $\alpha = 0.7$

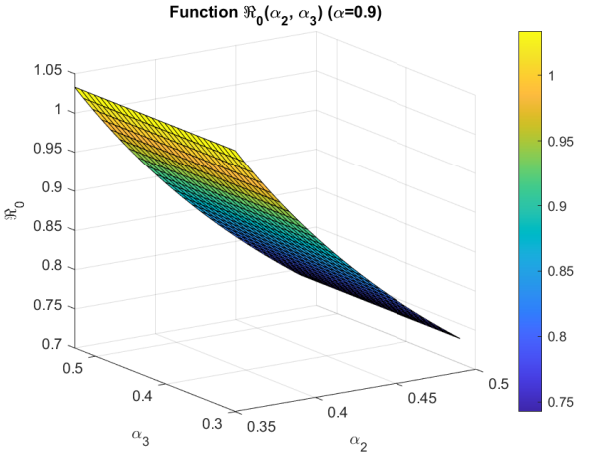

(d) $\Re_0(\alpha_2, \alpha_3)$ for $\alpha = 0.9$

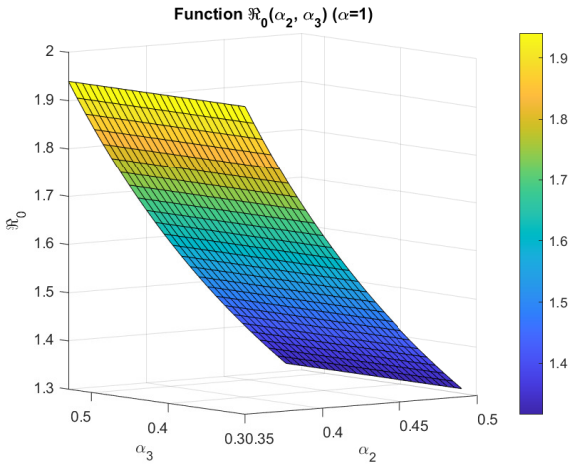

(e) $\Re_0(\alpha_2, \alpha_3)$ for $\alpha = 1$

Figure 5.1: Joint variation of α_2^α and α_3^α in $\Re_0$ for different $\alpha-$values.

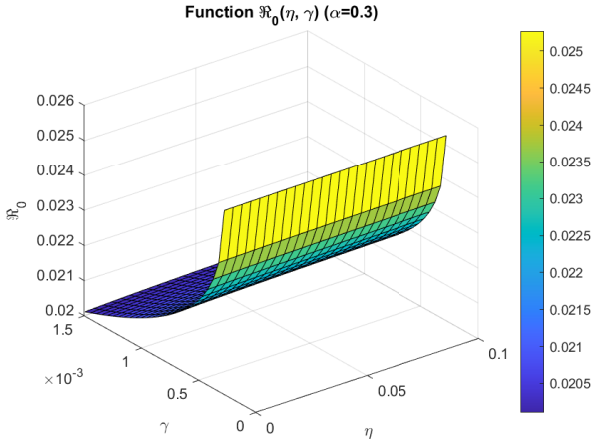

(a) $\Re_0(\eta, \gamma)$ for $\alpha = 0.3$

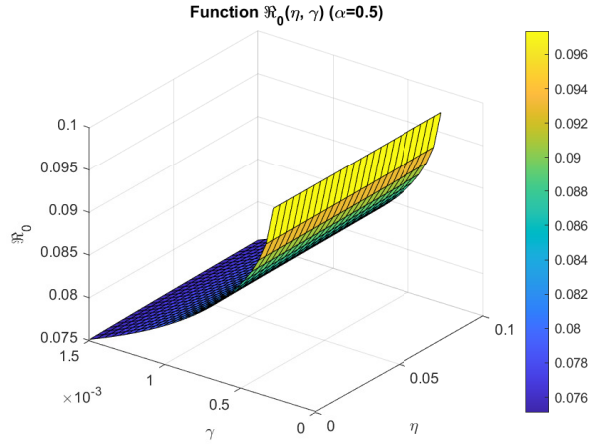

(b) $\Re_0(\eta, \gamma)$ for $\alpha = 0.5$

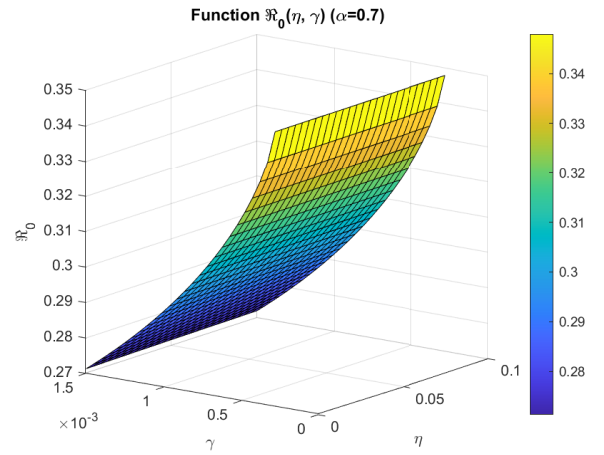

(c) $\Re_0(\eta, \gamma)$ for $\alpha = 0.7$

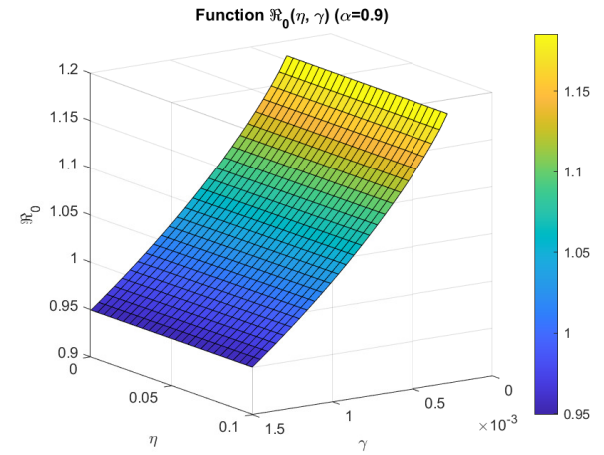

(d) $\Re_0(\eta, \gamma)$ for $\alpha = 0.9$

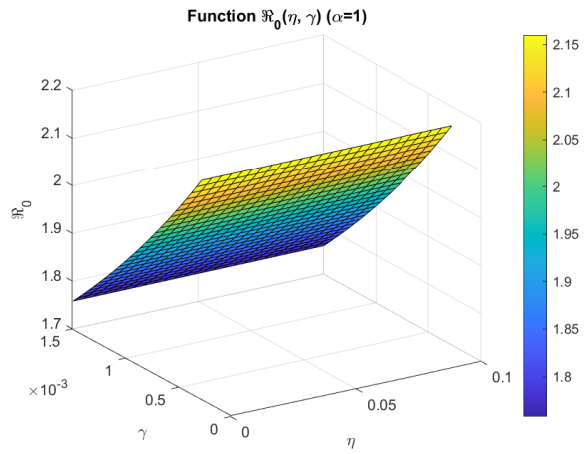

(e) $\Re_0(\eta, \gamma)$ for $\alpha = 1$

Figure 5.2: Joint variation of η^α and γ^α in $\Re_0$ for different $\alpha-$values.

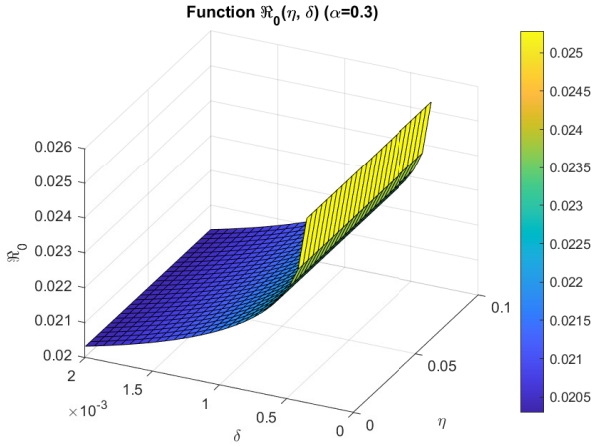

(a) $\Re_0(\eta, \delta)$ for $\alpha = 0.3$

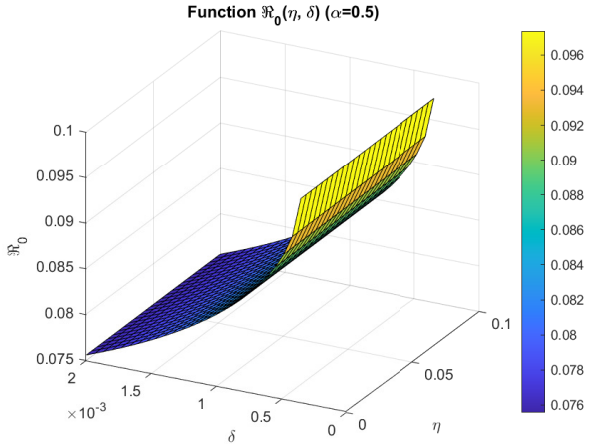

(b) $\Re_0(\eta, \delta)$ for $\alpha = 0.5$

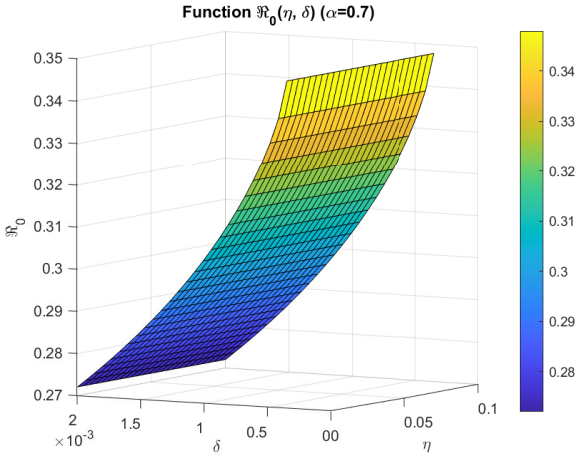

(c) $\Re_0(\eta, \delta)$ for $\alpha = 0.7$

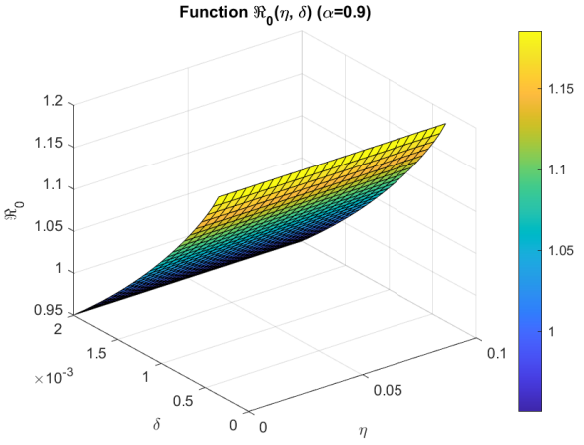

(d) $\Re_0(\eta, \delta)$ for $\alpha = 0.9$

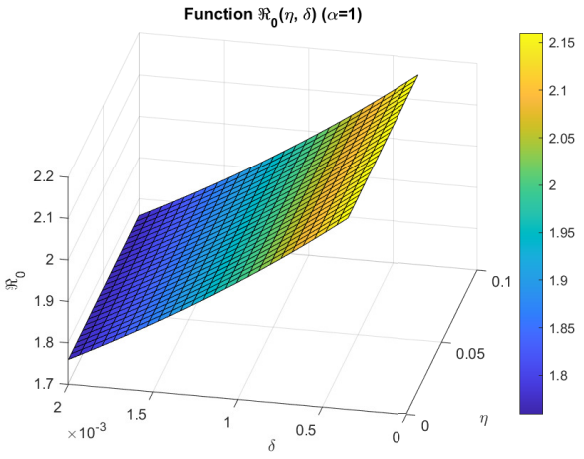

(e) $\Re_0(\eta, \delta)$ for $\alpha = 1$

Figure 5.3: Joint variation of η^α and δ^α in $\Re_0$ for different $\alpha-$values.

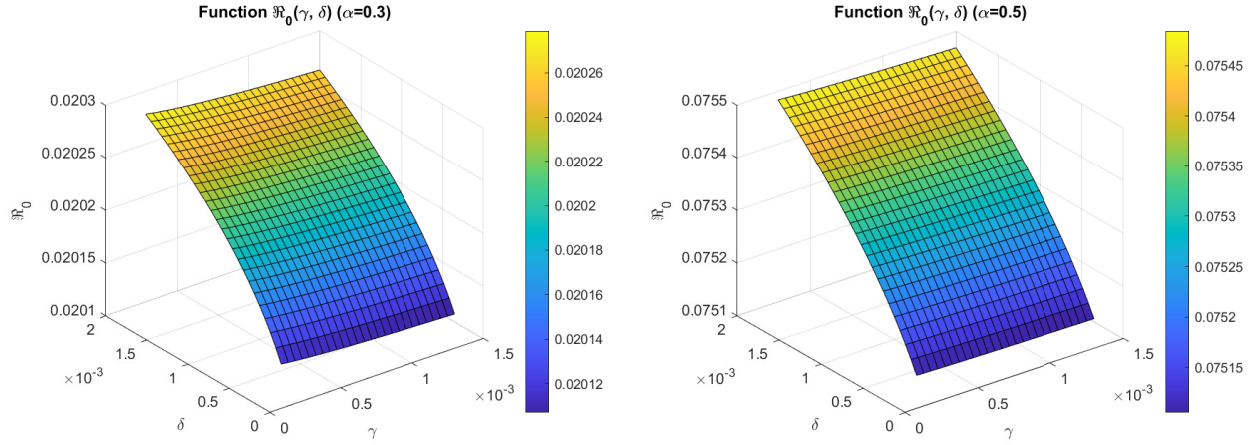

(a) $\Re_0(\gamma, \delta)$ for $\alpha = 0.3$

(b) $\Re_0(\gamma, \delta)$ for $\alpha = 0.5$

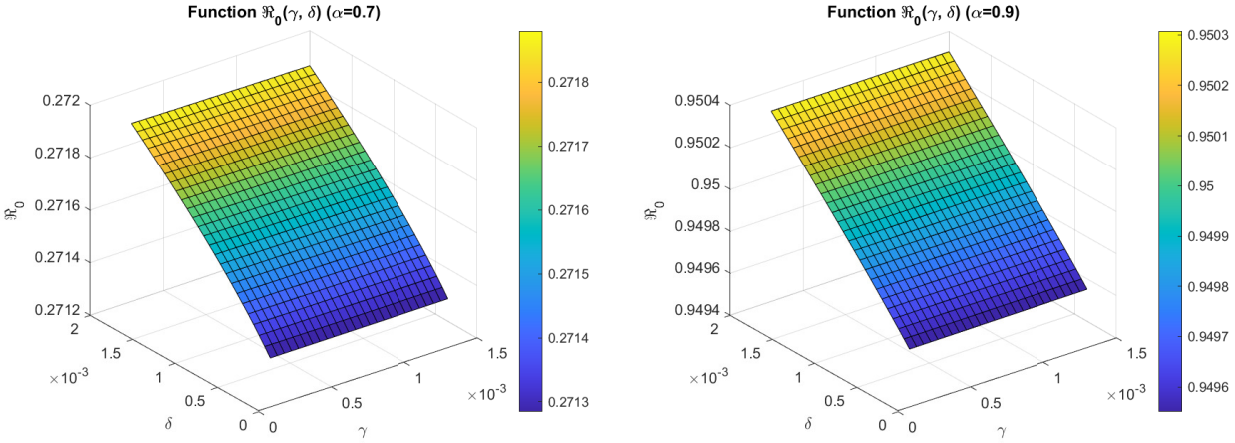

(c) $\Re_0(\gamma, \delta)$ for $\alpha = 0.7$

(d) $\Re_0(\gamma, \delta)$ for $\alpha = 0.9$

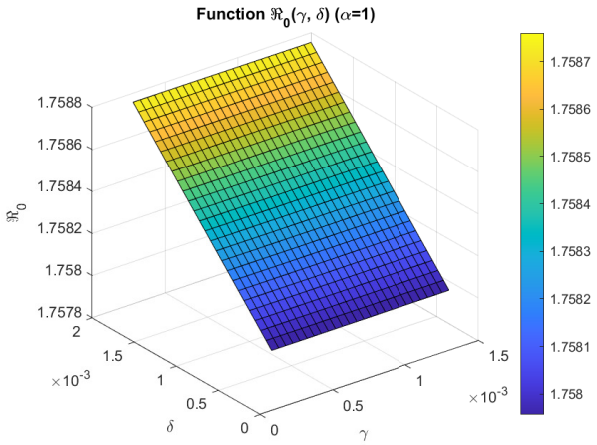

(e) $\Re_0(\gamma, \delta)$ for $\alpha = 1$

Figure 5.4: Joint variation of δ^α and γ^α in $\Re_0$ for different $\alpha-$values.

5.2. Compartmental study

In the compartment of people with normal-weight for the different $\alpha-$values under study, we have a growth in this compartment, where for higher α's a greater number of cases are reported. Then, begins a decrease where the lowest values are reached for the higher $\alpha-$values. This means that for higher $\alpha-$values the output of this compartment is higher, which is the opposite objective because the idea is to maintain a higher number of people with ideal weight, see Figure 5.5a. Quantitatively, we started in this compartment with 874.1400, and at the end of the study (15 years) for $\alpha = 0.3$ which reported the highest number of cases was 407.016 which means a reduction of 467.124 (more than half with respect to the initial value). For $\alpha = 1$, at the end of the study reported 218.687 meaning a reduction from the initial value, this means a reduction of 655.453. Observing Figure 5.5, the other behavior for $\alpha-$values studied is between 0.3 and 1, (see Figure 5.5a), so we can conclude that in this compartment at the end of the study, the outputs are significant and the objective is to achieve the highest number of healthy people.
In the compartment of overweight individuals at the beginning of the study, there is a growth that then stabilizes, where the final value is significantly higher than the initial value for all the fractional orders studied. During the longer time of the study and at the end of the study, higher $\alpha-$values report higher number of overweight individuals, see Figure 5.5b. At the end of the study for $\alpha = 0.3$ (lowest $\alpha-$value that reported the lowest reported number of cases) was 860.304 and for $\alpha = 1$ (highest $\alpha-$value that reported the highest number of cases) was 1,349.65 which represents a high number of reported cases considering that we started with 1.2000. All these cases will become obese or diabetic if they do not improve their lifestyle, which affects their health significantly.
For the compartment of obese individuals at the beginning of the study there is a decrease in the number of cases for all the $\alpha-$values under study, see Figure 5.5c. Approximately the number of cases reported with obesity starts to increase for the different $\alpha-$values reaching the highest values reported for the highest $\alpha-$values. We can observe that for $\alpha = 1$ it was reported 4.09616, and for $\alpha = 0.3$ it was 2.08284, the other fractional orders studied the reported values are between $\alpha = 0.3$ and $\alpha = 1$. Remembering that we started with 1.5000, the increase of individuals in this compartment is qualitatively significant. In comparison with the overweight compartment in the obese, a lower number was reported, but if the person does not change lifestyle from overweight to obese, will become obese, see Figures 5.5c and 5.5d.
In the diabetics compartment during the whole study there is a growth of the reported cases with respect to the initial value 100.0000, see Figure 5.5d. We can observe that overweight and obesity have a strong impact on diabetes. At the beginning lower $\alpha-$values report a higher number of cases but approximately at 3 years of study the opposite process happens and at the end of the study higher $\alpha-$values report a higher number of diabetics. Quantitatively, we have at the end of the study that for $\alpha = 0.3$ it was reported 874.534, and for $\alpha = 1$ it was 5,379.01 and as the other $\alpha-$values studied the values reported are between those reported for $\alpha = 0.3$ and $\alpha = 1.0$ then the study at the end reports that the diabetic cases are in the interval $[874.534; 5,379.01]$ which is a significant increase with respect to the initial value 100.0000. This evidences the need to apply control in overweight and obese cases due to the impact they have on diabetes and that upon reaching the diabetic state the situation is irreversible because diabetes has no cure at present.
All the results obtained contribute to providing information on the behavior of overweight and obesity obtained from the model. By studying different $\alpha-$values, it allows us to observe different behaviors and with them design different, more effective strategies for controlling overweight and obesity, taking into account several possible scenarios (depending on the $\alpha-$value) and appropriate time. In this case, we show the need for control strategies due to the growth of diabetics in the population coming from the increase in overweight and obese people, because this disease has a strong influence on the increase in diabetes in the population.
The variation of the parameter β_1 in the model was studied; this is directly associated with the social impact that leads a person with normal-weight to become overweight. We only studied the overweight compartment because the construction of the model will directly affect that compartment. The variation of this parameter independently will show us if only social pressure will affect the dynamics. We can observe that when we increase the $\alpha-$value for all the different values of β_1 studied ($\beta_1 = 0.1, 0.25, 0.40, 0.50, 0.70$) we have an increase in the number of overweight people. The number of overweight people in the population increases over time and the greater β_1 the number reported is higher. This increase for these variations of the parameter and the fractional order is not quantitatively or qualitatively significant, since the variation in the number of individuals is not impactful and the tendency of overweight behavior does not change for the variations of the parameter, see Figures 5.6a-5.6e.

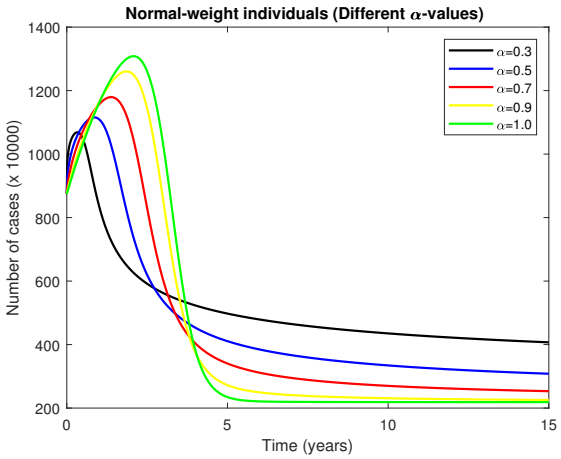

(a) Normal-Weight Individuals

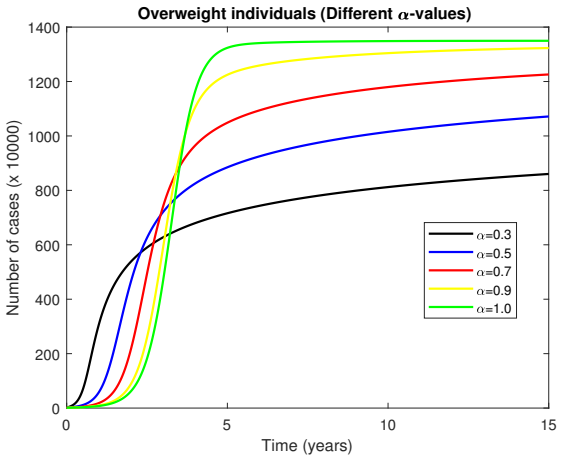

(b) Overweight Individuals

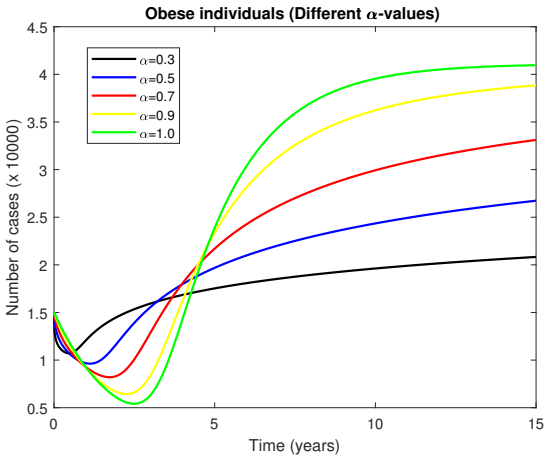

(c) Obese Individuals

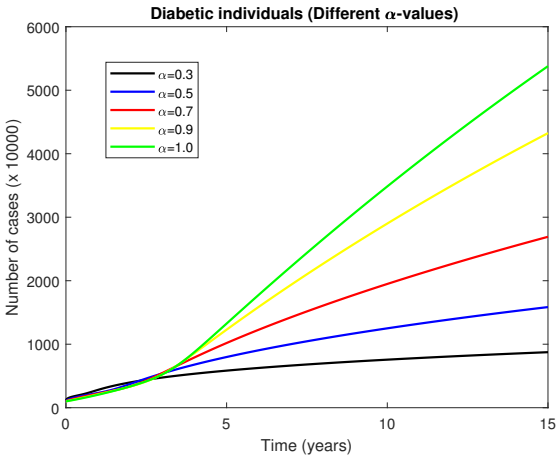

(d) Diabetic Individuals

Figure 5.5: Behavior of the compartments of Model (3.1) for the scenario under study and different $\alpha-$values.

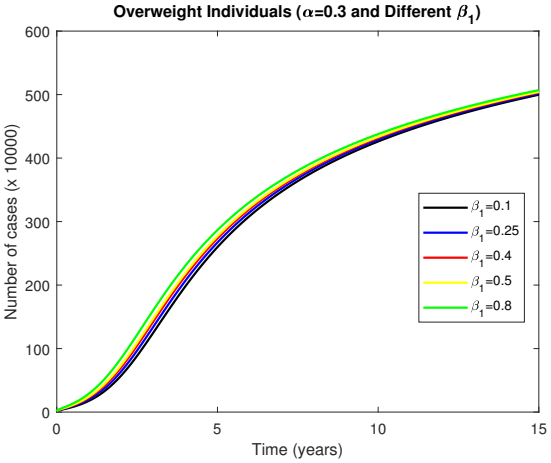

(a) Variation of β_1 for $\alpha = 0.3$

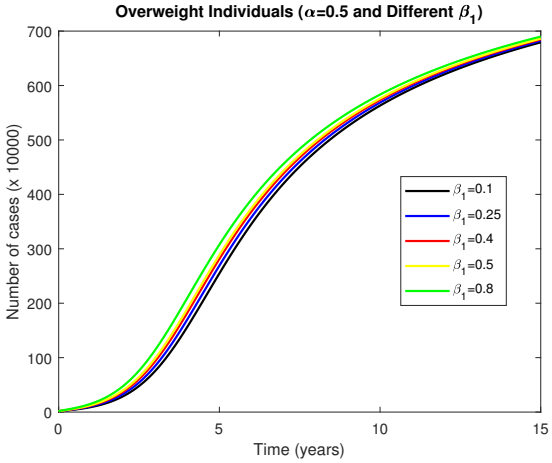

(b) Variation of β_1 for $\alpha = 0.5$

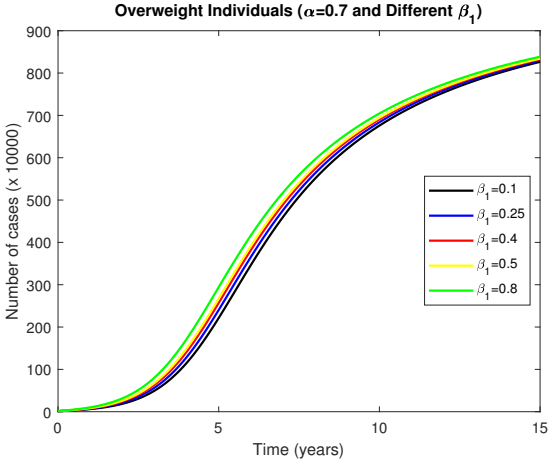

(c) Variation of β_1 for $\alpha = 0.7$

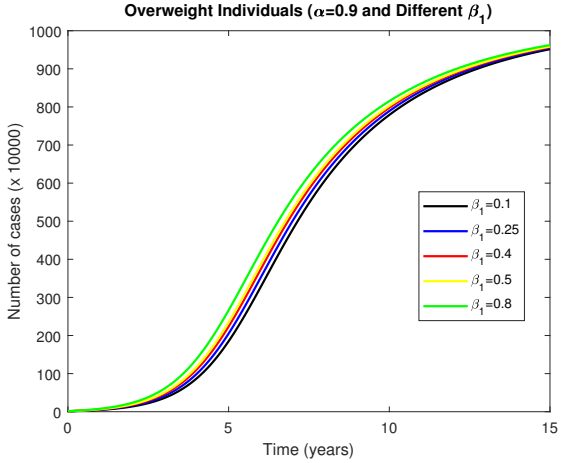

(d) Variation of β_1 for $\alpha = 0.9$

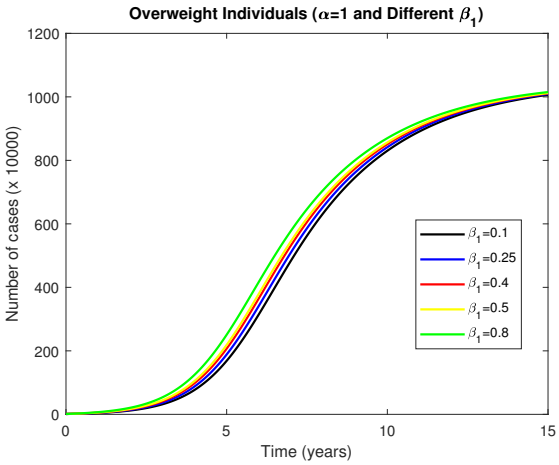

(e) Variation of β_1 for $\alpha = 1$, overweight individuals

Figure 5.6: Behavior of the overweight compartment when $\beta_1 = 0.05, 0.1, 0.3, 0.5, 0.7$ for different $\alpha-$values, overweight compartment.

6. Conclusion

In this paper, we presented a mathematical model to study obesity and overweight, and their relationship with diabetes. The model enables us to study the behavior of normal-weight, overweight, and obese individuals, as well as their interactions and the influence of social factors (social pressure). For the construction of the model, we used fractional order derivatives in the Caputo sense taking advantage of this modeling technique with respect to the memory effect. Using the next-generation matrix method, we find the basic reproduction number and show the local and global stability of the disease-free equilibrium point. Sensitivity indices were calculated with respect to the basic reproduction number for the parameters associated with weight gain due to social pressure and the diagnosis of diabetes not associated with body weight. The sensitivity index is negative for both, which means that an increase in these parameters will mean a decrease in the $\Re_0$. This means that as people are diagnosed with diabetes for reasons other than body weight, they enter the diabetic compartment and do not actively influence other individuals and also that social pressure alone will not significantly influence the increase in overweight and obesity. To validate the model, we performed computational simulations with data from the literature and other assumed data validated by specialists. In the study of the weight and diabetic groups, the normal-weight population decreased significantly, the overweight and obese increased and the diabetic group grew throughout the study. We can observe that the higher the $\alpha-$values, the higher the number of cases reported for the overweight, obese, and diabetic groups, and the opposite occurs for the normal-weight groups. This behavior shows the need to strategies with the objective of ensuring that people achieve a healthy lifestyle and a normal-weight and consequently reduce the impact of diabetes due to causes associated with body weight. We study the variation in the simulations of the parameter β_1, since this parameter is related to weight gain due to social pressure (which can lead to an unhealthy lifestyle). The study of this parameter will allow us to know if social pressure is an important factor in the increase in overweight people and, as a consequence, in the increase in cases of diabetes. This variation in the impact of social pressure (β_1) in our study did not cause significant effects on the dynamics (it was checked directly in the $\Re_0$ with the sensitivity analysis), particularly in the increase in overweight individuals. We can conclude that for our study, intervening only in the social pressure exerted on the individual will not be able to reduce the number of overweight individuals, so we have to intervene in human interactions. In future work, we intend to study different real scenarios and estimate parameters for them and propose, based on the results obtained regarding the behavior of the system, the problem of optimal control of reducing overweight and obesity and, as consequences, diabetes.

Article Information

Acknowledgements: The authors would like to express their sincere thanks to the editor and the anonymous reviewers for their helpful comments and suggestions.

Author's contributions: All authors contributed equally to the writing of this paper. All authors read and approved the final manuscript.

Conflict of Interest Disclosure: No potential conflict of interest was declared by the author.

Copyright Statement: Authors own the copyright of their work published in the journal and their work is published under the CC BY-NC 4.0 license.

Supporting/Supporting Organizations: No grants were received from any public, private or non-profit organizations for this research.

Ethical Approval and Participant Consent: It is declared that during the preparation process of this study, scientific and ethical principles were followed and all the studies benefited from are stated in the bibliography.

Plagiarism Statement: This article was scanned by the plagiarism program. No plagiarism detected.

Availability of data and materials: Not applicable.

References

[1] WHO, *Obesity and overweight 2021*, available at https://www.who.int/news-room/fact-sheets/detail/obesity-and-overweight
[2] F.Q. Nuttall, *Body mass index: Obesity, BMI, and health: A Critical review*, Nutr. Res., **50**(3) (2015), 117-128.
[3] M. Akram, *Diabetes mellitus type 2: Treatment strategies and options: A review*, Diabetes Metab. J., **4**(9) (2013), 304-313.
[4] A. Golay, J. Ybarr, *Link between obesity and type 2 diabetes*, Best Pract. Res. Clin. Endocrinol Metab., **19**(4) (2005), 649-663.
[5] T. Yang, B. Zhao, D. Pei, *Evaluation of the Association between obesity markers and type 2 diabetes: A cohort study based on a physical examination population*, J. Diabetes Res., **19**(4) (2021), Article ID 6503339, 9 pages, doi: 10.1155/2021/6503339.
[6] K. Ejima, D. Thomas, D.B. Allison, *A Mathematical model for predicting obesity transmission with both genetic and nongenetic heredity*, Obesity (Silver Spring), **26**(5) (2018), 927–933.
[7] S. Kim, So-Yeun Kim, *Mathematical modeling for the obesity dynamics with psychological and social factors*, East Asian Math. J., **34**(3) (2018), 317-330.
[8] L.P. Paudel, *Mathematical modeling on the obesity dynamics in the Southeastern region and the effect of intervention*, Univers. J. Math. Appl., **7**(3) (2019), 41-52.
[9] S.M. Al-Tuwairqi, R.T. Matbouli, *Modeling dynamics of fast food and obesity for evaluating the peer pressure effect and workout impact*, Adv. Differ. Equ., **58** (2021), 1-22.
[10] S. Bernard, T. Cesar, A. Pietrus, *The impact of media coverage on obesity*, Contemp. Math., **3**(1) (2021), 60-71.
[11] R.S. Dubey, P. Goswami, *Mathematical model of diabetes and its complications involving fractional operator without singular kernel*, Discrete Contin. Dyn. Syst. - Ser. S., **14**(7) (2021), 2151–2161.
[12] Sandhya, D. Kumar, *Mathematical model for Glucose-Insulin regulatory system of diabetes Mellitus*, Adv. Appl. Math. Biosci., **2**(1) (2011),39-46.
[13] S. Anusha, S. Athithan, *Mathematical modeling of diabetes and its restrain*, Int. J. Mod. Phys. C, **32**(9) (2021), 2150114.
[14] W. Banzi, I. Kambutse, V. Dusabejambo, E. Rutaganda, F. Minani, J. Niyobuhungiro, L. Mpinganzima, J.M. Ntaganda, *Mathematical model for Glucose-Insulin regulatory system of diabetes Mellitus*, Int J Math Math. Sci., **2**(1) (2021), Article ID 6660177, 12 pages.
[15] E. M. D. Moya, A. Pietrus, S. Bernard, *Mathematical model for the Study of obesity in a population and its impact on the growth of diabetes*, Math. Model. Anal., **28**(4) (2023), 611–635.
[16] R. Figueiredo Camargo, E. Capelas de Oliveira, (1 Ed.), *Cálculo fracionário*, Livraria da Fısica, Sao Paulo, 2015.
[17] H. Kheiri, M. Jafari, *Optimal control of a fractional-order model for the HIV/AIDS epidemic*, Int. J. Biomath, **11**(7) (2018), 1850086, doi:10.1142/S1793524518500869.
[18] K. Diethelm, (1 Ed.), *The Analysis of Fractional Differential Equations*, Springer-Verlag Berlin Heidelberg, 2014.

[19] L. Carvalho de Barros et al., *The memory effect on fractional calculus: An application in the spread of COVID-19*, J. Comput. Appl. Math., **40**(3) (2021), 72, doi:10.1007/s40314-021-01456-z.

[20] M. Saeedian et al., *Memory effects on epidemic evolution: The susceptible-infected-recovered epidemic model*, Phys. Rev. E, **95**(2) (2017), 022409, doi:10.1103/PhysRevE.95.022409.

[21] D. Baleanu, F.A. Ghassabzade, J.J. Nieto, A. Jajarmi, *On a new and generalized fractional model for a real cholera outbreak*, Alexandria Eng. J., **61**(11) (2022), 9175-9186. doi: /10.1016/j.aej.2022.02.054.

[22] N. Z. Monteiro and S. R. Mazorque, *Fractional derivatives applied to epidemiology*, Trends Comput. Appl. Math., **22**(2) (2021). doi:10.5540/tcam.2021.022.02.00157.

[23] M. Vellappandi, P. Kumar, V. Govindaraj, *Role of fractional derivatives in the mathematical modeling of the transmission of Chlamydia in the United States from 1989 to 2019*, Nonlinear Dyn., **11** (2023), 4915–4929 doi: 10.1007/s11071-022-08073-3.

[24] M. Inc, B. Acay, H. W. Berhe, A. Yusuf, A. Khan, S. Yao, *Analysis of novel fractional COVID-19 model with real-life data application*, Results Phys., **23** (2021), 103968. doi: 10.1016/j.rinp.2021.103968.

[25] K. Diethelm, *A fractional calculus based model for the simulation of an outbreak of dengue fever*, Nonlinear Dyn., **71** (2013), 613–619, doi: 10.1007/s11071-012-0475-2.

[26] E.M.D. Moya, A. Pietrus, S.M. Oliva, *Mathematical model with fractional order derivatives for Tuberculosis taking into account its relationship with HIV/AIDS and diabetes*, Jambura J. Biomath., **2**(2) (2021), 80-95.

[27] Z. Odibat, N. Shawagfeh, *A fractional calculus based model for the simulation of an outbreak of dengue fever*, Appl. Math. Comput. **186**(1) (2013), 286-293.

[28] C.M.A. Pinto, A.R.M. Carvalho, *Diabetes mellitus and TB co-existence: Clinical implications from a fractional order modelling*, Appl. Math. Modell., **68** (2019), 219-243.

[29] C.M.A. Pinto, A.R.M. Carvalho, *The HIV/TB coinfection severity in the presence of TB multi-drug resistant strains*, Ecol. Complexity, **32(Part A)** (2019), 1-20.

[30] W. Lin, *Global existence theory and chaos control of fractional differential equations*, J. Math. Anal. Appl., **332**(1) (2007), 709-726.

[31] O. Diekmann, J.A.P. Heesterbeek, M.G. Roberts, *The construction of next-generation matrices for compartmental epidemic models*, J. R. Soc. Interface, **7**(47) (2010), 873-885.

[32] P. Van Den Driessche, J. Watmoughs, *Reproduction numbers and sub-threshold endemic equilibria for compartmental models of disease transmission*, Math. Biosci., **180** (2002), 29-48.

[33] O. Diekmann, J.A.P. Heesterbeek, J.A.J. Metz, *On the definition and the computation of the basic reproduction ratio in model for infectious diseases in heterogeneous populations*, J. Math. Biol., **28** (1990), 365–382.

[34] E. Ahmed, A. M. A. El-Sayed, H. A. A. El-Sakau, *Onsome Routh-Hurwitz conditions for fractional order differential equations and their applications in Lorenz, Rössler, Chua and Chen systems*, Physics Letters A, **358**(1) (2006), 1-4.

[35] Fatmawati, M. A. Khan, E. Bonyah, Z. Hammouch, E. M. Shaiful, *A mathematical model of tuberculosis (TB) transmission with children and adults groups: A fractional model*, AIMS Math. **5** (2020), 2813-2842.

[36] C. M. A. Pinto, A. R. M. Carvalho, *A latency fractional order model for HIV dynamics*, J. Comput. Appl. Math. **312** (2017), 240-256.

[37] A. R. M. Carvalho, C. M. A. Pinto, D. Baleanu, *HIV/HCV coinfection model: a fractional-order perspective for the effect of the HIV viral load*, Adv. Differ. Equations., (2018), 1-22.

[38] C. Castillo-Chavez, Z. Feng, W. Huang, *On the Computation of $\mathfrak{R}_0$ and Its Role on Global Stability*, In: Mathematical Approaches for Emerging and Reemerging Infectious Diseases: An Introduction, Springer-Verlag, New York, (2002), 229-250, doi:10.1007/978-1-4613-0065-6.

[39] F.N. Ngoteya, Y. Nkansah-Gyekye, *Sensitivity Analysis of Parameters in a Competition Model*, Appl. Comput. Math. **4(5)** (2015), 363-368.

[40] N. Chitnis, J.M. Hyman, J.M. Cushing, *Determining important parameters in the spread of malaria through the sensitivity analysis of a mathematical model*, Bull. Math. Biol. **70(5)** (2008),1272-96.

[41] M. Zamir, G. Zaman, A.S. Alshomrani, *Sensitivity Analysis and Optimal Control of Anthroponotic Cutaneous Leishmania*, PLoS ONE **11(8)** (2016), e0160513, doi: 10.1371/journal.pone.0160513.

[42] K. Diethelm, N.J. Ford, A.D. Freed, *A Predictor-Corrector Approach for the Numerical Solution of Fractional Differential Equations*, Nonlinear Dyn. **29** (2002), 3-22.

[43] K. Diethelm, N.J. Ford and A.D. Freed, *Detailed Error Analysis for a Fractional Adams Method*, Numer Algorithms **36** (2004), 31-52.

[44] K. Diethelm, A.D. Freed, *The FracPECE Subroutine for the Numerical Solution of Differential Equations of Fractional Order*, In: Forschung und wissenschaftliches Rechnen 1999 (1998), 57–71.

[45] Centers for Disease Control and Prevention. National Center for Health Statistics, *About Underlying Cause of Death 1999–2019. CDC WONDER Online Database*, available at http://wonder.cdc.gov/ucd-icd10.html

[46] Centers for Disease Control and Prevention. National Center for Health Statistics, *About Underlying Cause of Death 2020. CDC WONDER Online Database*, available at https://www.cdc.gov/diabetes/pdfs/data/statistics/national-diabetes-statistics-report.pdf